



**Miguel  
Castro Silva**

**Simulação Numérica de Deformações e Tensões em  
Soldadura**

Numerical Simulation of Strains and Stresses in Welding





**Miguel  
Castro Silva**

## **Simulação Numérica de Deformações e Tensões em Soldadura**

Numerical Simulation of Strains and Stresses in Welding

Dissertação apresentada à Universidade de Aveiro para cumprimento dos requisitos necessários à obtenção do grau de Mestre em Engenharia Mecânica, realizada sob a orientação científica do Doutor António Manuel de Bastos Pereira, Professor Associado com Agregação do Departamento de Engenharia Mecânica da Universidade de Aveiro (DEM-UA) e coorientação do Doutor Fábio António Oliveira Fernandes, Investigador Júnior do Departamento de Engenharia Mecânica da Universidade de Aveiro (DEM-UA).

Este trabalho teve o apoio financeiro dos projetos UIDB/00481/2020 e UIDP/00481/2020 - FCT - Fundação para Ciência e Tecnologia; e CENTRO-01-0145-FEDER-022083-Programa Operacional Regional do Centro (Centro2020), no âmbito do Acordo de Parceria Portugal 2020, através do Fundo Europeu de Desenvolvimento Regional.



**o júri / the jury**

presidente / president

**Prof. Doutor Rui António da Silva Moreira**

Professor Auxiliar

Universidade de Aveiro – Departamento de Engenharia Mecânica

vogais / committee

**Prof. Doutor Daniel Gil Afonso**

Professor Adjunto

Universidade de Aveiro – Escola Superior de Design, Gestão e Tecnologia de Produção Aveiro - Norte

**Prof. Doutor António Manuel de Bastos Pereira**

Professor Associado c/ Agregação (Orientador)

Universidade de Aveiro – Departamento de Engenharia Mecânica



**agradecimentos**  
acknowledgements

A realização deste trabalho contou com a colaboração do Professor António Bastos e do Professor Fábio Fernandes aos quais expresso o meu reconhecimento pelas contribuições e toda a disponibilidade prestada.

À minha família e aos meus amigos, um agradecimento especial por tudo. Seguimos juntos!





**palavras-chave**

Soldadura; Laser; DP600; Simulação Numérica; Tensões e Deformações

**resumo**

A soldadura é dos métodos mais conhecidos na indústria para unir uma grande variedade de materiais. Este processo cria inevitavelmente tensões e deformações nos componentes devido à alta intensidade de energia libertada pela fonte de calor. Nos dias que correm torna-se quase obrigatório quantificar estas alterações nas peças que passam pelo processo de soldadura. Só assim é possível cumprir rigorosos parâmetros de qualidade, garantindo que a peça cumpre a função atribuída. É muito comum recorrer a métodos experimentais para fazer esta análise. No entanto, o uso de métodos computacionais em simulação de processos de soldadura tem crescido significativamente. A simulação numérica, baseada no Método de Elementos Finitos, surge para facilitar aos engenheiros a prevenção e análise de fenómenos complexos.

No presente trabalho foram desenvolvidos dois modelos de simulação numérica do processo de soldadura através de laser em chapas de *Dual-Phase* 600. Foram testados 2 tipos de juntas: topo a topo e em T. As deformações e tensões causadas pelo processo foram quantificadas com recurso ao *software* Simufact.



**keywords**

Welding; Laser; DP600; Numerical Simulation; Stress-Strain

**abstract**

Welding is one of the best known methods in the industry for joining a wide variety of materials. This process inevitably creates stresses and strains in the components due to the high energy intensity released by the heat source. Nowadays it is almost mandatory to quantify these changes in the parts that go through the welding process. This is the only way to comply with strict quality parameters ensuring that the part fulfils the assigned function. It is very common to use experimental methods to do this analysis. However, the use of computational methods in welding process simulation was being increasing significantly. Numerical simulation, based on the Finite Element Method, appears to make it easier for engineers to predict and analyse complex phenomena.

In this work two numerical simulation models of the welding process by laser were developed on Dual-Phase 600 steel plates. Two types of joints were tested: butt and in T. The deformations and stresses caused were quantified using the Simufact software.



# Contents

1. CHAPTER 1 - INTRODUCTION.....	1
1.1. Context and motivation .....	1
1.2. Objectives .....	2
1.3. Document structure.....	2
2. CHAPTER 2 – STATE OF THE ART .....	6
2.1. Section 1 - Introduction .....	6
2.2. Section 2 - Laser Welding .....	12
2.3. Section 3 - Numerical Simulation .....	40
2.4. Section 4 - Material .....	56
3. CHAPTER 3 – NUMERICAL MODEL .....	67
3.1. Pre-processing stage .....	67
3.2. Post-processing stage.....	80
4. CHAPTER 4 – GENERAL CONCLUSIONS.....	121
4.1. Conclusions .....	121
4.2. Future work.....	125
REFERENCES.....	128



# List of Tables

Table 1 – Material parameters and their influence [5] .....	10
Table 2 – Geometry parameters and their influence [5].....	12
Table 3 - Weldability of dissimilar metal combinations [12] .....	16
Table 4 - Overview of welding types [12] .....	17
Table 5 - Relative joining efficiencies of different welding processes [12] .....	18
Table 6 – Solid-state laser overview [8].....	21
Table 7 – Gas laser overview [8] .....	21
Table 8 – Residual stress distribution on types of welding sequence [2] .....	36
Table 9 - Overview of tolerances in welding process [39] .....	37
Table 10 - Relations in welding simulation [45].....	44
Table 11 – Differences between the simplified mechanical models [45] .....	47
Table 12 – Parameters of heat source model [3].....	51
Table 13 – Types of finite elements [52] .....	53
Table 14 – Error percentage of numerical simulation [45] .....	56
Table 15 - Mechanical properties of AHSS [3].....	57
Table 16 – Mass density [3] .....	60
Table 17 – Elastic properties [3] .....	60
Table 18 - Thermal expansion coefficient [3].....	62
Table 19 – Specific heat of DP600 [3].....	62
Table 20 – Thermal conductivity of DP600 [3] .....	63
Table 21 – Dual-phase microstructure constitution [26].....	63
Table 22 - Chemical composition of DP 600 [26] .....	65
Table 23 – Clamping conditions and steps overview of butt joint models .....	69
Table 24 – Clamping conditions and steps overview of T-joint model .....	70
Table 25 – Heat source parameters .....	71
Table 26 – Temperatures properties .....	73
Table 27 – Increment and steps control .....	79
Table 28 - Results resume (model 1 – butt joint).....	86
Table 29 – Results summary (model 2 – butt joint).....	94
Table 30 – Results summary (model 3 – T joint).....	107





# Acronyms

AHSS - Advanced High-Strength Steel

AWI - Abaqus welding interface

AWS - American Welding Society

BM - Base material

DP - Dual Phase

FE - Finite element

FEM - Finite element method

FZ - Fusion zone

GMA - Gas metal arc

HAZ - Heat affected zone

HSS - High strength steel

MIG - Metal arc welding

MMAW - Manual metal arc welding

PM – peak mode

TEM - Transverse Electromagnetic Mode

TIG - Tungsten arc welding

TWB – Tailored welded blank

WPP - Welding process parameters

WPS - Welding Procedure Specification



# List of Figures

Figure 2.1 - Unrestricted and restricted material behaviour [1].....	7
Figure 2.2 - Residual stress distribution [6].....	8
Figure 2.3 - Different types of welding distortion [4].....	9
Figure 2.4 – Thermomechanical properties vs temperature [5].....	10
Figure 2.5 - Effect of pass width [5].....	11
Figure 2.6 – Effect of welding speed [5].....	11
Figure 2.7 – Types of fusion welding [8].....	14
Figure 2.8 - Wavelength vs absorption ratio [8].....	15
Figure 2.9 - Tailor welded blanks in car body [23].....	19
Figure 2.10 – Conventional process vs tailored welded blank technique [25].....	20
Figure 2.11 - Equipment of Nd:YAG solid-state laser [28].....	23
Figure 2.12 – Energy level diagram [29].....	23
Figure 2.13 – Laser welding equipment of DEM-UA [26].....	24
Figure 2.14 - Continuous and pulsed laser beam mode.....	25
Figure 2.15 - Difference between conduction and keyhole processes [31].....	26
Figure 2.16 – Laser beam distribution [26].....	26
Figure 2.17 - Different profiles of TEM for laser [32].....	27
Figure 2.18 – Internal and external defects [26].....	29
Figure 2.20 - Transverse section micrograph [12].....	30
Figure 2.21 – Pulse [9].....	31
Figure 2.22 - Laser spot size [9].....	32
Figure 2.23 – Effective penetration for a 50% and 80% overlap [36].....	32
Figure 2.24 - Different welding joining arrangements [11].....	34
Figure 2.25 – Penetration depth at different roughness levels [37].....	35
Figure 2.26 - Laser welding with different gaps between plates [8].....	38
Figure 2.27 - Energy balance during laser welding Nd:YAG [3].....	38
Figure 2.28 – Types of model in FEM for welding simulation [45].....	43
Figure 2.29 - Multidisciplinary relations in the welding simulation process [45].....	44
Figure 2.30 - HAZ and FZ comparison between numerical simulation and real tests [17].....	45
Figure 2.31 - Analysis stages [42].....	46
Figure 2.32 - Double ellipsoidal heat source shape [17].....	49

Figure 2.33 Conical heat source shape [17] .....	51
Figure 2.34 – Clamping vs stress [4].....	54
Figure 2.35 - Summary of three generations of AHSS [56].....	57
Figure 2.36 – Car body structure.....	58
Figure 2.37 – True stress-strain curve obtained from tensile test for DP 600 [4].....	61
Figure 2.38 – DP600 microstructure [59] .....	64
Figure 2.39 – TTT diagram during thermal cycles [60].....	65
Figure 2.40 – Parameterized CCT (continuous cooling transition) [4].....	65
Figure 3.1 – Butt joint model .....	68
Figure 3.2 – T joint model.....	68
Figure 3.3 – Butt joint (model 1) clamping conditions at step A (top) and steps B+C (bottom) .....	70
Figure 3.4 – T-joint clamping conditions at step A (left) and steps B+C (right).....	70
Figure 3.5 – Heat source geometry in T-joint (left) and in butt joint (right) .....	71
Figure 3.6 –Trajectories of T-joint (up) and butt joint (down) .....	72
Figure 3.7 – Thermal conductivity .....	73
Figure 3.8 – Specific heat capacity .....	74
Figure 3.9 – Young’s modulus .....	75
Figure 3.10 - Density.....	75
Figure 3.11 – Thermal expansion coefficient.....	76
Figure 3.12 – Flow curves.....	77
Figure 3.13 – Butt joint mesh.....	78
Figure 3.14 – T-joint mesh.....	78
Figure 3.15 – Positioning of transverse and longitudinal lines of butt joint models.....	80
Figure 3.16 – Positioning of top and bottom surfaces of butt joint models .....	81
Figure 3.17 - Positioning of transverse and longitudinal lines of vertical plate (model 3 - T joint) .....	81
Figure 3.18 – Positioning of left and right surfaces (model 3 - T joint) .....	82
Figure 3.19 - Positioning of transverse and longitudinal lines of horizontal plate (model 3 – T joint).....	83
Figure 3.20 - Positioning of top and bottom surfaces (model 3 – T joint).....	83

Figure 3.21 - Positioning of transverse lines to calculate Y and Z displacement on butt joint models .....	84
Figure 3.22 - Positioning longitudinal lines to calculate X displacement on butt joint models .....	84
Figure 3.23 – Positioning of transverse lines to calculate X and Y displacement (model 3 – T joint).....	85
Figure 3.24 - Positioning of longitudinal lines to calculate Z displacement (model 3 – T joint) .....	85
Figure 3.25 - Longitudinal stress mapping in butt joint (model 1 – butt joint).....	86
Figure 3.26 – Longitudinal residual stress along transverse lines (model 1 – butt joint) ...	87
Figure 3.27 - Longitudinal residual stress along longitudinal lines (model 1 – butt joint) .	88
Figure 3.28 – Transverse stress mapping in butt joint (model 1 – butt joint) .....	88
Figure 3.29 – Transverse residual stress along transverse lines (model 1 – butt joint) .....	89
Figure 3.30 – Transverse residual stress along longitudinal lines (model 1 – butt joint) ...	90
Figure 3.31 – Top view of Z displacement (model 1 – butt joint) .....	90
Figure 3.32 – Side view of Z displacement (model 1 – butt joint) .....	91
Figure 3.33 – Z displacement along transverse lines (model 1 – butt joint) .....	91
Figure 3.34 – Top view of Y displacement (model 1 – butt joint).....	92
Figure 3.35 - Y displacement along transverse lines (model 1 – butt joint) .....	92
Figure 3.36 – Top view of X displacement (model 1 – butt joint).....	93
Figure 3.37 - X displacement along longitudinal lines (model 1 – butt joint) .....	93
Figure 3.38 – Mapping of longitudinal stress in butt joint (model 2 – butt joint).....	94
Figure 3.39 – Longitudinal residual stress along transverse lines (model 2 – butt joint) ...	95
Figure 3.40 – Longitudinal residual stress along longitudinal lines (model 2 – butt joint) ...	96
Figure 3.41 – Mapping of transverse stress in butt joint (model 2 – butt joint).....	96
Figure 3.42 – Transverse residual stress along transverse lines (model 2 – butt joint) .....	97
Figure 3.43 – Transverse residual stress along longitudinal lines (model 2 – butt joint) ...	98
Figure 3.44 – Top view of Z displacement (model 2 – butt joint) .....	98
Figure 3.45 – Side view of Z displacement (model 2 – butt joint) .....	99
Figure 3.46 - Z displacement along transverse lines (model 2 – butt joint).....	99
Figure 3.47 – Top view of Y displacement (model 2 – butt joint).....	100
Figure 3.48 – Y displacement along transverse lines (model 2 – butt joint).....	100

Figure 3.49 – Top view of X displacement (model 2 – butt joint).....	101
Figure 3.50 - X displacement along longitudinal lines (model 2 – butt joint) .....	102
Figure 3.51 – Comparison of longitudinal residual stress along transverse line of butt joint models .....	103
Figure 3.52 - Comparison of longitudinal residual stress along longitudinal line of butt joint models .....	103
Figure 3.53 - Comparison of transverse residual stress along transverse lines of butt joint models .....	104
Figure 3.54 - Comparison of transverse residual stress along longitudinal lines of butt joint models .....	105
Figure 3.55 - Comparison of Z displacement of butt joint models .....	105
Figure 3.56 - Comparison of Y displacement of butt joint models.....	106
Figure 3.57 - Comparison of X displacement of butt joint models.....	106
Figure 3.58 – Mapping of the stress in z-direction (model 3 – T joint).....	108
Figure 3.59 - Transverse residual stress along transverse lines of vertical plate (model 3 – T joint) .....	109
Figure 3.60 - Mapping of the stress in x-direction (model 3 – T joint) .....	109
Figure 3.61 - Transverse residual stress along transverse lines of horizontal plate (model 3 – T joint).....	110
Figure 3.62 - Transverse residual stress along longitudinal line (model 3 – T joint) .....	111
Figure 3.63 - Mapping of the stress in y-direction (model 3 – T joint) .....	111
Figure 3.64 - Longitudinal residual stress along transverse lines of horizontal plate (model 3 – T joint).....	112
Figure 3.65 - Longitudinal residual stress along transverse lines of vertical plate (model 3 – T joint).....	112
Figure 3.66 - Longitudinal residual stress along longitudinal line (model 3 – T joint) ....	113
Figure 3.67 - Overview of X displacement (model 3 – T joint).....	114
Figure 3.68 – Side view of X displacement (model 3).....	114
Figure 3.69 – X displacement along transverse lines of the vertical plate (model 3 – T joint) .....	115
Figure 3.70 – X displacement along longitudinal lines of horizontal plate (model 3 – T joint) .....	115

Figure 3.71 - Overview of Y displacement (model 3 – T joint).....	116
Figure 3.72 – Y displacement along transverse lines of the horizontal plate (model 3 – T joint) .....	117
Figure 3.73 – Y displacement along transverse lines of the vertical plate (model 3 – T joint) .....	117
Figure 3.74 – Overview of Z displacement (model 3 – T joint) .....	118
Figure 3.75 – Z displacement along transverse lines of horizontal plate (model 3 – T joint) .....	119
Figure 3.76 - Z displacement along longitudinal lines of the vertical plate (model 3 – T joint) .....	119

# 1. CHAPTER 1 - INTRODUCTION

This first chapter is where the context of the project developed for the master's thesis is explained. The proposed objectives are clearly detailed. Finally, the whole structure of the document is explained.

## 1.1. Context and motivation

---

Any product that is developed needs to guarantee certain quality parameters. To ensure that this happens, it is necessary to know and master all the manufacturing processes that are associated with product development. This work consists in the study of the consequences that the welding process has for the parts.

The welding process inevitably leads to a deformation of connected components. The high amount of heat in a localized area produces mechanical and metallurgical changes due to thermal cycles. The presence of internal stresses reduce the strength of the structure near the welded joint area. They are dependent on many variables such as the material, welding parameters and clamping conditions. The major concern of the industry is how to predict the material behaviour to improve the product quality and save time and money. Laser welding is a recent method, still being investigated. It is a fusion process that performs the weld without filler material. To join the parts, this technology releases a high amount of energy in a concentrated zone that heats the material until it melts.

The whole welding process is quite complex and not linear. To understand the material behaviour and the respective stresses and strains in the components caused by the heat input, finite element method analysis must be used. Numerical simulation is widely used in various areas of engineering, since it makes it possible to achieve results of complex problems, dependent on many variables. This method is very useful because it can improve the prototype conception without experimental tests, which would take a long time to develop



and would involve a great waste of money. The knowledge of the mechanical and thermal properties of the material and understanding how the welding process will change these properties can be used to optimize the joining process. Consequently, the quality of the product will be higher. Confirming the reliability of the welded joint and checking if tolerances are satisfied without doing real tests is one of the most important advantages that simulation offers.

## 1.2. Objectives

---

Numerical simulation of welding process in the Mechanical Engineering Department of the University of Aveiro is not very common. The importance of developing this work is high as it is the starting point for future work in this area. The main objective of this work was to start the numerical simulation of the welding process using Simufact software. It is divided into small topics as follows:

- i. Initial research to master the concepts of the welding process, especially the laser beam welding;
- ii. Understand the material properties and how they depends on the heat input;
- iii. Study the different types of numerical simulation models;
- iv. Learn how numerical simulation software works;
- v. Develop a numerical simulation model of the welding process;
- vi. Analyse the strains and internal stresses generated by the heat input;
- vii. Take conclusions about the obtained results;
- viii. Propose future work to continue this research.

## 1.3. Document structure

---

This part explains how the document is divided, giving a brief summary of the 4 main chapters.

The *first chapter* includes a brief introduction to the work done, the project context and the motivation, as well as the main objectives and how the work is divided.

The *second chapter* is the state-of-the-art. It is extensive since it intends to cover all aspects relevant to this work. Furthermore, since this is the first time that this type of work has been developed, it needed further research to have a good knowledge of the theme. It consists of three large sections: laser welding, numerical simulation and material. The first section is related to laser welding. A presentation of the laser welding process is made, starting with a general overview, mentioning the progress of the laser over the years. Moreover, a summary of available welding types and the various applications of this technology is done. The advantages and drawbacks are mentioned in detail. The working principle of the laser, from the equipment to the composition of the system, are at the end of this chapter. In this chapter it is possible to understand the differences between pulsed or continuous beam and the modes (conduction vs keyhole). A quick introduction to heat affected areas is made. There are many laser categories that are dependent on the environment in which they work and their characteristics. An introduction to the laser that will be used is made (Nd:YAG). The parameters to perform the welding are mentioned, as well as their respective influence on the welding quality. Finally, the characteristic defects that are caused due to the high heat input are mentioned.

The second section covers all aspects of numerical simulation. Initially, a brief introduction mentions the relationship with industry and history and their development over time. This method has its obstacles, and its limitations are explained. After that, an introduction is made to the numerical simulation of the welding process. The various possible models are presented in detail, such as mechanical, thermal and metallurgical models, followed by the elements responsible for the discretization of the model.

The third section focuses on the material. Initially an introduction to Advanced High-Strength Steel (AHSS) steel is made, followed by the properties of DP600 as well as its composition and microstructure. This section also includes the advantages and disadvantages of using this type of steel and the optimum laser welding parameters that are specific to this material. Finally, a comparison is made between the experimental results versus the results obtained using the Finite Element Method (FEM).

The development of a numerical simulation model was done in the *third chapter*. This chapter is divided into 2 characteristic steps of the numerical simulation model: pre-processing stage and post-processing stage. In the first stage (pre-processing), the model is defined with the characteristics of the welding process. Then, the different components that are part of the model are generated and the respective mesh is produced. The material properties are then defined taking into account that they are temperature dependent. As in any numerical model, to have the ability to simulate the process as it actually happens in reality, it is necessary to define the boundary conditions. To finish this step, the robot is defined, as well as the path, welding speed, heat source geometry and the power to be used. This step is extremely important so that the results are close to the actual process. Finally, the last step, post-processing, is where the various results are presented.

The *fourth chapter* is the end of the work and where the results, discussions and final conclusions are presented. In addition, suggestions for future work are made in order to continue the work developed. The constraints felt during the work are also mentioned.



## 2. CHAPTER 2 – STATE OF THE ART

A literature review necessary to carry out the work is present in this chapter. The state of the art is divided into three main sections: welding, numerical simulation and material. Each section is divided into large topics that are sub-divided into small areas for a more detailed explanation. Initially, a general introduction is made, describing the main concepts covered throughout this work.

### 2.1. Section 1 - Introduction

---

This is an introduction to the developed work with some theoretical considerations. An overview is made where a problem is presented to understand exactly what this work is about. Some topics such as stress and deformation as well as the material behaviour are mentioned.

#### 2.1.1. Welding problem

The material is represented by the spheres shown in the following figures. Figure 2.1. (left) shows the material behaviour without restrictions. This change is due to an external stimulus, in this case heat input. Initially the material is at room temperature (A), expands in response to heat input (B) and then, after the cooling process, returns to its initial shape (C). Although the final shape is identical to the initial, there are few internal stresses that have been created that are not detected by naked eye. What usually happens in the welding process is represented in Figure 2.1. (right), i.e. there are restrictions on the width of the weld bead. Through the scheme, it is possible to see that the material behaves differently due to the imposed restrictions. After the process, the material does not return to its initial shape and consequently suffers a permanent deformation. This happens whenever the material is subject to a process of phase transformation. What happens in the welding process is exactly

the same, but instead of being in a concentrated material sphere, it is along the entire weld bead.

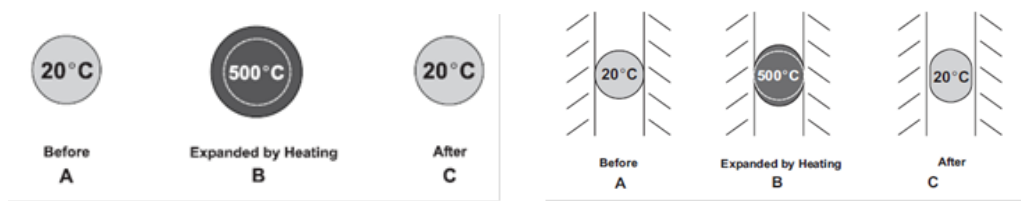


Figure 2.1 - Unrestricted and restricted material behaviour [1]

The previous case was a good example of the problem that happens in the welding process. The existence of internal stresses is a disadvantage in the structures and may even compromise their function and consequently quality. Further, it will be explain how these internal strains and stresses can be predicted by engineers with non-evasive methods such as numerical simulation. For now this is just an introduction to recognize the problem of this type of joining process.

### 2.1.2. Residual Stresses

To better understand how residual stresses appear in the material, the process will be explained in detail. Residual stresses are self-equilibrating internal stresses existing with no external forces on its boundary [2]. They are those that remain in the body, even after external stimuli are removed. There are several causes for the emergence of these stresses, such as thermal or mechanical loads or even phase transformation. The internal stresses should always be quantified because they compromise the quality of the product. It is also important to know the magnitude to predict the resistance to fracture [3]. In welding, they are created due to the non-uniform thermal cycles of the part, which cause volume changes.

As seen above, welding always causes a change in the stress/strain state of the parts due to the thermal cycles to which the material is subjected. The material expands due to heat input and is compressed against the side walls elastically [4] [5]. The cooling step takes place between the melting point and the solidification of the material. At this stage the material undergoes a contraction that causes the so-called residual stresses. After the process, the

material can fracture if the generated stresses are high, or deform if the existing stresses are reduced. What happens most of the time is the deformation of the parts since it is necessary to reach the fracture stress for the fracture to happen. Residual stress distribution is going to appear in longitudinal and transversal direction of the welding direction. The equilibrium condition is present during all the process. It should be noted that before the welding process starts there may be residual stresses but they are usually close to zero. The following Figure 2.2 illustrates typical internal stresses in both directions caused by thermal cycles. When the room temperature is reached, as seen in the following figure, the longitudinal residual stresses are under tension state (+) in the centre of the weld bead and are in compression state (-) in the lateral zones.

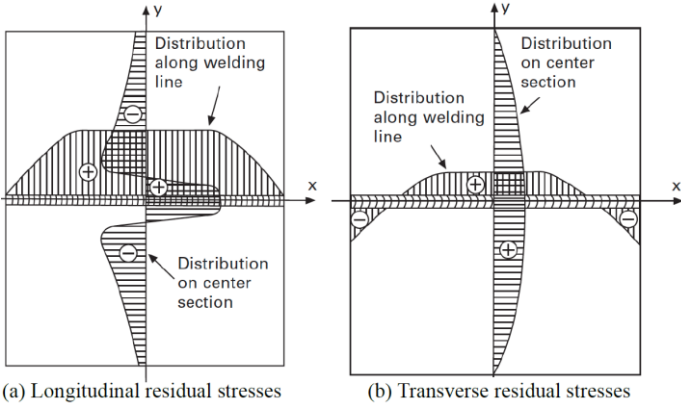


Figure 2.2 - Residual stress distribution [6]

### 2.1.3. Deformations

Deformations are the way the material reacts to the presence of residual stresses. The material always try to obtain a state of equilibrium. Since there are residual stresses, the material tends to adapt its shape. The distortions are always present in any welding. The work of an engineer is trying to predict, through numerical simulations, these deformations [3]. Minimizing the deformations is one of the largest challenges of the welding industry, avoiding compromising the integrity of the parts.

The next Figure 2.3 shows some examples of the type of deformations that can exist due to the welding process. The transverse and longitudinal shrinkages are due to the contraction

of the weld bead in different directions [1]. Rotational distortion is caused when there is a non-uniform expansion of the weld bead, leaving one area of the piece narrower than the other. Angular distortion occurs when there is an irregular thermal distribution along the thickness of the part. Consequently, residual stresses are generated which cause a rotation of the part around the welding bead. This type of deformation is a very common in T-joints. Bending has the same cause as angular distortion but in another direction [4]. It is a shrinkage in the longitudinal direction, due to the presence of non-symmetrical residual stresses caused by different thermal gradients. Finally, buckling happens because of instability of compressive stresses.

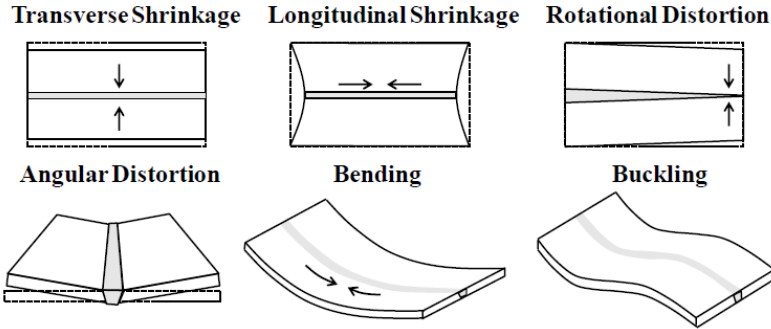


Figure 2.3 - Different types of welding distortion [4]

2.1.4. Influence parameters

There are three main factors that influence the magnitude of the deformations present in welded parts. These factors are related with the material, welding parameters and geometry of the plates.

2.1.4.1. Material

The fact that the material to be used already has internal stresses, changes the behaviour of the part during the welding process. In addition, the thermomechanical properties of the material have influence on the presence of deformations. The most important properties are those that change according to temperature, such as yield stress, thermal conductivity, specific heat, coefficient of expansion and Young modulus [5]. Table 1 shows the influence of the material parameters on the stresses and strains and their explanation.



Table 1 – Material parameters and their influence [5]

Parameter	Influence	Reason
↑ yield stress	↑ internal stresses and strains	-
↑ coefficient of expansion	↑ internal stresses and strains	-
↑ thermal conductivity	↓ internal stresses and strains	A high thermal conductivity ensures a higher heat distribution across the part, so the thermal gradients are smaller
↑ specific heat	↓ internal stresses and strains	The higher the specific heat, the more heat is transferred to the material, so the maximum temperature in the melt bath is lower
↑ Young modulus	↓ internal stresses and strains	-

In Figure 2.4, it is possible to see the behaviour of the thermomechanical properties of a general steel according to temperature. The density of the material and the expansion coefficient have little changes with temperature variation. However, the specific heat and thermal conductivity increase proportionally with temperature. The heat transfer coefficient, yield stress and Young modulus are the properties of materials that decrease with increasing temperature.

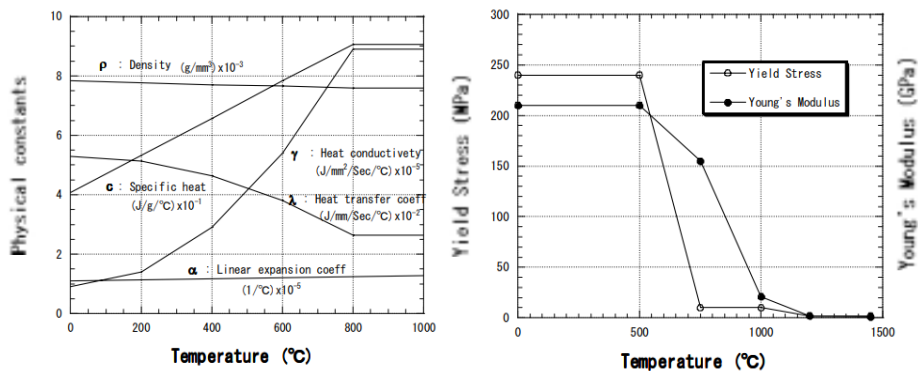


Figure 2.4 – Thermomechanical properties vs temperature [5]

#### 2.1.4.2. Process

The welding parameters are also an important factor since the amount of energy chosen and its sequence will have an influence on the type of deformations present in the weld part. A

greater amount of energy used to join the two metal sheets will automatically have more deformations [5]. To avoid this, it is common to have a preheating of the components to be welded to ensure less thermal variation and consequently less stress and strain. The width of the passes has a high influence on the deformation direction. According to Figure 2.5, narrow passes will have low longitudinal distortion but will cause high transverse distortion. The opposite happens with wide passes.

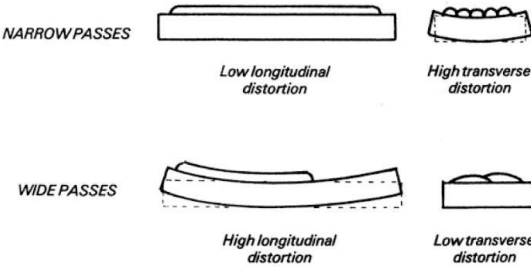


Figure 2.5 - Effect of pass width [5]

Welding speed is the parameter that most affects the rotational distortion also known as the scissor effect. If the welding speed is low (Figure 2.6-a) the plates tend to close. If the speed is high the plates will open as shown in Figure 2.6-b.

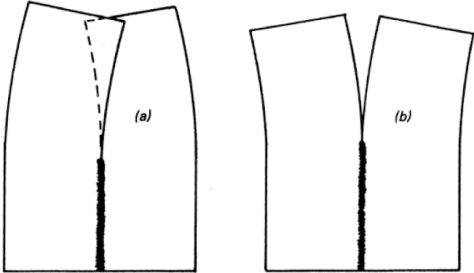


Figure 2.6 – Effect of welding speed [5]

**2.1.4.3. Geometry**

Finally, the geometry of the joint to be welded has an impact on the existing deformations. Different thicknesses and dimensions will behave differently since the overall stiffness of the assembly is different. The following Table 2 shows the influence of the geometry related parameters.

Table 2 – Geometry parameters and their influence [5]

Parameter	Influence
↑ higher stiffness	↑ internal stresses and ↓ strains
↑ clamping system	↑ internal stresses and ↓ strains
↑ weld bead	↑ strains
↓ plate thickness	↑ distortions

## 2.2. Section 2 - Laser Welding

---

This section is entirely dedicated to the welding process. Initially, a brief introduction to laser welding is made. After that the advantages, disadvantages and respective applications of this type of welding are presented. A presentation of the various types of lasers currently available is given. The laser equipment is described in this chapter. The two operating modes (keyhole vs. conduction) and the types of beam (continuous vs pulsed) are explained in detail. Since this type of welding uses large amounts of energy, defects and the areas affected by heat are mentioned. Finally, all the parameters that need to be defined in order to perform the welding are mentioned, as well as the standards that need to be met.

### 2.2.1. Introduction

Welding is the most common and widely used joining method in many manufacturing industries, such as automotive and aviation, because of its advantages [7]. It is the process of connecting material that is done by heating surfaces in order to reach a melting point. The materials to be joined can have the same composition or not (dissimilar materials). The solidification point is reached after the cooling down of the components. During welding it is common for the material to change its phase and deform due to the various internal stresses created by heat input. Microstructures changes are not visible but have impact on the joint and consequently the performance of the component. The concept of joining two materials goes back to the Bronze Age, when this technique was developed due to the need to mix

copper with tin to form bronze [8]. During the middle ages the steel art was developed and automatically many steel pieces were joined by archaic techniques.

#### **2.2.1.1. Laser history**

The laser appeared when engineers discovered that light had large amounts of power density. It is important to realize that light is an energy source in form of heat. It is absorbed and can be transmitted long distance without losing its features [9]. The acronym laser stands for “Light Amplification by Stimulated Emission of Radiation”. Laser beam is monochromatic, because it only has a colour associated to a specific wavelength. Unlike other lights that emit in various directions, laser has only one direction, i.e. it is highly directional light. The first steps of welding using a laser were taken by engineer Theodore Harold [3]. He invented a laser ruby at Hughes Research Laboratories (California, USA) in 1960. Two years later the first laser diode semiconductor was made by American scientists Robert N. Hall and Marshall Nathan from General Electric Research Center and Watson Research Center, respectively. Other stepping stones followed such as the invention of the first Nd:YAG laser by J. E. Geusic in 1964 and the production of the first CO<sub>2</sub> laser by C.K.N. Patel in Bell laboratories. In the year 2003, the first disk laser was tested.

#### **2.2.1.2. Types of welding process**

There are many types of welding processes according to their heat source application. Gas welding is when gases are used with the addition of oxygen to generate heat. The generated flame creates a melting zone that, after cooling, unites the components. Electric Resistance Welding (ERW) is when two materials are joined through the heat generated by the passage of an electric current. In this type of welding the components have to be under a certain pressure that can only be released after the electric current, that generated heat, passes to the material to form the joint. Solid State Welding (SSW) is another type of process characterized by joining materials together due to the pressure created between the components. The molten phase is not reached and no material is added. The most common processes are friction welding and cold welding. Thermit Welding (TW) is a process based on an exothermic reaction. The excess heat released by the reaction serves as heat source to fuse the two materials in a casting. Electron Beam Welding (EBW) is a process that uses an electron to generate large amounts of energy. The following Figure 2.7 shows some of the

existing welding types in more detail. Pressure welding occurs when an external force is applied, which, due to the plastic deformation caused in the material, is able to join the parts.

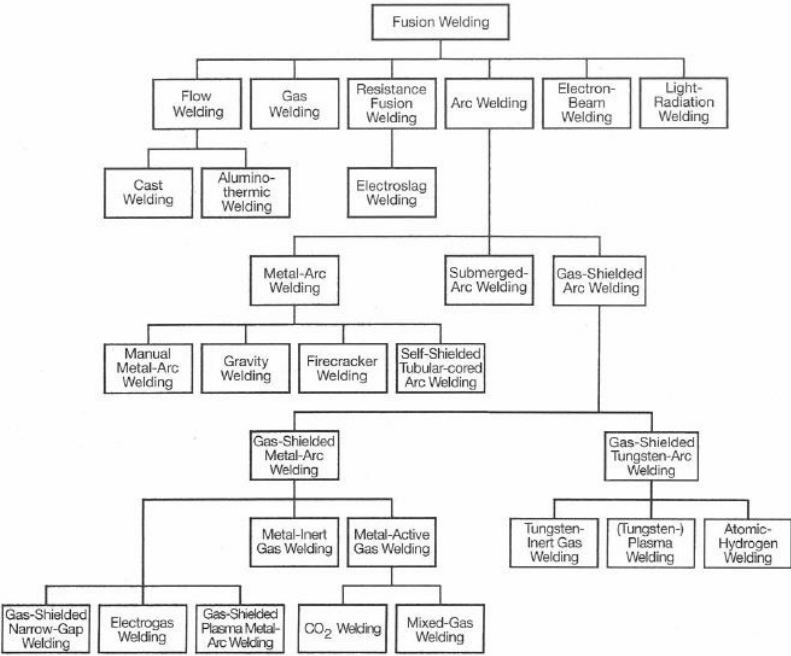


Figure 2.7 – Types of fusion welding [8]

This modern, technological and high-quality tool is increasing mainly because it has several benefits compared to conventional processes. One of the main advantages is the small heat affected zone (HAZ), a typical characteristic of this technology due to the capacity to concentrate a high amount of energy in a small area [10]. The investment required for laser welding is high. However, due to the high efficiency of this process, it is profitable. It is crucial to understand how laser technology works to control the parameters which will influence the weld. The impact of the parameters and how these are chosen has already been studied in several articles, which will be mentioned later. Incorrect values will strongly affect the final results and compromise quality. The laser beam is very powerful and so the material will reach high temperatures in a concentrated area in a short time. Understanding how the material properties change with temperature is a big challenge but it is fundamental to perform a reliable weld. An important advantage of laser technology is the ability to weld materials with different composition, normally very difficult to join with conventional processes.

### 2.2.1.3. Absorption Ratio

It is directly related to the wavelength of the laser beam and its intensity. It also depends on the temperature of the material since conductivity is a temperature-dependent property [1]. The following graph (Figure 2.8) shows the relationship between the degree of absorption and the wavelength of different metals. The units of the abscissa axis are in micrometres. Analysing the graph, it is possible to conclude that metals have a high degree of absorption in the visible (typical wavelengths from 380 to 740 nanometers) and UV (wavelength between 400 and 10 nanometers) spectrums.

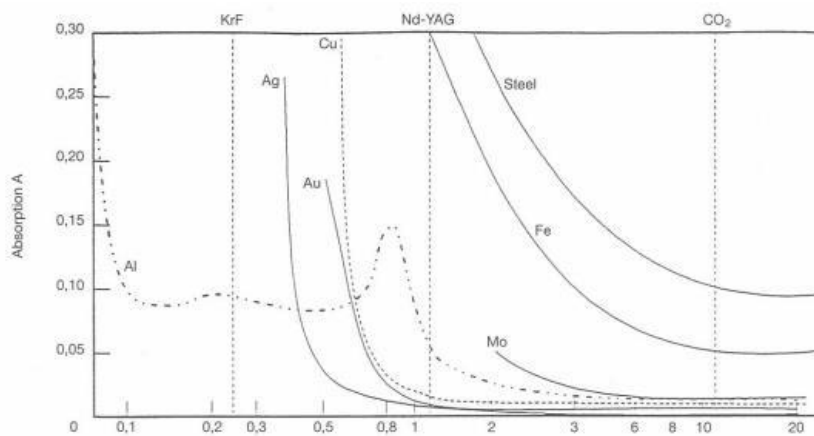


Figure 2.8 - Wavelength vs absorption ratio [8]

### 2.2.1.4. Weldability

The capacity of a material to be welded is known as weldability. If the material is joined with traditional welding techniques, such as Metal Inert Gas (MIG) and Tungsten Inert Gas (TIG), it can also be joined with the laser method. Nevertheless, some combinations of materials can lead to defects after the welding process such as brittle welds and/or shrinkage cracks [11]. In the practical guideline of Laser Welding it is possible to see tables that show the relationship between material standard and the laser weldability.

Laser welding is one of the most effective joining processes today due to the use of a high power and high energy density laser beam, compared to conventional processes such as arc or plasma. Consequently, the penetration of the weld is deeper and narrower, making laser welding an efficient technological process for welding metals with different compositions

and properties. When two different materials are joined, their compositions are different and because of that mechanical properties are dissimilar. Usually this type of welding presents problems, compromising the joint performance because of the different residual stress of the material. A varied diversity of different steel grades and dissimilar materials have been successfully welded together using laser welding technology [10]. In Table 3 it is possible to see some weldability combination between different metals.

Table 3 - Weldability of dissimilar metal combinations [12]

	W	Ta	Mo	Cr	Co	Ti	Be	Fe	Pt	Ni	Pd	Cu	Au	Ag	Mg	Al	Zn	Cd	Pb	Sn
W																				
Ta																				
Mo																				
Cr			P																	
Co		F	P	F	G															
Ti		F				F														
Be		P	P	P	P	F	P													
Fe		F	F	G				F	F											
Pt		G	F	G	G			F	P	G										
Ni		F	G	F	G			F	F	G										
Pd		F	G	G	G			F	F	G										
Cu		P	P	P	P	F	F	F	F											
Au		-	-	P	F	P	F	F	F											
Ag		P	P	P	P	P	F	P	P	F	P		F							
Mg		P	-	P	P	P	P	P	P	P	P	F	F	F	F					
Al		P	P	P	P	F	F	P	F	P	F	P	F	F	F					
Zn		P	-	P	P	F	P	P	F	P	F	F	G	F	G	P	F			
Cd		-	-	-	P	P	P	-	P	F	F	F	P	F	G		P	P		
Pb		P	-	P	P	P	-	P	P	P	P	P	P	P	P	P	P	P	P	
Sn		P	P	P	P	P	P	P	F	P	F	P	F	F	P	P	P	P	P	F

■	Excellent
G	Good
F	Fair
P	Poor

### 2.2.2. Advantages

There are several advantages that allow laser welding to gain popularity in the industry of metal joining. Below are the main characteristics of laser welding mentioned by many authors [13] [14] [15] [16] [17] [18] [19]. The laser process is a very flexible, reliable and fast method with high efficiency, easy to automate and monitor. The automated laser adjusts the welding parameters of all process according to the interactions and respective output of the sensors and controllers [11]. Another advantage of this equipment is the possibility to join dissimilar materials without adding filler material, ensuring the same quality compared with processes that add material. It is known as an autogenous weld because the filling procedure is ensured by melting the base material. By using laser, the workpiece has minimal or non-existent deformation/distortions after welding because the beam has high energy

density. However, it is in a concentrated area because of its small diameter. Furthermore, the equipment has a precise control capability, allowing small parts to be welded. Consequently, due to lower thermal expansion, the part will have a narrow HAZ and a small fusion zone (FZ). Additionally, if a comparison is made between the laser technique and other welding technologies, the profit will be higher in the first one because of its performance and lower cost (cost-effective solutions). It is also possible to increase productivity because with laser welding, the post rework will be reduced. The laser welding process is capable of welding parts up to 32 cm thick with a single pass [8]. Since there is no contact between the machine and the part, as in more traditional cases, there is less wear and tear on the equipment. To get a better idea of how this type of process is better than the others, the following Table 4 shows a summary of the most common welding processes nowadays with its advantages and disadvantages.

Table 4 - Overview of welding types [12]

	<b>Laser</b>	<b>Electron beam</b>	<b>TIG</b>	<b>Resistance</b>	<b>Ultrasonic</b>
Rate	↑	↑	↓	↑	↓
Low heat input	↑	↑	↓	↑	↑
Narrow HAZ	↑	↑	↓		↑
Weld bead appearance	↑	↑	↓		↑
Clamping	↑	↓	↓		
Equipment reliability	↑		↑	↑	
Deep penetration	↓	↑		↓	
Welding in air	↑	↓		↑	
Weld magnetic materials	↑	↓	↑	↑	↑
Weld reflective material	↓	↑	↑	↑	↑
Weld heat-sensitive material	↑	↑	↓	↓	↑
Joint access	↑			↓	↓
Environment, noise, fume	↑	↑	↓	↓	↓
Equipment costs	↓	↓	↑		
Operating costs					
↑ point of merit		↓ point of disadvantage			

The laser welding process has the best joining efficiency comparing with other welding methods. This means less energy is needed to do the same welding and consequently the area affected by the laser beam (HAZ) will be lower [20]. The following Table 5 compares the efficiencies for the different types of welding processes.



Table 5 - Relative joining efficiencies of different welding processes [12]

Process type	Joining efficiency $\frac{mm^2}{kJ}$
High-frequency resistance	65 - 100
Electron beam	20 - 30
laser	15 - 25
Submerged arc welding	4 - 10
Manual metal arc	2 - 3
Tungsten inert gas	0.8 - 2
Oxyacetylene flame	0.2 - 0.5

### 2.2.3. Disadvantages

As in all processes, laser welding also has its disadvantages [19] [21] [22]. During the welding the material reaches the boiling point due to a high amount of heat which also has some drawbacks. Any material that is subjected to thermal cycles (cooling and heating) generates residual stress and structural distortions. Consequently, the final product is going to be affected by structural defects, such as cracks, porosity or incomplete fusion. Presence of high magnitude residual stresses is going to compromise the final product quality and have direct consequences on tolerances. Residual stresses have a very large impact on material fatigue. Thin plates will always be more prone to high distortion and residual stress problems due to the existence of less material to dissipate the heat input. Depending on the thickness of the plate, sometimes it is necessary to make a previous preparation of the joint. Another disadvantage is the high cost of the equipment and the respective maintenance, even if it is easy to get the return due to the high productivity of the process. Although it is possible to weld a wide variety of materials, high reflective materials, like aluminium, copper, gold, will have more difficulty to absorb energy. For a good welding, the position and alignment of the parts to be welded is fundamental [8]. In laser welding, this aspect has even more relevance because the metal sheets must be placed in a position that allows the focal point of the laser beam to reach the parts. This turns out to be a disadvantage because sometimes it takes time to ensure that.

## 2.2.4. Applications

Significant progress has been made in product quality due to the use of laser welding. Main industries, such as automotive, aeronautical and ship building are the ones that most benefit from this technology advantages. They are increasingly replacing traditional welding techniques for this one. One of the greatest examples of the application of this technology is the automotive industry. Nowadays, environmental issues have a greater impact in our society. Car manufacturers are obliged to meet strict targets for emissions. Laser welding allows different materials to be joined, which is also one of the main challenges in vehicle manufacturing. Figure 2.9 shows where the technique is currently used in car body structure.

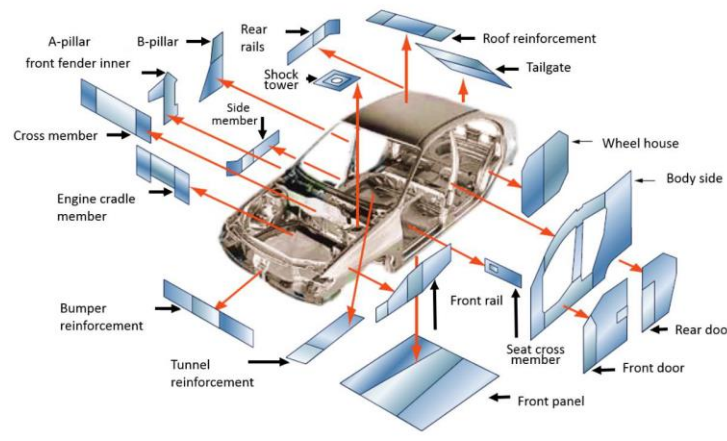


Figure 2.9 - Tailor welded blanks in car body [23]

Currently cars are made through the technique of tailored welded blank (TWB), which consists in producing car components from different material sheets. The number of assembly parts will be smaller and consequently the sealing operations will be lower, reducing the manufacturing costs. With this technique it is possible to reduce about 25% to 30% of total weight because the laser welding process does not add material [12]. Compared to a car that is made using a traditional metal joining technology (that adds material), this will need a less powerful engine because it is lighter. Consequently, it will have lower consumption and release less CO<sub>2</sub>. In Figure 2.10, it is possible to see the difference between conventional and tailored welded blank techniques. There are still other applications, but they are less common. Bastos et al. [24] developed an investigation where laser welding is used to repair and maintain cracks in the conventional welding process (TIG for example).

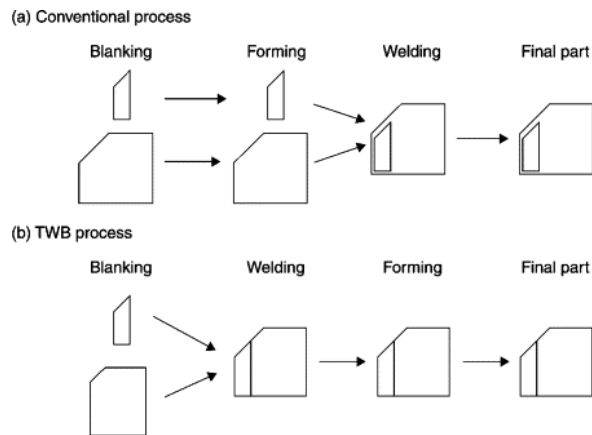


Figure 2.10 – Conventional process vs tailored welded blank technique [25]

## 2.2.5. Types (Solid, gaseous, semiconductor)

The right choice of laser depends on the application area, the materials to be welded and the characteristics of the work. There are many laser types available in the industry and it is crucial to select the correct category to use its full features. The main difference between lasers is the active medium they use and the wavelength of the source. The welding lasers can be divided into different types, such as: solid-state, liquid, gaseous and semiconductor [11] [26].

### 2.2.5.1. Solid-state

The active medium in solid state laser category is a solid crystalline material. Usually the most used crystal is the YAG (Yttrium Aluminium Garnet). It is possible to use others, like ruby or glass, but it is not very common nowadays. This type of laser has specific characteristics, such as low energetic return near 2% and the beam can be conducted through fiberglass cable [3]. This type of laser is more dangerous when using invisible radiation, since it can cause serious eyes damage. There are two main lasers, the Yb:YAG and the Nd:YAG, that use Ytterbium and Neodymium ions, respectively. The Nd:YAG is the most common used solid-state laser in industries due to its great heat absorption capacity with the metal, so a brief description of it will be made. It has good quality, high speed welding, high penetration and low distortions [19]. Nd:YAG is compatible with optical fibres and it is easy

to automate which is a key feature of today's manufacturing processes. Fernandes et al. [10] concluded that good quality welds were performed with an Nd:YAG pulsed laser in DP600 steel samples. After finding appropriate parameters, it was possible to obtain a well welded joint that demonstrated to be more resistant than the material itself. Pereira et al. [13] studied the welding capability of new third-generation GEN980T steel with Nd:YAG laser welding with different parameters and concluded that it performs a reliable weld. In the following Table 6 it is possible to see the different wavelengths and the respective active substances of the available solid-state lasers.

Table 6 – Solid-state laser overview [8]

Laser	Host Material	Active substances	Wavelength [ $\mu\text{m}$ ]
Ruby	Ruby	Chromium ions ( $Cr^{3+}$ )	0.694
Nd:glass	Glass	Neodymium ions ( $Nd^{3+}$ )	1.06
Nd:YAG	YAG	Neodymium ions ( $Nd^{3+}$ )	1.06

### 2.2.5.2. Gaseous

A Gaseous laser uses a mixture of gases as active medium, like He-Ne, carbon dioxide, excimer. This laser type has an energetic return near 10% [3]. This type of laser can only conduct the laser beam with mirrors. The laser efficiency is directly related to the chosen gas. The work principle is very simple: the light is produced through an electrical discharge that occurs inside the compartment where the gas is stored (active medium). The following Table 7 shows an overview of the different wavelengths of gaseous lasers.

Table 7 – Gas laser overview [8]

Spectrum radiation	Host Material	Wavelength [nm]
UV (ultraviolet)	ArF	193
	KrF	248
	XeCL	308
Visible	HeNe	632
	Ar (green)	514.5
	Ar (blue)	488
IR (infrared)	CO <sub>2</sub>	106000

### 2.2.5.3. Semiconductor

Fiber, disk and diode are some examples of semiconductor lasers. The energetic return is very high compared with others laser types (disk 25%, laser 30%, diode 40%). One of the

advantages of this type of laser is that the laser beam can be conducted using fiberglass cable. However, diode laser type has a smaller beam quality, but can perform a deep welding.

#### **2.2.5.4. Hybrid laser**

Hybrid welding came about to compensate for these disadvantages by combining two processes into one. The advantages of using electric arc welding is that it is very easy to operate and has extremely low costs, compared with laser welding. The disadvantages of one process are the advantages of the other process, and vice versa. With this welding technique it is possible to decrease energy costs and increased welding speed [27]. Some hybrid solutions exist to compensate and overcome the drawbacks of laser welding [19]. LHAW is a hybrid arc welding laser that combines laser and electric arc welding (like MIG/MAG). GMA is a gas metal arc which reduces the propensity for cracking, fragile phase formation and porosity. Multi-kilowatt CO<sub>2</sub> laser has the capability of producing deep penetration welds at high welding speeds.

#### **2.2.6. Equipment**

All welding equipment and system composition should meet some requirements in order to insure a good weld quality [11]. These specifications are mentioned in norms, such as “ISO/DIS 15609.4 - specification and quality of welding procedures for metallic materials”; ”ISO 11145 Optics and photonics – laser and laser-related equipment”; and others. The work principle of the laser is relatively simple, since it plays the role of an amplifier. The laser system is composed of the following items responsible for providing the right laser beam: energy source, active medium and resonant optical cavity. The energy source is a component where the power is generated [26]. The energy excites the electrons and consequently energizes the active medium. The active medium is where the electrons are stimulated by the power pump from the energy source. These components allow the amplification of the laser beam. Figure 2.11 shows a schematic of a Nd:YAG laser system.

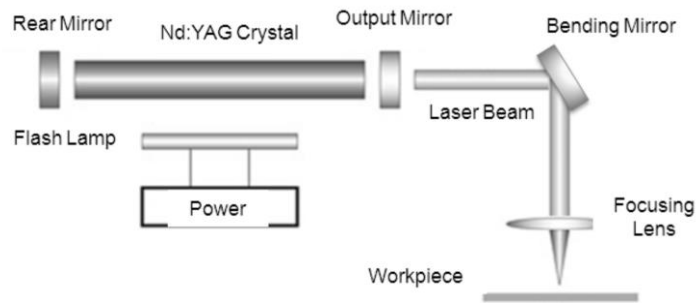


Figure 2.11 - Equipment of Nd:YAG solid-state laser [28]

There are four energy levels as you can see in Figure 2.12: the 1<sup>st</sup> level corresponds to the lower energy level (ground energy), the 2<sup>nd</sup> is the excited energy level [29]. Between the 3<sup>rd</sup> and the 4<sup>rd</sup> levels the electrons are released when they are at the highest energy level. The laser is transported in optical fibres and to change directions the system uses a bending mirror/lens [3]. The resonant optical cavity is composed of two reflector mirrors and it is where the photons oscillate due to the light stimulation process. The rear mirror is a high reflector mirror and is responsible for reflecting the entire energy. The output mirror is a semi-reflector, which means that it reflect less than 100% of the total radiation. Some percentage of the radiation is stored and the remainder radiation, which is not reflected by this mirror, is responsible for transmitting it, generating the laser beam.

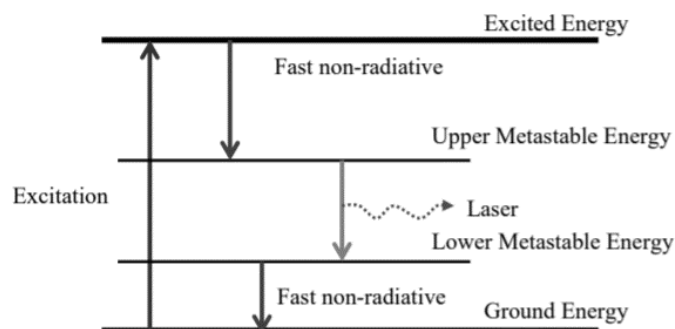


Figure 2.12 – Energy level diagram [29]

In the Mechanical Engineering Department of the University of Aveiro (DEM-UA) there is a laser welding machine [26]. This is an open mobile workstation SISMA-SWA300. This device allows welding on parts of various dimensions without limitations. The touch screen

showed in Figure 2.13 allows defining the parameters for executing the welding, such as the definition of the path along the various axes (X,Y,Z) as well as the on/off of the power source. This machine has already been used to perform numerous tests in the area of laser welding.

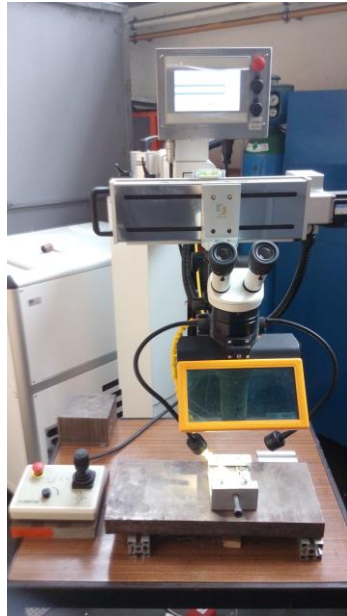


Figure 2.13 – Laser welding equipment of DEM-UA [26]

### 2.2.7. Beam operation mode (continuous vs pulsed)

The laser beam can work in continuous or pulsed wave [26] [12]. In continuous operation mode, the laser beam output is constant over time. On the other hand, pulsed welding, also known as peak mode (PM), is a great way to reduce the average temperature of the process because the beam varies in time, i.e. it is constantly switched on and off. This makes it possible to achieve high energy in a short period of time. There are many ways to apply the pulsed operation technique: pumping, mode-locking and switching. Pulsed pumping uses capacitors that store large quantities of energy that are linked to the excitation source [30]. Then, when needed, capacitors quickly release large amounts of energy into the environment. Although mode-locking uses ultra-short pulses from femtoseconds ( $10^{-15}$ ) to second in contrast with q-switching that uses short pulses between  $10^{-12} - 10^{-15}$  seconds,

it is very powerful. For a better understanding of the existing types of beam operation and its differences, Figure 2.14 shows a diagram of a continuous and pulsed form.

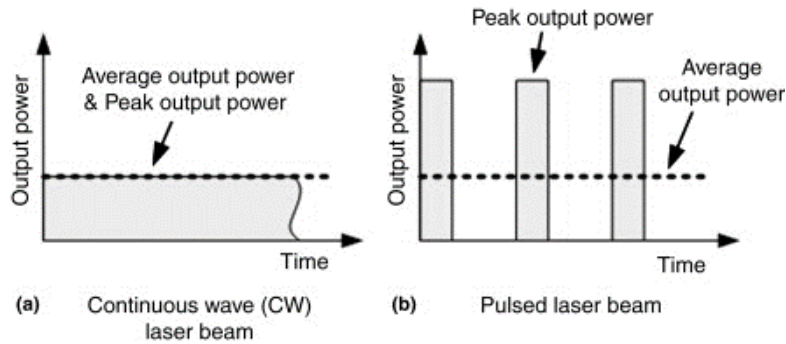


Figure 2.14 - Continuous and pulsed laser beam mode

### 2.2.8. Welding modes (Conduction vs Keyhole)

The power density in the workpiece is directly related with the amount of penetration with which the beam reaches the part. It can be divided into conduction and keyhole [19]. Both are capable of working with beam in pulsed or continuous wave mode.

In conduction mode, penetration is lower because high power densities are not reached [17]. Consequently, changes in the material state only occur in the welded area (solid-liquid-solid). This mode occurs when the welding speed is high. So the laser beam is only a short period of time in a certain surface area and the power distribution will be lower: between  $100 - 10^4$  W/mm<sup>2</sup>. It is normal to see a semi-circular weld, due to the absorption of the laser beam on the part [19]. However, conduction mode generates a weakly penetration weld beam [12] [17]. The energy released by the laser beam is deposited on the part surface.

Keyhole or deep penetration mode happens when the power distribution is dense, normally higher than  $10^4$  W/mm<sup>2</sup> [17]. The reason why this takes place is because the material is not able to transfer all that energy and, consequently, part of it is absorbed and a hole is formed in the section. This process is characterized by causing evaporation of the material due to the high temperatures during the heating cycle of material caused by high power intensities [19]. Once the material evaporates, i.e. disappears from the surface, the laser beam will



penetrate deeper and deeper into the workpiece, forming a keyhole in the melt pool. This hole is stabilized by the pressure from the vapour being produced [12]. Through the lateral view present in Figure 2.15 it is possible to see the difference between the two processes and its beam absorption.

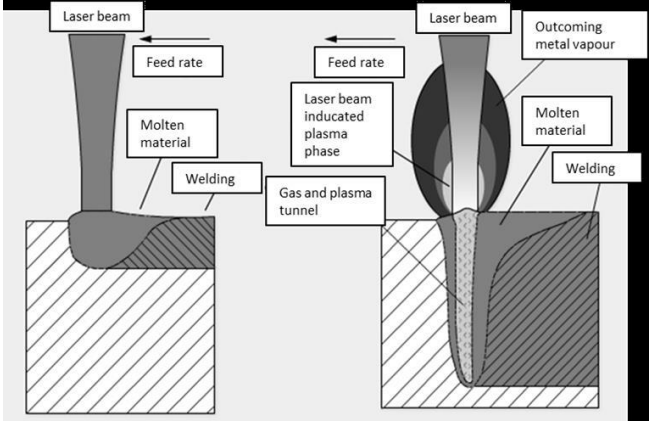


Figure 2.15 - Difference between conduction and keyhole processes [31]

### 2.2.9. Laser space distribution

The energy distribution along its diameter is not always constant and can change according to the active medium used [9]. Transverse Electromagnetic Mode (TEM), represents the laser beam energy profile in the plane perpendicular to the laser propagation direction [26]. As can be seen in Figure 2.16, the model type is designated by  $TEM_{xy}$  where the x and y indices represent the number of points in the horizontal and vertical directions, respectively.

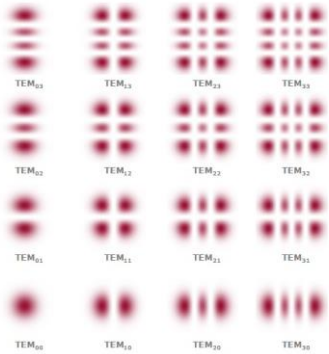


Figure 2.16 – Laser beam distribution [26]

With higher index values, it is more challenging to focus the beam to a fine spot to achieve a high power density [9]. Many combinations of transverse electromagnetic modes are available. Moreover, multi-mode laser is the equipment that has the capability to operate in different modes. Figure 2.17 shows three different examples of basic beam modes produced by different laser, where it is possible to see the projection and a 3D profile of the laser beam distribution.

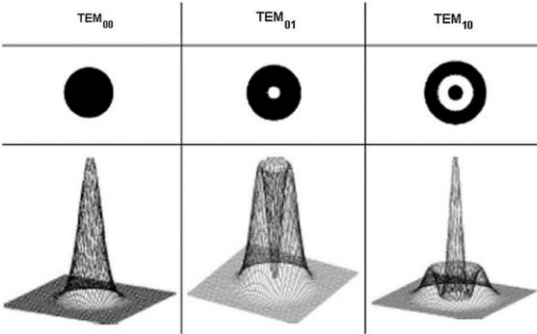


Figure 2.17 - Different profiles of TEM for laser [32]

2.2.10. Defects

Some internal and external defects may inevitably appear during or after the welding process. This happens mainly due to the thermal cycles, inherent heating and high cooling, to which the part is subjected, and consequently changes the material properties due to the phase transformation. Those imperfections compromise the final product result and unfortunately cannot always be prevented. Sometimes the part can be rejected by quality control, depending on the requirements, size tolerances and applications of the product, being an unnecessary waste of money and time. Laser welding has a great advantage, as it does not need to add material to do the weld. Consequently the change in volume during the process will be significantly smaller. The defects are also dependent on the material types and their combinations, the equipment and the welding parameters chosen [11]. Steels that contain a higher carbon level in their microstructure will be more sensitive to rapid cooling. The same occurs in material that does not compensate the rapid contraction of the workpiece due to strong heat laser intensity. Materials that vaporize quickly and have in their

composition alloy elements (which have melting points much lower than the principal material) will have more problems comparing with other steels. Some problems can be solved with pre-heating and post treatments like galvanization. However, one of the advantages of laser welding is that it is a fast process. By following these steps, the production time will be substantially higher, losing the advantage of using this process.

After welding, it is important that the weld bead has a uniform composition, in width and depth of penetration. Additionally, the evaluation of the metallurgical quality is fundamental since it evaluates the internal structure of the weld. External defects are those that are most easily visible and normally they are related to the joint. It is also important to take into account that imperfections on the weld bead shape can compromise the integrity of the welded part and sometimes are not visible.

Internal defects can be divided in four main groups: incomplete fusion, void, porosity and cracks. Incomplete fusion occurs due to poor laser beam radiation absorption and consequently there is no connection between the materials. It is very difficult to detect by visual inspection because it usually occurs in areas that are not totally seen and farthest away from the beam. To detect this type of imperfection it is necessary to use destructive tests, like the bending test. If a small load causes a break in the weld joint, it can be an indicator that an incomplete fusion occurred. The porosity is related with deficient gas vaporization during the process, causing voids, which are small air bubbles retained in the weld. This defect of gases release normally occurs with small welding speeds associated with a high heat input. These gases disappear because they evaporate and consequently leave porosity in the surface of the weld. It can be minimized adjusting the laser parameters to ensure less instability of the keyhole and consequently minimum fluid flow [19]. With a higher welding speed and a higher laser beam quality it is possible to reduce the number of pores per unit of weld length.

Cracking is one of the most typical defects in laser welded structures. It happens during the solidification process, when the material does not have freedom to contract during the cooling cycle [19]. There are several ways to reduce cracking such as using a high pulse rate, adding a filler or using preheat treatment [12]. There are two types of cracking present in a

weld: solidification cracking and liquation cracking. The first occurs during the weld metal solidification. Metals that have a high thermal expansion, large solidification range and big solidification shrinkage are conducive to have this type of cracks present in the fusion zone. The liquation cracking represents the cracks resulting from the solidification process of the liquated material. These cracks are mainly present in the melted zone as a result of a huge quantity of alloying addition.

In Figure 2.18 it is possible to see some of the typical intern defects of laser welding. The following numbers represent: 1 - pores, 2 - undercut, 3 - incomplete fusion, 4 – crater, 5 – cracking, 6 – weld spatter.

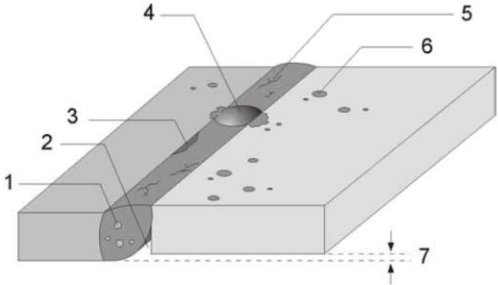


Figure 2.18 – Internal and external defects [26]

2.2.11. Heat Affected Zones

Laser welding has one of the most powerful density sources in the welding area, with a heat source intensity between  $10^{10} - 10^{12}$  W/m<sup>2</sup>. The laser beam focus is very precise with a small spot diameter, which creates a concentrated fusion zone profile. Due to the input of high energy and the absorption by the surface, material evaporation occurs and a hole is formed. In Figure 2.19, it is possible to see three different areas: the lighter area corresponds to the material which has not been affected by heat; the other areas are the HAZ and the darkest colour is the FZ.

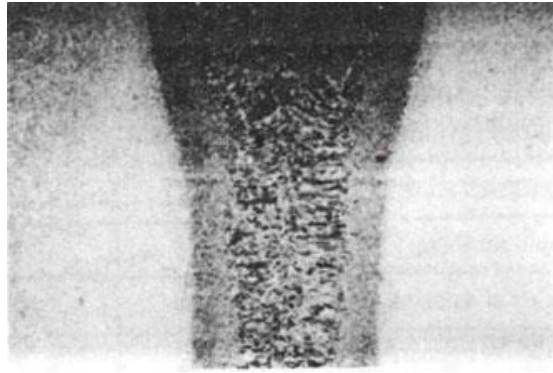


Figure 2.19 - Transverse section micrograph [12]

The base material corresponds to all the material that is not affected, thermally and mechanically, by the welding process. Due to the enormous amount of heat released by the laser beam, HAZ and FZ are the areas affected and whose properties changed during the process. HAZ is the part of the material that is between BM and FZ [11]. The inner zone of HAZ, near the FZ, is harder than the outer zone (soft zone) due to the martensite formation [19]. By doing a review on welding residual stress, the authors agree that it occurs at the HAZ, but the distribution is still confusing [2]. FZ is the only zone that was melted during the process. The formation of these zones is directly related to the welding process (cooling and heating cycles) and respective parameters (welding speed, energy input and heat source distributions) [33]. Other factors like material thickness, welding conditions, pre-treatments, joint length and geometry also affect the cooling rate and consequently have effects on the HAZ and FZ shapes [1]. The maximum residual stress are located at the HAZ of the parts [33]. A lower welding speed causes a higher presence of residual stresses. Analysing these affected zones is always important because they are sensitive areas since they have suffered many microstructural changes.

#### 2.2.12. Parameters

It is always necessary to choose and adjust the parameters in order to obtain quality and reliable welds according to the type of welding, the material and the respective thickness. It is crucial to understand how welding parameters affect the residual stress. In laser welding, the parameters are divided in four main categories related with the laser, machine, workpiece and material. Although they are divided, they interact among each other and sometimes are

strongly dependent. According to much theoretical research and engineering experience, the weld width largely depends on process parameters such as laser power, welding speed, laser focal position, gap width and shielding gas [34].

**2.2.12.1. Laser Parameters**

As mentioned above, the laser beam can work in pulsed or continuous mode. In addition, there are beam parameters that need to be set, such as pulse duration, shape, frequency and energy, spot size, power density, the overlapping of the pulse and others. The pulse duration corresponds to the time interval in which the pulse is acting on the part [11] [26] [35]. Large intervals mean that the part is subjected to the laser beam for a longer time and consequently will have a longer heating cycle, leading to a bigger melt area. Frequency is a parameter that is related to the laser pulse duration and its repetition. In others words, it represents the amount of laser pulses that reach the weld part in the first second. The maximum possible frequency depends on the selected power and pulse duration parameters. Pulse energy has to be adjusted according to the joint geometry and the material. This parameter is directly related to penetration, i.e. in the keyhole process the laser beam power has to be higher than the conduction process. The power should be as low as possible, since high amounts of energy will heat the plate quickly and consequently increase the development of defects. Pulse shape is the geometry of the laser pulse. It characterizes the way that power acts in a specific time interval. This can be constant or variable over time as shown in Figure 2.20.

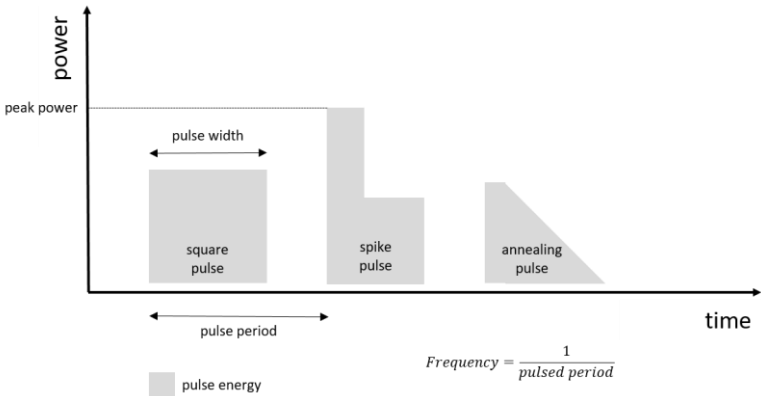


Figure 2.20 – Pulse [9]

Spot size corresponds to the area of the laser beam that acts on the part and it is different from the beam diameter. Laser beam diameter is constantly being changed along the optical path and is related with focal length, as it can be seen in Figure 2.21. Normally beam diameters increase with the amount of power generated by the laser [9]. The average power density across laser beam diameters is between 6 and 13 W/mm<sup>2</sup>.

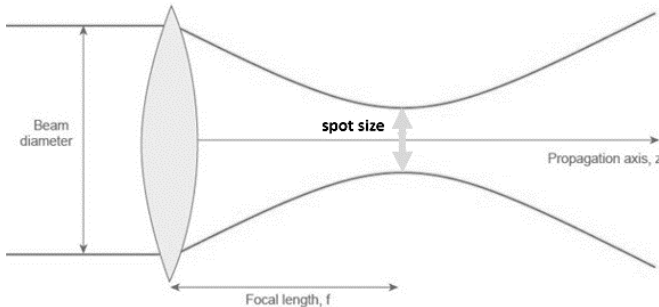


Figure 2.21 - Laser spot size [9]

Power density represents the power that reaches a certain area. To guarantee the connection of the components, it is crucial to ensure enough power to achieve the material melting points. There is a direct relation between the power chosen and the thickness of the part: large thicknesses need high amounts of energy. In pulsed welding, it is necessary to set an overlap, expressed as a percentage. It represents the overlapping area of the molten material by the current pulse over the previous pulse. In Figure 2.22 it is possible to see an example of different overlaps and conclude that there is a higher penetration of the laser beam when the percentage of overlap is higher. There are other parameters such as the beam quality, related with intensity distribution and divergence, polarization and the wavelength.

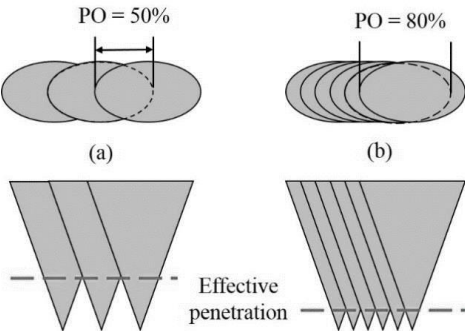


Figure 2.22 – Effective penetration for a 50% and 80% overlap [36]

### **2.2.12.2. Machine parameters**

The machine parameters are directly linked to the machine. The conductance type is related with how the laser beam is conducted during the generation process [11]. It can be through mirrors or fibre optics and depends on the laser category (solid state, semiconductor or gaseous). The focus parameter is associated with focal length, focal position, and depth of focus. The welding is performed at the point where the light beam has the highest energy intensity, which is the focal point. The gas type used as well as the flow (debit) and the supply method are parameters that need to be taken into consideration. Defining the correct welding speed is a very challenging procedure for the reason that they are dependent on several factors and will have direct consequences on the workpiece. High speed will cause porous and the risk of hardening will be high due to rapid weld cooling. Low speed is responsible for producing weld sagging. The higher the percentage of pulse overlap, the lower the welding speed. Other parameters such as the diameter and the distance to the workpiece of the gas nozzle need to be defined. The beam angle incidence of the laser beam also influences the weld.

### **2.2.12.3. Workpiece parameters**

Workpiece parameters depend exclusively on the weld part. The thickness of the material, the surface conditions and coating type are some considerations that have to be taken into account [11]. As a reference, high power and low welding speeds are used for parts with high thicknesses [8]. It should be noted that there are reflective surfaces which consequently make the laser welding process difficult to perform. In thick welds, especially in technologies that use material addition, a seam preparation is necessary, which is inevitably linked with width and shape. The thickness of the plate has a significant impact since it is related to the amount of energy it can absorb from the laser beam [12]. Because of this, new joint geometries have been discovered, facilitating the product manufacturing process. There are several possible types of joints such as butt joint, edge joint, tee joint and others. Each geometry has its advantages and inconveniences [13]. There are joints where access to both sides is restricted and will make the whole welding process difficult. The following figure helps to better understand the joints that are possible to weld nowadays. There are several possible geometries present in Figure 2.23.



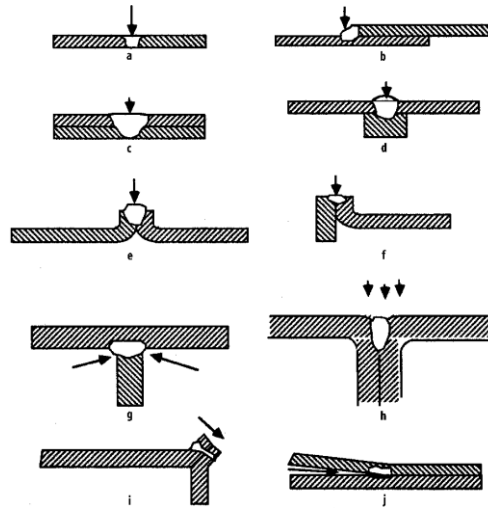


Figure 2.23 - Different welding joining arrangements [11]

The correlation between surface edge preparation and the absorption ratio of the laser beam has been explored by the author [37]. The theory said that the absorption has tendency to be higher in rough surfaces. If the material reaches the melting point, the absorption ratio will decrease to a constant value and then stabilize. However, some research proves that laser welding can be improved with other parameters like optimizing the laser beam or adapting the parameters of the heat input instead of paying attention to the surface preparation. The results of this study show that the effect of the roughness present on the surface is a critical factor during the entire welding process.

In some welding processes the plate edges need a surface preparation. The preparation of the joint helps to decrease the roughness of the edge surface [37]. The polished surface will increase the abortion ratio. The conclusion was that the joint edge should be prepared to achieve a surface roughness near to  $6.3 \mu\text{m}$ . The following Figure 2.24 shows the relationship between penetration and surface roughness of low alloyed steel S355, with plate thickness 20 mm and welding speed equal to 2 m/min.

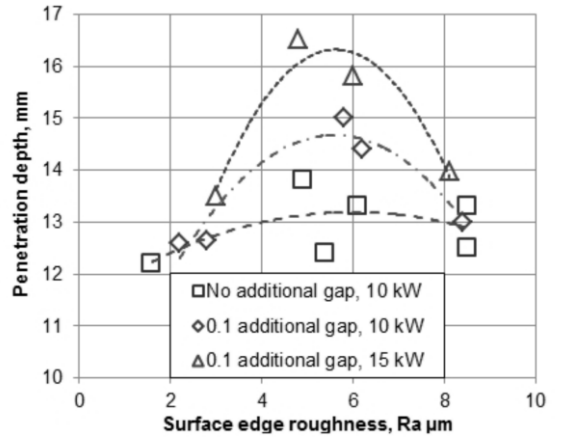


Figure 2.24 – Penetration depth at different roughness levels [37]

#### 2.2.12.4. Material parameters

Finally, it is necessary to determine the material parameters. These parameters are entirely related to the material's properties [11]. Sometimes a pre-treatment is necessary to increase the efficiency of the weld and to avoid the appearance of defects. Further on, in Section 4 dedicated exclusively to the material, all the parameters used in welding are described in detail.

#### 2.2.13. Influence of changing parameters

Knowing how the different parameters influence welding is crucial to make a quality weld. Tsung-Ping Hung et al. [38] simulated the effects of varying the laser parameters in AISI 1045 and AISI 4140 steels surfaces and they concluded that higher laser diameter will reduce the hardening area. Without changing other parameters, a higher focal point position increases the width of FZ and HAZ [3]. This parameter has a significant impact on welded joint defects when the laser beam has a high amount of energy with high speed. The author concluded that heat input has an influence on the residual stress distribution [2]. However, the impact of this influence is still being discussed. According to the author, the heat input strongly affects the value and distribution of residual stress. However, other author agree that heat input has just a little impact in the welding residual stress. The heat input increases with a combination of increased power and decreased welding speed [3]. The amount of heat released by the laser beam is directly related to the magnitude of the residual stresses,

although it is not a linear effect [2]. The high heat-input can lead to softening and a loss of strength in the areas near the HAZ [3]. This has a significant impact on the hardness inside FZ and HAZ. High power intensity is responsible for an extreme penetration and consequently a concavity on the top of the part due to deeper penetration, while low energy release will not make complete penetration. The author discovered that stress distribution can be manipulated by changing the weld sequence [2]. According to the author, the welding sequence has a significant impact on residual stress distribution near the welded zone. Another research was done to compare the effect of the welding sequence on residual stress [2]. The conclusion was that the welding sequence has less effect on residual stress. In Table 8 the author compared the effects of the welding sequence on residual stress based on the type of welding sequence and concluded that different types of welding sequences influence the residual stress distribution.

Table 8 – Residual stress distribution on types of welding sequence [2]

<b>Welding Sequence</b>	<b>Residual Stress Part</b>	<b>Tensile Residual Stress</b>	<b>Compressive Residual Stress</b>
Single-pass butt welded	Longitudinal	Near the weld	Far the weld
	Transverse	Middle of plate	End of the weld
Multi-pass butt welded	Longitudinal	Near the weld bead along the weld line	Far from the weld line
	Transverse	Upper surface of the plate	Bottom plate surface
Circular patch welds	Circumferential	Patches central region and HAZ	Far from the weld bead and HAZ
	Radial	Patches central region	-

Higher welding speed is going to reduce the top of FZ and HAZ areas. However, the increase of this parameter does not guarantee the decrease of surface imperfections because these are caused by the high power density released by the laser beam [3]. Last but not least, restraint and clamping have a significant influence in the final result such as the location and the time in which they are active [4]. The author studied whether there is an ideal time for the application of clamping systems. The study was done for stainless steel and indicates that the time to final weld distortion can be achieved in minutes, for two steel beams welded by four welds. The time to obtain 40% of the final distortion is about five minutes, and to achieve 80%, ten minutes are necessary.

### 2.2.14. Tolerances

Although laser welding does not add material, it is possible to have a gap between the two parts to be welded. The gap between the plates in butt joint assemblies should be slightly lower than half the beam diameter [12]. This is the only way to ensure that the laser beam does not pass straight through the joint. In case of large gaps, the laser beam is rotated but that is not advisable due to overheating of the weld. The following equations (Equation 1 and Equation 2) show the tolerated gap allowed for butt and lap joints, respectively. Where  $\beta$  is the coefficient of thermal expansion ( $^{\circ}\text{C}^{-1}$ ),  $\Delta T$  is the temperature change ( $^{\circ}\text{C}$ ),  $w$  is the weld width (m),  $t_p$  is the sheet thickness (m),  $g$  is the gap width (m) and  $A$  and  $B$  are constants. Table 9 shows an overview of allowed tolerances of different joint types. These values are important to keep in mind because tolerances in industrial production are critical to guarantee the welding quality [39].

$$g = A \cdot \beta \cdot \Delta T \cdot w \quad (1)$$

$$g = B \cdot \beta \cdot \Delta T \cdot 2 t_p \quad (2)$$

Table 9 - Overview of tolerances in welding process [39]

Weld construction	Maximum split [mm]	Maximum height discrepancy [mm]	Maximum position tolerance laser spot	
			Rectangular on the seam [mm]	Perpendicular on the seam [mm]
Butt Joint	0.1	0.2	$\pm 0.05$	$\pm 0.25$
Lap joint	0.1	-	Not critical	$\pm 0.25$
Corner joint (no filler material)	0.25	-	$\pm 0.05$	$\pm 0.25$
Flange joint	0.125	$\pm 0.5$	$\pm 0.15$	$\pm 0.25$
Edge joint	0.125	$\pm 0.25$	$\pm 0.1$	$\pm 0.25$
Corner joint ( $40^{\circ} < \alpha < 60^{\circ}$ )	0.25	-	$\pm 0.125$	-
Corner joint ( $60^{\circ} < \alpha < 80^{\circ}$ )	0.25	-	$\pm 0.15$	-
Outside corner joint	0.2	0.5	$\pm 0.05$	$\pm 0.25$

Figure 2.25 shows a weld of two plates with different gaps. It is known that larger gaps will create more weld irregularities. It is possible to conclude that with a minimum gap there are practically no defects. As the gap between plates increases, a concavity begins to appear at the top of the weld [8]. If the gap reaches the permitted limit, the weld is defective and it has no quality requirements.

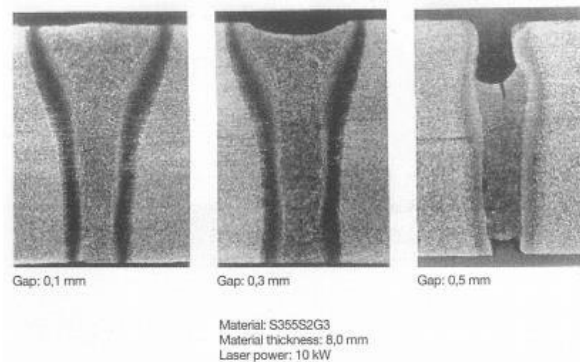


Figure 2.25 - Laser welding with different gaps between plates [8]

### 2.2.15. Heat transfer during the process

During the process, laser energy is lost by convection, conduction and radiation. The theory of heat flow was developed by Fourier. Describing and quantifying these effects into a heat transfer equation is crucial. A calculation of energy lost by radiation and convection during laser welding of titanium alloy was made by the Lemkeddem et al. [40] with FEM analysis. These losses, which have a significant influence on the welding areas, should be considered separately in a two dimensional model. They concluded that laser energy dissipates (heat loss) on surface by convection and radiation represents 7% of the energy balance. Other papers suggest using a single heat transfer equation, combining all heat lost into a single heat transfer coefficient. Figure 2.26 shows a diagram of the losses in the laser welding process. The heat is dissipated by the melting area by convection and radiation. Conduction also occurs between this area and the base material.

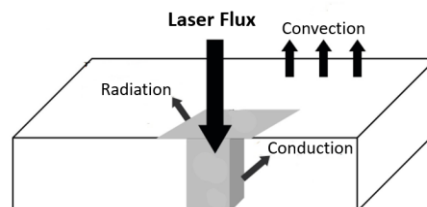


Figure 2.26 - Energy balance during laser welding Nd:YAG [3]

### 2.2.16. Standards

Finally, it is important to know that the welding process has standards and norms that must be met such as quality requirements (EN ISO 3834), operator qualification (EN 1418, ISO 14732) and procedure specification (WPS) [11]. ISO 25901 contains general terms and definitions valid to welding processes. During welding, an inspection is made to verify tolerances and measure the temperatures. After the welding some visual examination is performed. In complex structures with very strict requirements, the verification is done with the help of technology resources like radiography, ultrasonic, magnetic or penetration tools. The general weld quality, imperfections and weld bead need to be validated and are only accepted after passing a series of strict criteria. One of the most important factor in welding is the achieved quality of the welded zone. To accomplish this, standard quality parameters need to be ensured. Some non-destructive inspections such as visual, surface crack, metallurgical (micro + macro) and magnetic penetration should be executed to approve the weld. Other experimental exams can be done to certify the welding quality like toughness, bend tests, tensile strength, and hardness tests. The norm EN ISO 17662 stipulates requirements for verification, validation and calibration of equipment used in welding processes. Due to a high amount of energy release from the laser, it is necessary to take safety measures, according to the rules, to avoid accident. It is crucial that people that work with the machine, such as operators, maintenance staff, always use their personal protection and are not in contact with direct or reflected laser beam. The international manual instructions about safety in laser equipment is available on 2006/25/EG.

There are several risks associated with the welding process such as explosion, blindness, autistic damage, fire, electrocution, burns, among others. Laser security starts when the equipment is installed. This procedure meets severe requirements and it is crucial that calibration rigidly follows the company manufacture guidelines. Maintenance procedures according to the defined plane are also important to guarantee safety. There are standards for other safety issues such as fume sampling, filters and eye protection, protective clothing, welding curtains. Ensuring that the entire process meets environmental requirements is also a key factor in certification procedure and very important nowadays.

At global, European and national level there are some regulator authorities of the welding activity such as the International Institute of Welding (IIW), the European Federation for Welding, Joining and Cutting (EWF) and the Portuguese *Instituto de Soldadura e Qualidade* (ISQ).

## 2.3. Section 3 - Numerical Simulation

---

This section is entirely dedicated to numerical simulation. Initially an introduction to numerical simulation is made, explaining its history, the concept and its limitations. The three existing models (metallurgical, thermal and mechanical) are presented in detail. Two heat sources are presented, as well as their parameters and how the heat is distributed. The concept of the discretization of the mesh and the existing elements are addressed in the middle of the section. Finally, a small approach to existing software is made.

### 2.3.1. Introduction

Numerical analysis is very popular in engineering and is increasing in recent years in all areas because it can predict real phenomena quite accurately. The use of this technology tool avoids spending large amounts of money on experimental tests such as prototypes that involve large amounts of material. In addition, the software allows to change parameters, re-creating the model easily in an interactive way until the final result is optimal. The model may consider the environment that interacts with it. Depending on the context, normally the results are available very quickly compared to real tests, which is excellent because it saves engineers a lot of time, by focusing on the essential: the results with reasonable accuracy.

Initially, a distinction must be made between a numerical method and an analytical method. A numerical method presents an approximation to the solution of the problem. The analytical method gives exact results (accurate solutions). The FEM is a numerical method and is used to find estimated solutions to complex problems where a solution is not known. Every day engineers face real problems that are quite complex and need to find a solution. This method

can be applied to the most diverse areas such as electricity, fluids, material behaviour, thermal, and so on.

Commonly, numerical approaches are necessary for engineering problems. They are the only ones possible because analytical methods do not enable solutions to real complex problems that behave in a non-linear way. The principle behind the FEM is the discretization. It consists in dividing a component into several smaller parts so that a mathematical description can be obtained for each one.

Numerical simulation of welding to predict the material behaviour is a complex process. Due to the intense laser heat, the material goes through several transformations [41]. Nowadays it is possible to simulate the entire production process of the product using numerical analyses. FE analysis allows us to predict the quality and durability of welded structures or components and with few resources and quickly, improve the welding process by changing the laser parameters always targeting the changes. Currently, due to the technology growth, it is possible to perform a complete simulation such as laser light propagation until structures stresses and strains [17]. The study of the interaction between laser and material permits us to know the amount of heat input and the flux of heat transfer.

Knowing how it behaves due to an external stimulus like heat, can improve the product quality, save time and reduce cost. The application of the finite element method to realistic, often complex, engineering problems often requires the availability of significant computational means. The development of the simulation models has been in line with the development of calculation capacity of the available software.

Finite Element Analysis (FEA) is a very important and efficient procedure to understand, predict and give information about the material behaviour during the welding process. With this type of information, it is possible to know exactly the consequences of heating and cooling cycles during the process and information about residual deformation. It is possible to minimize the stresses and deformation in weldment. Furthermore, it is possible to reduce costs and decrease development time since it is not necessary to make prototypes [42].



Numerical simulation is relatively recent compared to other fields of engineering. This happens because powerful resources, such as computers with great processing capacity, are needed to run the simulations. The first research incorporating FEM was done by Courant [43]. The first work using analytic mathematical equations to predict residual stresses and strains was done by Rodger and Fletcher in 1938 [30] [22]. After approximately 30 years and with more evolved technology, in 1970, the first welding numerical model using the FEM were developed by Brust, Rybicky, Barber, and Masubuchi. The first application of welding simulations in industry was began near 1990 in USA, Japan and others European countries such as France and Germany [22].

#### **2.3.1.1. Obstacles and limitations**

Numerical simulation of welding process is always very complex due to non-linearity phenomena, depending on many parameters. Numerical welding simulation is “complex because it is a multiphase simulation with heating, melting, and solidification, with phase transition between solid and fluid states” [42]. The main obstacle in simulating the welding process is that the heat source is moving and consequently the displacements and stresses in the welded parts are not uniform [41]. There are also other parameters that make simulation so difficult, such as boundary conditions, thermal and mechanical properties, welding technique and its parameters and joints geometry. This process has high heating and cooling cycles due to its powerful laser beam. Dal and Fabbro [17] did an overview in welding simulation and the author concluded that the limit of welding simulation is the heat source definition. The changes in mechanical properties occur due to the strong incidence of heat in material (thermal changes) and the author advises further studies of heat transfers to validate the models.

#### **2.3.2. Models**

Simulate the welding process normally can have many objectives always with the aim of improving the quality of the joint. It can predict the influence of welding parameters on the shape of the weld pool helping to optimize the parameters [44]. It is also possible to study the consequences of the welding process and it can quantify the deformations and internal stresses created in the part. Since the objective of this work is related to the second task,

more emphasis will be given to this topic. It is crucial to understand that there are three main models available to perform the welding simulation with different purposes [45]. They are ordered from the most complex to the most simplified model: thermomechanical-metallurgical, thermomechanical and simplified mechanical. Figure 2.27 shows a schematic with the existing models. The metallurgic model is the only one that studies the phase transformation associated to the thermal cycles to which the material is subjected. The thermal model focuses on how energy is transferred through the heat source. Finally the mechanical model is the simplest one and studies the elastic and plastic behaviour of the material due to the incidence of large amounts of energy. Each model will be explained in more detail below.

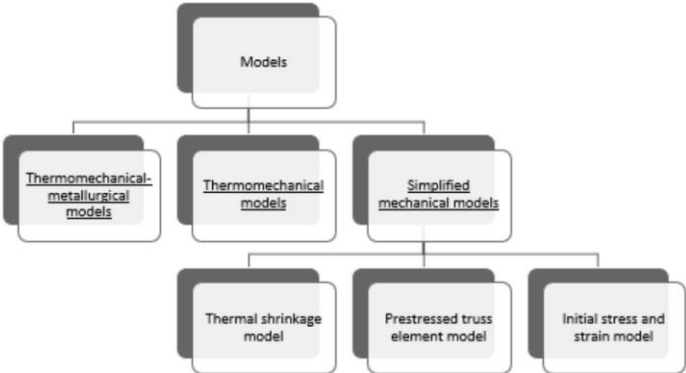


Figure 2.27 – Types of model in FEM for welding simulation [45]

It is important to recognize that to simulate the real behaviour of the material, it is necessary to combine the different types of models, because the microstructure of the material, the thermal behaviour and the mechanical behaviour are always directly related. Simulations that do not take these three into consideration will always be less accurate; however, they can give some important information quickly. The simulation precision, the amount of input parameters and the computation time of the analysis have to be considered and adapted according to the problem and the type of expected results.

To perform the simulation, it is necessary to have a multidisciplinary knowledge of different areas because microstructure, heat flow and deformations are directly connected [46]. The following Figure 2.28 shows in a simple way the existent relations. The interactions between

thermo-mechanical-metallurgical models are explained in Table 10. The microstructure is influenced by thermal expansion. If the phase changes, the volume of the material, the heat conductivity and the heat capacity will also change. Additionally, plastic and elastic material behaviour is strongly dependent on the microstructure of the material. Back at the beginning, the microstructure is going to transform if the thermal fields change and so on.

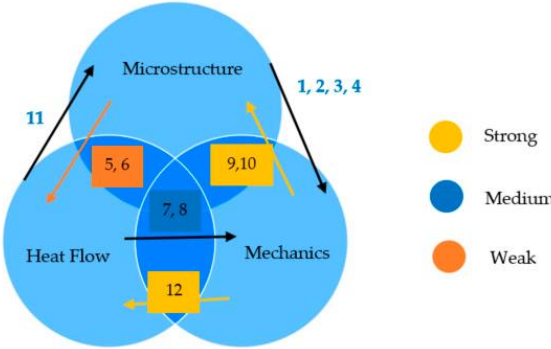


Figure 2.28 - Multidisciplinary relations in the welding simulation process [45]

Table 10 - Relations in welding simulation [45]

Interaction	Description
1	Thermal stresses due to microstructure changes
2	Elastic and plastic behaviour
3	Phase transformation origins volumetric changes
4	Microstructural changes are coupled with plastic stresses
5	Material’s microstructure can influence thermal properties
6	Phase transformation origins latent heat
7	Deformation evolution has influence on thermal boundary conditions
8	Plastic and elastic stresses can influence heat generation
9	Deformations are from microstructural evolution
10	Phase transformations are influenced by stress
11	Thermal cycles have a direct link on thermal cycles
12	Deformations are caused by temperature changes

**2.3.2.1. Metallurgical Model**

The metallurgical model is the most complex model since it takes into account all physical factors: mechanical, thermal and metallurgical [45]. Some examples of these factors are the elastoplastic material behaviour, viscosity behaviour in the molten zone and phase transformation in the weld seam. It is the only model that can predict phase transformation and the affected heat zone, such as FZ and the HAZ. This model only has interest for research

purposes because the results are very precise. The reason why this type of model is not very common in the industry is because the processing time for these models is extremely high, which sometimes makes it unrealistic. Moreover, expensive equipment with high processing capacity is needed.

To perform metallurgical models, detailed material data is required. Besides, it is crucial that all data is temperature dependent since laser welding has a very wide temperature range. Working with constant values would be an incorrect approach. Metallurgical analysis is normally used to improve the accuracy of the thermal and mechanical model [47]. To quantify the stresses and strains in a precise way, it is necessary to incorporate the phase transformations of the material in the model [33]. This model is the only one that allows predicting the areas affected by the heat generated. Kumar et al. [17] used the 3D Gaussian double ellipsoidal heat source and determined reasonable results of HAZ and FZ comparing numerical simulation with experimental tests. The following Figure 2.29 shows the comparison between numerical simulation (left side) and experimental test (right side) of heat affected zones of a metallurgical model.

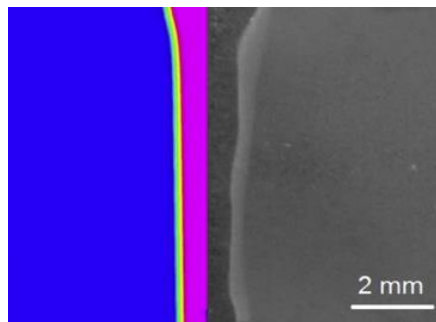


Figure 2.29 - HAZ and FZ comparison between numerical simulation and real tests [17]

### 2.3.2.2. Thermo-mechanical Model

The thermo-mechanical model performs a thermal and mechanical analysis in the same simulation, which means that results are directly related. There are two possibilities to make this simulation. “For simple welding simulations it is considered that the heat source distribution is constant and has a circular area” [3]. This method is not at all reliable and only serves to have a quantitative feedback of what happens. To simulate the process in a realistic way it is necessary to choose a heat source model responsible to determine the

precision of the thermal model. For a simulation close to reality the material properties should be temperature dependent [45]. It is the most used model because the applicability of this numerical model is in research and industry. It is efficient to predict correct distortion with a lower computing time than the previous model. Nonetheless, it is only possible to calculate the average level of stress. To obtain the mechanical changes of the material due to the welding process it is also necessary to simulate the thermal fields. Welding simulation is a complex problem so, in the thermomechanical model, the analysis is performed in two stages: the thermal analysis followed by mechanical simulation [46]. It is done in this sequence because while software is doing the mechanical analysis, it is necessary to update constantly the temperature history.

To execute the FEM analysis, it is necessary to define first the input parameters to have the 3D finite element model: mesh, material properties, boundary conditions and the equivalent heat source [48] [22] [45]. It is very difficult to calculate the stresses and strain deformations and the temperature distribution at the same time because they are directly connected. The temperature is assumed as the key aspect here, i.e., if some alterations in temperature occur, the stresses and strains of the part will be affected. However, variations on mechanical properties do not cause any change in the temperature field. Figure 2.30 shows a diagram of the analysis stages of the thermo-mechanical model [4]. Initially, the thermal properties of the material are defined. Then, the heat source used to perform the thermal analysis is chosen. The results will be the temperature fields during the welding process, which will serve as input for mechanical analysis. After defining the mechanical properties, which are dependent on the temperature, it is possible to obtain the stresses and strains.

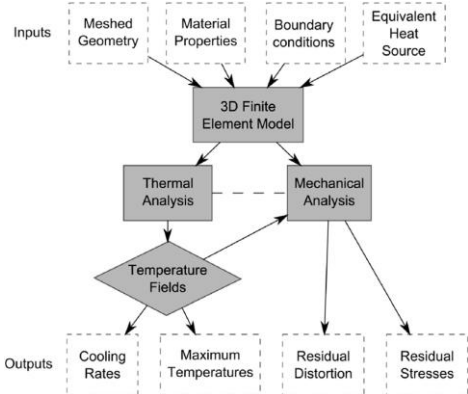


Figure 2.30 - Analysis stages [42]

The non-linear thermal simulation is performed to know exactly the temperature fields in the nodes, such as cooling rates and maximum temperatures. The data collected in the previous step is going to be one of the input data to execute the mechanical analysis to obtain residual distortion and residual stress fields. There are two possible approaches to non-linear thermal simulation: in the steady state the temperature remains constant; in the transient state, temperatures keep changing with time. The second option is better for the welding process since there is a high variation on the temperature gradient.

**2.3.2.3. Mechanical model**

The mechanical model is considered the simplest model in welding simulation because it gives a small amount of information and consequently needs low computation time to achieve the results [3] [45]. The quality of the results is pretty good but only to predict the correct distortion. This is the reason why it is used mainly in industry. It is a simplified mechanical model divided in three sub models: thermal shrinkage model, prestressed truss element model and initial stress and strain model. Analysing Table 11 it is possible to see the differences between the simplified mechanical models.

Table 11 – Differences between the simplified mechanical models [45]

<b>Model</b>	<b>Material Data</b>	<b>Variables</b>	<b>Applicability</b>
Thermal Shrinkage model	Material shrinkage at the model nodes of the welded volume	Welding sequence	<ul style="list-style-type: none"> <li>- Small computation effort</li> <li>- Low number of material parameters</li> <li>- Any general-purpose FE software can easily incorporate this kind of model</li> </ul>
Prestressed Truss element model	1D elements connecting the nodes of the weld line	Longitudinal shrinkage mechanism	<ul style="list-style-type: none"> <li>- Mesh quality and element type is not important</li> <li>- Calculation is done in very short time</li> <li>- Low number of material parameters</li> </ul>
Initial stress and strain model	The stresses and strains in each element of weld	Distortion, plastic deformation and the existing stress state	<ul style="list-style-type: none"> <li>- Can be applied for 3D or shell meshes</li> <li>- Requires low number of material and is very fast to run</li> <li>- The distortion can be minimized by changing the work conditions (e.g. welding sequence)</li> </ul>

### 2.3.3. Heat Source

In this topic, a detailed description of each heat source and its parameters will be made. The heat source is a high power density font that moves along the welding trajectory. The heat source model describes, according to the mathematical equations, the way the heat reaches the material and the correspondent weld pool. One of the reasons why it is mandatory to compare the numerical results with real tests values is because it is necessary to adjust the heat source parameters. Performing a dynamic and appropriate calibration and modifying geometric shape creates a more efficient and accurate model. If the calibration is neglected, it will not be possible to recreate the temperature distribution fields that affect the welded part and consequently the determination of the stresses and strains caused by the heat input will be very different from reality. Describing how energy is supplied to ensure the weld is probably the most important factor in numerical analysis model [45]. The heat source model and its shape should always be adapted to the problem in question [49]. Different welding processes or even different joints arrangements have different models and geometries.

It is important to remember that the first person who started studying moving heat source modelling was Rosenthal in 1935 [50]. However, he assumed, to simplify the problem, that the heat source was represented by a point. According to the literature [49] [3] [17] there are two main heat sources: the double ellipsoidal model proposed by Goldak (1984), which is typically used for arc welding process, and the conical model studied by Gauss and normally applied in numerical simulation of laser welding or electron beam.

#### **2.3.3.1. Heat sources generations**

According to the author [3], the heat sources are divided into 5 generations. They are divided by the degree of difficulty of implementation and their accuracy. The 1<sup>st</sup> generation does not predict heat flux because the distribution of heat is represented by a point. Consequently it is impossible to calculate the weld pool. The 2<sup>nd</sup> generation considered the heat flux distribution outside the melted zone. The physical parameters of the melts are not considered. The models of the generations previously mentioned (1<sup>st</sup> and 2<sup>nd</sup>) only need the power density distribution, flux or temperature data to perform the analysis. The prediction of the liquid and gas interface started to be modelled on the 3<sup>rd</sup> generation. These results allow the prediction of the shape of the weld pool. It was possible to start calculating the heat flow

from the laser beam in its fullness. However, high processing capacity is needed to simulate the mentioned models because of the amount of data, such as pressure distribution from the arc, mass flow rate into the weld pool and surface tension on liquid surface of the pool. The Navier Stokes equations are differential equations that allow the determination of a set of parameters, such as velocity, pressure, temperature, and density, describing the flow of fluids (liquid and gaseous). The 4<sup>th</sup> generation introduces this fluid dynamic equation on the heat source model. The last generation, the 5<sup>th</sup> one, is the first that considers the magneto-hydrodynamics equation. The last two generations are not common in laser welding simulation.

**2.3.3.2. Double-ellipsoidal Heat Source**

This heat source was suggested by J. Goldak et al. [17]. The heat is distributed in both directions from front and rear part of the ellipse. This model simulates the heat drag and that is the reason why the front of the heat source is larger than the back. [41] The Goldak model consists in two ellipsoids placed in two perpendicular planes as showed in the following Figure 2.31.

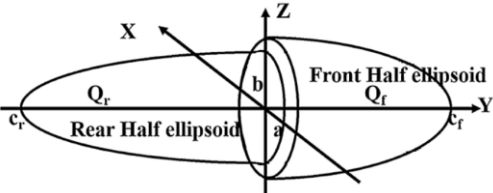


Figure 2.31 - Double ellipsoidal heat source shape [17]

Currently, this heat source model is very popular in finite element analyses because it is a very useful tool when the process is carried out using melt in welding. In addition, it covers many types of welding processes and is mainly used for gas metal arc (GMA) welding. The next mathematical equations show the heat transferred from heat source. The following equations (Equation 2 and Equation 3) represent the heat transferred from the front and rear of the heat source model. “Where  $Q_f$  and  $Q_r$  are volumetric heat flux density in front and rear part of the model;  $Q$  is total power source;  $a, b, c_f$  and  $c_r$  are width, depth and length of the front and the rear part of the molten pool;  $f_f$  and  $f_r$  are constants which influence energy flow



intensity into the material ( $f_f + f_r = 2$ );  $k, l, m$  are coefficients enabling modification of the liquid metal pool shape” [17].

$$Q_f(x, y, z) = \frac{6\sqrt{3} f_f Q}{a b c_f \pi \sqrt{\pi}} \exp\left(\frac{-k x^2}{a^2}\right) \exp\left(\frac{-l y^2}{b^2}\right) \exp\left(\frac{-m z^2}{c^2}\right) \left[\frac{W}{m^3}\right] \quad (3)$$

$$Q_r(x, y, z) = \frac{6\sqrt{3} f_r Q}{a b c_r \pi \sqrt{\pi}} \exp\left(\frac{-k x^2}{a^2}\right) \exp\left(\frac{-l y^2}{b^2}\right) \exp\left(\frac{-m z^2}{c^2}\right) \left[\frac{W}{m^3}\right] \quad (4)$$

### 2.3.3.3. Conical Heat Source

This model is widely used in laser welding simulation because its conical shape reflects a good reproduction of the welding processes whose heat source releases a high amount of energy [41]. In other words, with this model, it is possible to simulate a concentrated heat source, such as the laser, which has a deep FZ [3]. Dean Deng [33] did FEM prediction of welding residual stress and distortion in carbon steel considering phase transformation effects and concluded that the temperature in the centre of the fusion zone using Gaussian distribution conical heat source was different from the reality. The temperature field and the shape of weld pool are strongly affected by the solidification of the material and the effect of the fluid flow. This heat source model is the one that adapts to the laser welding process using Nd:YAG [3]. It has a good representation of the high intensity of energy released through a laser beam with a small diameter. To describe the geometry of this heat source there are 3 parameters that need to be defined: radius of top, radius of bottom and depth. The shape and parameters of the conical heat source are present in the Figure 2.32. The values for defining the shape of the heat source vary greatly with the type of joint and the thickness of the plate. The author [3] used the dimensions present in the Table 12 to perform an overlap welding of two metal plates.

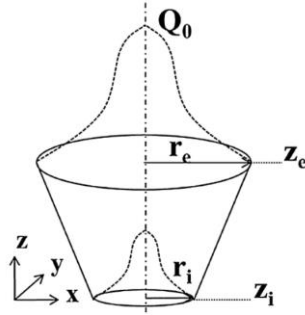


Figure 2.32 - Conical heat source shape [17]

Table 12 – Parameters of heat source model [3]

Symbol	Dimension	Value [mm]
$r_e$	Radius of top	0.65
$r_i$	Radius of bottom	0.50
$r_c$	Radius at the height of z	3.4
$z_e$	Z position of top	1.25
$z_i$	Z position of bottom	-1.26

Conical heat source flow density into the material in dependence of coordinate's data can be described by the follow Equation 5. The  $Q_0$  corresponds to the maximum value of the volumetric heat flux density and the  $x, y, z$  are the coordinates of the heat source point. The radius change in the direction of the depth is defined in Equation 6. Where  $r_i - r_e$  is the difference between the upper and lower conical radius dimension and the  $z_i - z_e$  represents the conical heat source length.

$$Q(x, y, z) = Q_0 \exp\left(-\frac{x^2 + y^2}{r_0^2(z)}\right) \left[\frac{W}{m^3}\right] \quad (5)$$

$$r_0(z) = r_e + \frac{r_i - r_e}{z_i - z_e} (z - z_e) \quad (6)$$

The conduction of the 3D conical heat source with Gaussian distribution is based on Fourier's Law and is governed by the Equation 7. Where  $c(T)$  characterizes the temperature dependent specific heat capacity and the  $k(T)$  is the temperature dependent thermal conductivity. The space coordinates are  $x, y, z$ ,  $T$  is the temperature,  $\rho$  the density and  $t$  the time period.

$$\rho c(T) \frac{\partial T}{\partial t} = \frac{\partial}{\partial x} \left( k(T) \frac{\partial T}{\partial x} \right) + \frac{\partial}{\partial y} \left( k(T) \frac{\partial T}{\partial y} \right) + \frac{\partial}{\partial z} \left( k(T) \frac{\partial T}{\partial z} \right) + q_v \quad (7)$$

### 2.3.4. Model discretization

#### 2.3.4.1. Mesh

Understanding how the model is discretized is fundamental to know the process. The mesh represents the discretization of the model into finite elements. In other words, it divides the large body into several small elements so that it is possible to study its behaviour. Choosing the mesh is always an iterative process since the model has to be constantly calibrated, through experimental analysis, until it represents the actual behaviour of the material. In the thermo-mechanical model, normally the thermal simulation is performed using a fine mesh to calculate the detailed temperature along the part [44]. Mechanical analysis typically used a coarser mesh. However, sometimes it is not possible and the meshes refinement needs to be the same. The type of element has significant impact on the quality of the simulation. It must be taken into account that although the more refined meshes have more detailed results, they have a longer processing time. Making a compromise between these two factors and having an extensive knowledge of the process are the keys to the analysis success.

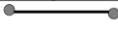


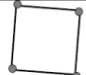


It is essential to study the convergence of the model mesh. This is an iterative procedure that aims to make results independent of the element size. Making an extremely refined mesh can solve this issue; however, it will result on a high computational time. According to the Sysweld software manual, the mesh is not part of the model calibration, which is exclusive to the welding parameters and material properties [8]. There are some general rules that can simplify the process of discretization of the model. To ensure a good compromise between the quality of the results and the mesh density, the element size should be equal to a third or a quarter of the width of the melt pool [44].

#### 2.3.4.2. Elements

There are several types of finite elements, from one-dimensional, to bidirectional and axisymmetric. These models are used when the problem can be analysed from the point of view of a 1D or 2D formulation. Three-dimensional finite elements, such as tetrahedron and hexahedron (first and second order), are the most common in the analysis of engineering

problems [51]. When conditions are imposed, such as a mechanical or thermal load, on the three principal directions it is necessary to use 3D finite elements. Table 13 shows the different FEM elements that exist in 1D, 2D and 3D.

Table 13 – Types of finite elements [52]

Finite element name	Type	Geometric Representation
One-dimensional finite element	Straight lines nodal	
	Curved lines nodal	
Two-dimensional finite element	triangular	
	quadrilateral	
Tridimensional finite element	hexahedron	
	Tetrahedron	

Tetrahedral elements offer advantages in the construction of the complex geometries mesh because of their shape, which makes it easier to do the discretization of the model and the fact that they only have one integration point [51]. As a consequence, when engineers choose to use tetrahedral elements, it is necessary to use more refined meshes. When obtaining reliable results is the main focus of the problem, the choice of hexahedral elements is made.

### 2.3.5. Boundary conditions

The defined mechanical and thermal boundary conditions have a significant impact on the simulations results. The relationship between the degree of freedom and the level of distortion as well as the effect on residual stresses affects the numerical simulation [4]. The time when the clamping conditions are active during and after the welding process has an influence on the final results [49]. The Figure 2.33 shows a graph with the relationship between the degrees of clamping versus the stress/distortion that occurs in the component.

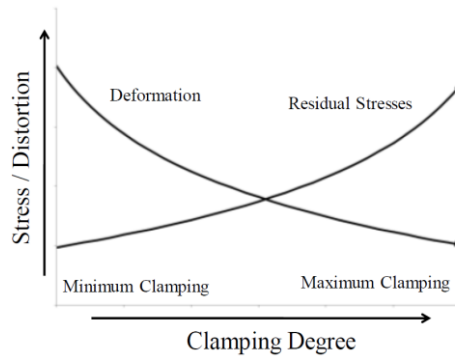


Figure 2.33 – Clamping vs stress [4]

### 2.3.6. Software

The world of numerical simulation is vast. As mentioned above, there are several numerical simulation models that can be used in welding simulation. The mechanical, thermal and metallurgical models are different, requiring different input parameters. Consequently, the approach for each one of them will be different. It is also necessary to understand to what purpose we want the results of the simulation. Complex solutions compromise the performance of numerical simulation because it will be time consuming [41]. The software available to perform the welding simulation are many, such as Abaqus, Ansys, Sysweld, Simufact welding, Sorpas and Geonx. The author performs a software comparison between Ansys, Abaqus e Sysweld [53].

Simufact is a relatively recent software, compared to Abaqus, [53] that has several applications, such as additive manufacturing and forming simulation. For the specific case of welding processes (thermal joining) there is Simufact Welding. It is composed of several modules: arc welding, laser beam, pressure welding, resistance spot welding, mechanical joining, brazing, electron beam and stress relief. A butt-welded plate was studied numerically and the results show that Ansys obtains the equivalent values to the Sysweld software [45].

Sysweld is the only presented software that was exclusively developed for welding analysis. The author compared this software to Abaqus, in an equivalent way, and concluded that Sysweld needs a large number of material parameters and has a much longer processing time

than Abaqus, due to the meshes and the necessity to process a lot of information [45]. Despite these disadvantages, the final results were equivalent.

Abaqus is one of the best known FEM codes. This software has already proven itself in the most diverse areas of FE analysis, but for the specific case of welding, it requires a rather complex process. To simulate welding, this software has a specific plug-in, the Abaqus Welding Interface (AWI), to generate the heat source. However, this plug-in is focused on welds where there is addition of material, which is not the case with laser welding. To simulate the moving heat source in laser welding it is necessary to use complex subroutines, which are made in Fortran. This programming language is exclusive for numeric computation. The developed and very popular subroutine for laser welding is DFLUX. W. Piekarska et al. [21] studied the “Application of Abaqus the temperature field in elements heated by moving heat sources”. The research that did the numerical analysis of thermal phenomena occurring during the process of laser welding concluded that knowledge of the temperature distribution along the material and the weld plate is crucial to optimize the laser welding process. The DFLUX subroutine of Abaqus makes it possible to analyse the temperature field with movable heat source. Therefore it is possible to determine numerically the kinetics of phase transformation in the solid state. This information allows us to estimate the composition of structure affected by the heating caused by the laser beam.

#### **2.3.6.1. Analysis error**

There is always an error in analysis relatively to the experimental values associated with the model. Bastos et al. [45] concluded that simulation analyses have an error percentage between 0% and 5% and it is possible to obtain deviations from 11% to 20% in a smaller number. According to the error percentages, the results can be considered accurate when comparing simulations with experimental tests. Table 14 shows the error percentage of 37 papers in which a comparison between experimental and FE analysis is made.

Table 14 – Error percentage of numerical simulation [45]

<b>Error</b>	<b>Papers</b>
0 – 5%	21.05%
6 – 10%	10.52%
11 – 15%	2.6%
16 -20%	7.9%

## 2.4. Section 4 - Material

---

In this section an introduction to the steel world is made, moving on to a more detailed description of what is AHSS. After that a brief description of DP 600 is made, where the main advantages and applications of this widely used steel are presented. The properties of DP600 are temperature-dependent, since the welding process has a large temperature variation. The chemical composition and microstructure of the material are presented below.

### 2.4.1. AHSS

Figure 2.34 shows several steels classified according to their category. The light grey are the mild steel, and the dark grey are the conventional high-strength steel (HSS) [54]. The various shades of blue represent the three generations of AHSS. Mild steel is easily deformable due to its microstructure composed exclusively of ferrite, with a maximum tensile strength of 280 MPa. High-strength steel has higher strengths compared to the mild steel, with a tensile strength in the range of 300 MPa. However, these steels have lost popularity to AHSS. They have much more attractive properties for vehicle manufacturers, such as reducing vehicle weight and ensuring greater safety. An overview of the mechanical properties of the more common AHSS can be seen in Table 15.

Table 15 - Mechanical properties of AHSS [3]

Class	Elastic Limit [MPa]	Ultimate shear strength [MPa]	Total Elongation [%]
HSLA 350/450	350	450	23 - 27
DP 300/500	300	500	30 - 34
DP350/600	350	600	24 - 30
TRIP 450/800	450	800	26 - 32
DP 500/800	500	800	12 - 20
CP 700/100	700	1000	12 - 15
DP 700/1000	700	1000	12 - 17
MS 1250/1520	1250	1520	4 - 6

It is important to understand the three different generations of AHSS. The first generation reached higher strength levels and has reduced formability [55]. The 2<sup>nd</sup> generation has excellent mechanical properties and good formability combined with high strength; however, the cost is high due to its composition. The last generation of AHSS, the 3<sup>rd</sup> one, is a class of steel focused on the improvement of formability compared to the 1<sup>st</sup> generation AHSS, without the disadvantages of the 2<sup>nd</sup> generation. It has mechanical properties between the 1<sup>st</sup> and 2<sup>nd</sup> generations, with multiphase microstructure with substantial amount of retained austenite [13].

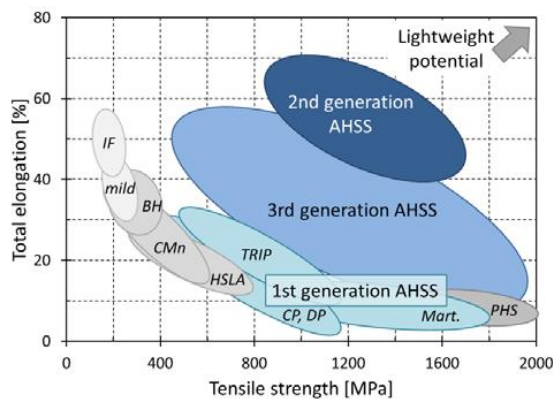


Figure 2.34 - Summary of three generations of AHSS [56]

#### 2.4.2. DP600

To produce car components, one of the most used AHSS steel in the industry is DP600. It is part of the new generation of high-strength steels that is revolutionizing the automotive industry due to its enormous advantages [13]. It provides a high durability and reduces the



weight of the components while retaining the structural stiffness. Dual-phase has a high performance of energy absorption and the use of this steel is growing because of environmental concerns. This type of steel is composed of two phases [10]. In its microstructure, it has approximately 15% of hard martensite in the form of islands distributed by a soft ferrite matrix. The microstructure of this steel will be explained in detail later on. The number present in the name designation represents the steel series, in this case it means that it has a tensile strength over 600 MPa. Therefore a distribution of hard martensite islands in a soft ferritic matrix and plus bainite to reduce the edge-cracking sensitivity [56]. In this way, dual phase steel achieves its strength. The following Figure 2.35 shows which types of steels are present in the car body structure.

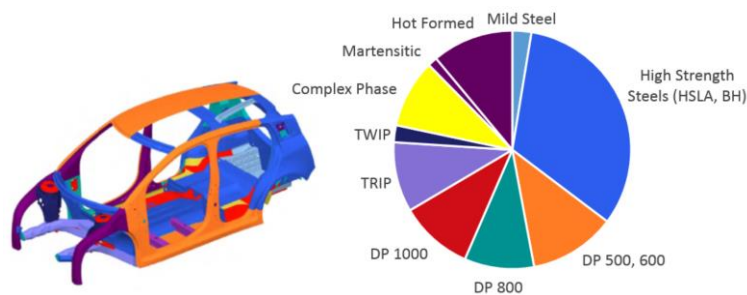


Figure 2.35 – Car body structure

### 2.4.3. Advantages and applications

Dual-phase steel has advantages of high strength, excellent ductility and low yield ratio. This material has good properties (strength with low weight) that allow the manufacture of components with less material quantity, reducing the thickness and therefore it is possible to produce lighter vehicles [13]. This will have an impact on vehicle performance through reduced fuel consumption and lower greenhouse gas emissions.

The EU imposes limits to reduce CO<sub>2</sub> emissions and the car industry has high interest in using this type of steel. By adopting this measure the automotive industry is able to reduce the weight of vehicles without compromising the structure of the car. In addition, this material offers better properties because it has a good relationship between vehicle safety and lightweight [13].

#### 2.4.4. Properties

This topic is an overview of the main properties of DP 600 steel. There are several properties related to the material, such as: mechanical, thermal, chemical, electrical, magnetic, optical and acoustic. However, only the properties that will have an influence on the stress and strain of the workpiece, which is the aim of this work, will be mentioned. Initially, an introduction is made, explaining the importance of having the properties dependent on the temperature and the cut off temperature approach. Subsequently, all the relevant properties for this work are presented, including the mechanical, thermal properties and others.

During the welding process, the material goes through a wide range of temperature, from room to boiling temperature in a matter of seconds. To carry out this work, it is necessary to take into account how the temperature will influence the material properties. Since the numerical simulation pretends to predict the real material behaviour, having temperature dependent properties is always a key factor. This happened for two reasons: first it should be borne in mind that acquiring these values is a complicated process because material reacts to the heat input in a non-linear way (change the phase), especially at high temperatures; second, some properties have no interest in being temperature dependent because they have no influence on stresses and strains results. Although many articles only mention few values that cannot cover the necessary range of temperatures of the welding process, it is always better than working with constant values, related to the room temperature. Additionally, FEM software today is very powerful and capable of interpolating data values. To avoid large amounts of data, which will overload the processing, it is enough to have values for every 100 °C, in order not to overload the simulation up to the melting point.

The author [3] proposes cut-off temperature for the mechanical analysis to cover the drawbacks that temperature dependent properties have. Above this higher temperature limit, the properties, which are temperature-dependent, remain unchanged.

The relevant properties are shown below: density, Young modulus and Poisson ratio (elastic), yield stress and strain (plastic), thermal expansion coefficient, specific heat capacity and

thermal conductivity. The author [45] concluded that knowing the thermal conductivity of the material is an essential parameter in numerical simulation because during thermal cycles (cooling and heating) phases transformations on HAZ and FZ happen. In relation to mechanical properties, the author came to the conclusion that Poisson ratio and Young modulus, thermal strain, yield strength, stress-strain curves are the main parameters that need to be taken into account.

**2.4.4.1. Density ( $\rho$ )**

This parameter generally decreases during heating cycle because of the thermal expansion of the metal. The author [3] proposes to use this value at room temperature (20 °C), because the density has insignificant influence on temperature field. However, another author proposes to use the density as a function of temperature (Table 16).

Table 16 – Mass density [3]

Mass density [kg/m <sup>3</sup> ]	Temperature [°C]
7594	0
7300	1000
7210	1200
7200	1500

**2.4.4.2. Elastic Behaviour**

In DP600 the elastic modulus starts from 210 GPa and decreases with temperature, as show in Table 17. This parameter has insignificant effect on stresses-strains and using a constant value of Young’s modulus at room temperature achieves better results [3].

Table 17 – Elastic properties [3]

Young Modulus [GPa]	Poisson ratio	Temperature [°C]
210	0.280	0
190	0.295	300
120	0.310	600
7200	0.330	800

**2.4.4.3. Plastic Behaviour**

It is when the material starts to deform plastically. It is represented by the yield stress and plastic strain. The author agree that to obtain simulation results similar to the real material

behaviour, yield stress has influence and must be considered temperature dependent [47]. This happens since this property is one of the most important to represent the mechanical behaviour of the material. Therefore, if this value is constant, the numerical simulation model only “predicts zero residual stress and no permanent distortion”. The plastic behaviour is strongly dependent on the temperature and needs to be take into account in simulation. In DP600 the yield stress value starts at 310 MPa and goes up to 345 MPa. The tensile stress is around 690 MPa [26].

The strain-stress curve describes the material behaviour during elastic and plastic stages. The author [4] tested the material at 7 different temperatures, using an extensometer to measure the strain. The results are present in the next Figure 2.36. Another author [47] concluded that these properties varied with temperature: the yield strength is going to decrease with the increase of the temperature.

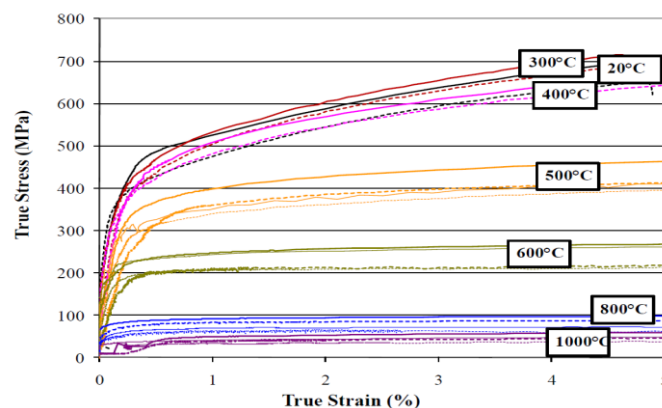


Figure 2.36 – True stress-strain curve obtained from tensile test for DP 600 [4]

#### 2.4.4.4. Thermal expansion coefficient ( $\alpha$ )

It represents the change in volume due to temperature (Table 18). It is a parameter that strongly depends on the lattice structure. This parameter quickly decreased during the austenitization and increase during melting. However, there is some contradiction as to whether or not this has effect on stresses and strain.

Table 18 - Thermal expansion coefficient [3]

Expansion coefficient	Temperature [°C]
$1.2 \times 10^{-5}$	0
$1.6 \times 10^{-5}$	400
$1.6 \times 10^{-5}$	800
$2.2 \times 10^{-5}$	1000
$2.5 \times 10^{-5}$	1200

#### 2.4.4.5. Specific heat capacity (*cp*)

This parameter represents the amount of energy that must be supplied to the material in the form of heat to increase the temperature by one unit (Table 19). The author [3] concludes that having this parameter dependent on the temperature does not have influence. Therefore, a constant value at room temperature is used.

Table 19 – Specific heat of DP600 [3]

Specific heat [J/kg. °C]	Temperature [°C]
520	0
550	200
600	400
750	600
1160	740
690	800
520	1100
610	1200
620	3000

#### 2.4.4.6. Thermal conductivity ( $\lambda$ )

It represents the ease with which heat passes through the material, i.e. whether or not the material is a good conductor. It has impact on the results of temperature fields' distribution. This parameter initially reduces with increasing temperature, stabilizing from a certain temperature as can be seen in the Table 20. [57] DP600 is a good thermal conductor due to the number of free electrons.

Table 20 – Thermal conductivity of DP600 [3]

Conductivity [W/(m. °C)]	Temperature [°C]
34.6	0
34.8	25
35	200
35	254
21.4	1100
25.5	1200
60	1300
70	1400
70	3000

Besides the mechanical and thermal properties, there are other properties related to the electrical and metallurgical parts of the material such as thermal metallurgical expansion and the specific electrical resistance. However, these are not relevant to this work.

## 2.4.5. Composition

### 2.4.5.1. Microstructure

During the welding process the microstructure of the component changes since the material in the welding zone passes through the solid, liquid and gaseous states [19]. Phase transformation occurs and consequently the mechanical and thermal properties of the areas affected by the heat of the laser beam are modified. By changing welding parameters, such as welding speed and others, it is possible to control the microstructure of the part. The principal phase of DP600, also called the matrix, is the ferrite. This low carbon steel has martensite islands in its composition, which normally represent one third of the main phase. The following Table 21 shows the microstructure proposed by the author [26]. However, we must be aware that there are other composition percentages, with small variation from the presented here.

Table 21 – Dual-phase microstructure constitution [26]

Phase	Volume Percentage (%)
Ferrite	70 - 75
Martensite	15 - 20
Bainite	7 - 13
Perlite/Austenite	< 2

During the solidification process, due to high cooling ratio, the austenite turns to martensite. Consequently, the material will become harder. The high ductility (good formability) depends directly on the amount of ferrite present in the microstructure of the steel. The percentage of martensite will determine the strength of the material (yield and tensile strength parameters) [58]. According to Figure 2.37 it is possible to see the microstructure of the material. Black areas represent the presence of martensite and lighter areas are the matrix, which is ferrite [59]. There is still bainite, austenite and perlite in the composition of the metal, as seen before, but with a much smaller representation than the others.

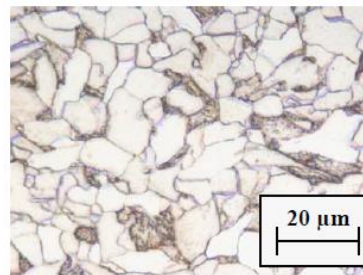


Figure 2.37 – DP600 microstructure [59]

#### 2.4.5.2. Diagrams (CTT and TTT)

The author [3] divides the solid state transformations, due to the existing thermal cycles, into 3 types: “the austenite transformation during heating cycle, the diffusion transformation and the martensite transformation during cooling cycle”. To analyse material transformations, there are many types of phase diagrams, related with changes in volume, temperature or even pressure. To understand the phase transformations due to temperature changes there are two options: Continuous cooling transformation (CCT) and time temperature transformation (TTT). Both diagrams represent the same thing but with differences in cooling method.

TTT is also known as isothermal transformation diagram. Figure 2.38 makes it possible to check how the microstructure is transformed according to temperature. The grey line represents the cooling process. The red, blue and green lines represent ferrite, perlite and bainite, respectively.

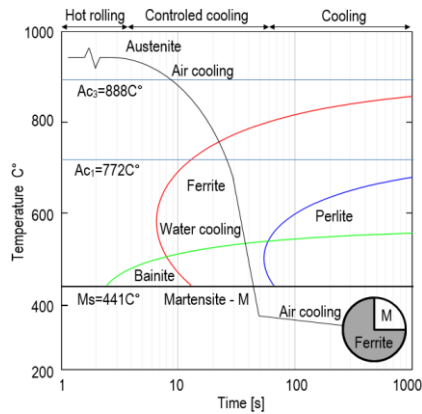


Figure 2.38 – TTT diagram during thermal cycles [60]

CCT is more common since the material is always cooling down, i.e. it is possible to see in the diagram the material behaviour over the range of different temperatures. It is used to model the phase transformations (Figure 2.39).

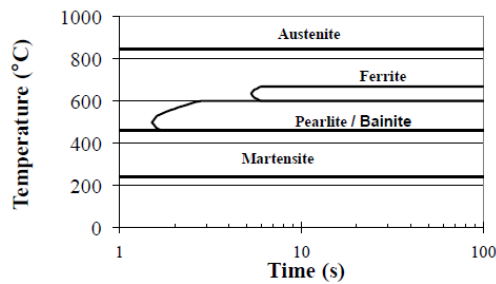


Figure 2.39 – Parameterized CCT (continuous cooling transition) [4]

### 2.4.5.3. Chemical Composition

Besides the microstructure of the material, the chemical composition is also important. Table 22 shows one of the suggested chemical compositions. Several authors [26] [4] [59] refer other chemical compositions of DP600 with other elements representing a very small percentage in the microstructure, such as the nickel (Ni) and vanadium (V) elements.

Table 22 - Chemical composition of DP 600 [26]

Mn	Si	C	Al	Cu	Cr	Mo	P	S
1.84	0.36	0.09	0.05	0.03	0.02	0.01	0.01	0.005





## 3. CHAPTER 3 – NUMERICAL MODEL

This chapter covers the development of the numerical models (pre-processing stage) and the correspondent results (post-processing stage). Three models were made based on 2 types of arrangements: butt and T-joint. All models intend to simulate Nd:YAG laser welding with keyhole using the conical volumetric heat source. The stresses and strains caused by the laser beam were studied and compared.

The numerical simulation was performed using Simufact. It is a software specific for welding simulations that is capable of predicting elastic-plastic and hardening material behavior. The great advantage of using this software is that it was developed exclusively for the welding process. The user interface is simple and makes it relatively easier to set and adjust the parameters, as it takes less time comparing to other software.

### 3.1. Pre-processing stage

---

This step consists of building the entire model such as the geometries, boundary conditions and all the other parameters including the material properties. The type of finite element to be used as well as the refinement of the mesh are also made in this step. The model development is an iterative process, that is, throughout the process many parameters were changed in order to improve the model. The values and model development methodology presented were the final ones.

#### 3.1.1. Problem description

The aim is joining two plates by using the laser Nd:YAG welding technique. The laser beam power is 4 kW and the welding robot moves at a speed of 3 m/min. These values were chosen because they are reasonable for this type of welding with the characteristics presented. Two

types of joints were studied: butt and T-joint. These two were chosen as they are among the most common welding configurations.

The butt joint model (Figure 3.1) consists of two metal plates with dimensions 20.0 x 20.0 mm with a thickness of 1.0 mm. They are connected with a butt joint and there is no gap between the plates.

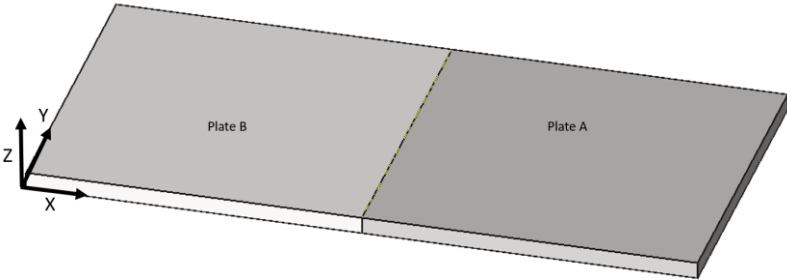


Figure 3.1 – Butt joint model

The T-joint model (Figure 3.2) involves welding two metal plates with a T-joint configuration. The horizontal plate has 20.0 x 41.0 mm. The vertical metal sheet has the dimensions of 20.0 x 20.0 mm and is positioned in the middle of the horizontal plate. Both metal sheets have 1.0 mm of thickness. Like in the butt joint models, there is no gap between the plates.

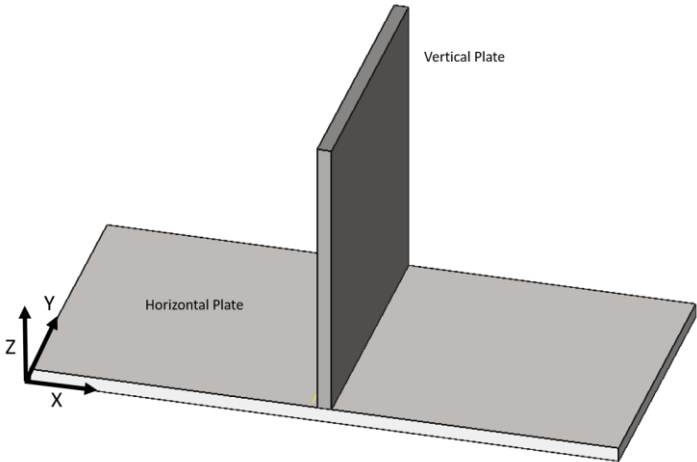


Figure 3.2 – T joint model

### 3.1.2. Steps and boundary conditions

There are two steps in the developed models. The welding step corresponds to the operation of the welding robot and the cooling step to the phase after the welding.

Regardless of the model in question, the dimensions of the mechanical boundary conditions are the same. It is a cuboid with 5 mm of width, 20 mm of depth and a height of 1 mm. To lock the plates and prevent them from moving during the welding, two types of mechanical fixtures are used in pairs: bearing and clamping. Both are rigid bodies. Bearing only allows the component to move in the same plane of the contact. Clamping is used when there is a need for applying force on the component. In order to press the clamping against the bearing, with the plate between them, a force needs to be applied. Stiffness and force mode were used. The force direction is normal to the component surface with a holding force of 1 kN and a constant translation stiffness of 5000 N/m.

In the butt joint models, there are 4 mechanical boundary conditions (Figure 3.3) to ensure the fixing of the plates: 2 bearing (red) and 2 clamping (green). The center of all boundary conditions is positioned about 7.5 mm, in transverse direction, from the center of the weld bead. The time when the boundary conditions are active is dependent on the model in question (Table 23). The objective of model 1 is to evaluate the maximum deformation so the plates are initially joined with a tack weld and then they are released to do the entire weld bead. The purpose of model 2 is to calculate the maximum stress on the part. So, the parts are clamped during the whole process.

Table 23 – Clamping conditions and steps overview of butt joint models

Model Nr	Purpose	Step		Plate A		Plate B	
				Clamp	Bearing	Clamp	Bearing
1	Maximum deformation	B	Welding (tack)	ON	ON	ON	ON
		C	Welding (joining)	ON	ON	OFF	OFF
		A	Cooling	ON	ON	OFF	OFF
2	Maximum stress	B	Welding (joining)	ON	ON	ON	ON
		C	Cooling	ON	ON	ON	ON

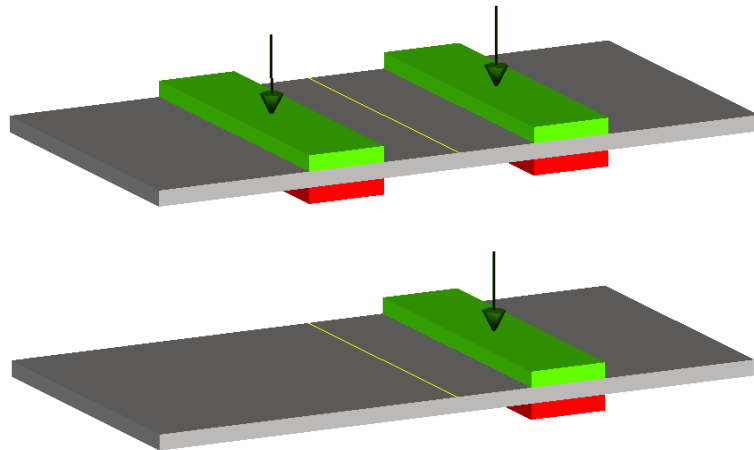


Figure 3.3 – Butt joint (model 1) clamping conditions at step A (top) and steps B+C (bottom)

For T-joint model (Figure 3.4), there are 6 mechanical boundary conditions to guarantee the fixing of the plates: 4 for the horizontal plate and 2 for the vertical. The distance between the center of the boundary conditions geometry and the center of the weld bead is approximately 12.5 mm in transverse direction. Only one model was developed with this joint arrangement. The aim is to predict the maximum deformation of the vertical plate. During the welding process, the vertical plate is free to move (Table 24).

Table 24 – Clamping conditions and steps overview of T-joint model

Model Nr	Purpose	Step		Horizontal plate		Vertical plate	
				Clamp	Bearing	Clamp	Bearing
3	Maximum deformation	A	Welding (tack)	ON	ON	ON	ON
		B	Welding (joining)	ON	ON	OFF	OFF
		C	cooling	ON	ON	OFF	OFF

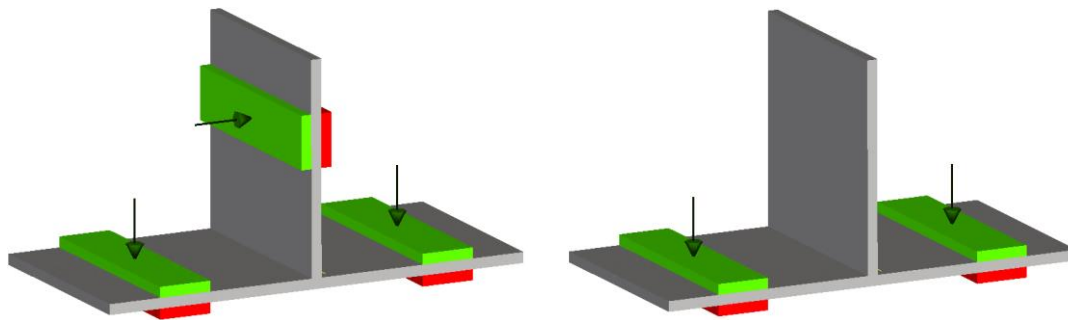


Figure 3.4 – T-joint clamping conditions at step A (left) and steps B+C (right)

### 3.1.3. Heat source and trajectory

The heat source chosen for the numerical analysis was the conical with Gaussian distribution (Figure 3.5) in keyhole mode because it represents the energy distribution of the laser process. The shape parameters are the same for all models, as shown in Table 25. The depth of the heat source is different in the T- joint model to ensure the correct energy distribution along the weld bead. The power intensity is constantly distributed inside the heat source.

Table 25 – Heat source parameters

Parameter	Butt joint [mm]	T-joint [mm]
Radius superior ( $r_u$ )	0.50	0.50
Radius inferior ( $r_i$ )	0.10	0.10
Depth ( $d$ )	1.00	1.00
Offset	0	0.47

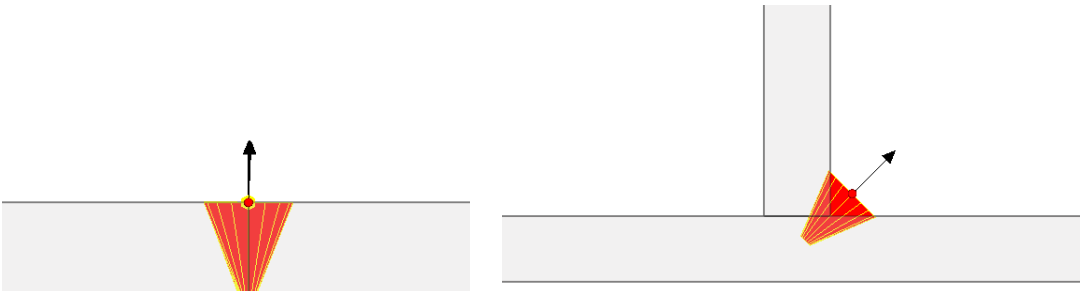


Figure 3.5 – Heat source geometry in T-joint (left) and in butt joint (right)

The trajectory describes the path of the heat source moving during welding process. Figure 3.6 shows the different trajectories of butt and T-joint, respectively. The weld bead has the total length of the plate (20 mm). In the models that aim to predict the maximum deformation, two tack welds were made and after that, the clamping were released. This is a widely used procedure adopted when it is necessary to hold the parts during the welding process without using clamping conditions. Tack welds have a length equal to twice the upper radius of the heat source.

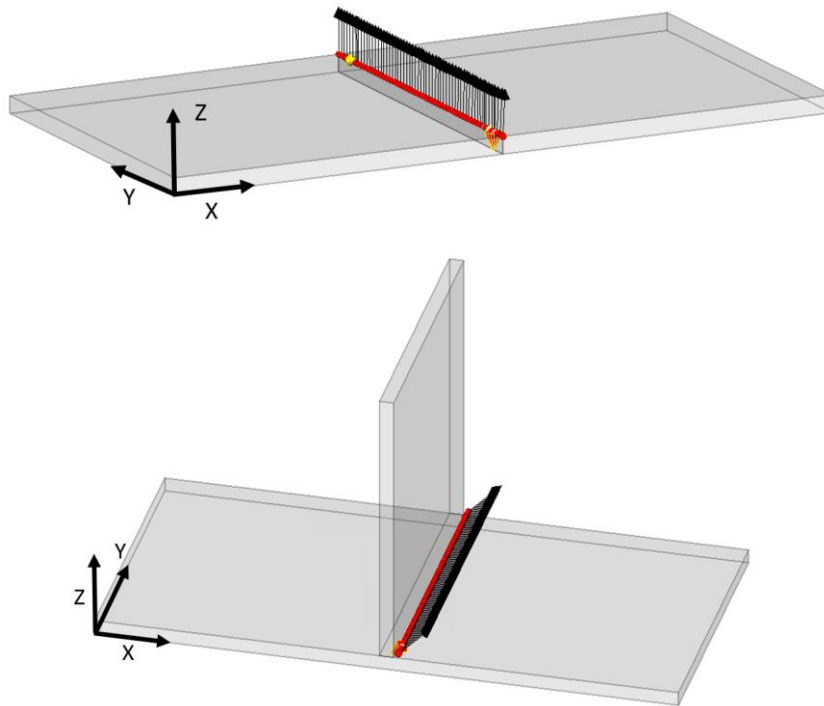


Figure 3.6 –Trajectories of T-joint (up) and butt joint (down)

### 3.1.4. Material

The material is high strength steel, very common nowadays in automotive manufacturing industries. The process was done without filler material. The software performs a thermal analysis, so it is necessary to define the material properties (mechanical and thermal) dependent on the temperature. This is the only way to guarantee a reliable simulation. A material very similar to the properties of DP600 was chosen. This material is already defined in the software library (S60QL-SPM-sw). Assumption of the initial phase fractions: 79% bainite, 21% ferrite.

#### 3.1.4.1. Thermal properties

Three constant parameters related to latent heat are required (Table 26). Solidus temperature is the temperature at which the material is completely solid. The melting temperature needs to be higher than solidus temperature because it represents the temperature at which the material is in liquid state. The latent heat for melting is the amount of energy that is required to change a material from the solid to the liquid state.

Table 26 – Temperatures properties

Parameter	Value
Solidus temperature [°C]	1462.92
Melting temperature [°C]	1509.95
Latent heat for melting [J/Kg]	256400.0

The thermal conductivity (Figure 3.7) should be temperature dependent because it describes how the heat is transferred in the material. The Fourier's law correlated the heat flux across a surface and the temperature gradient.

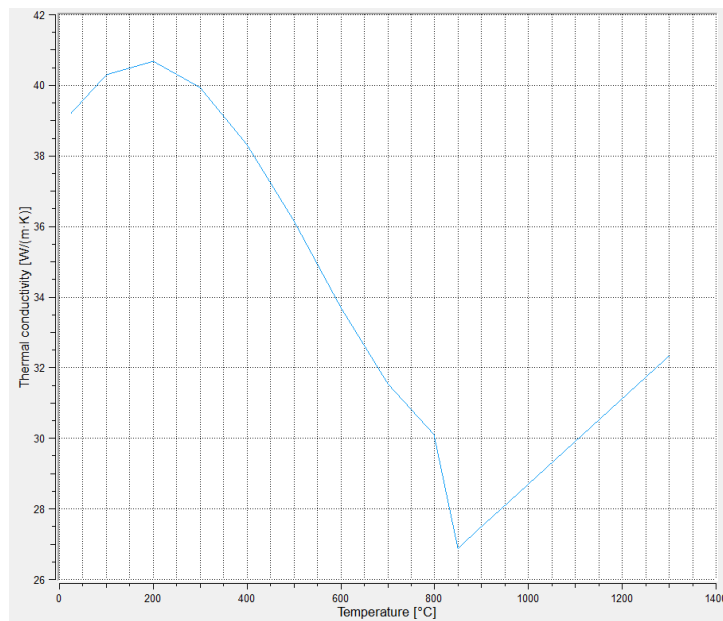


Figure 3.7 – Thermal conductivity

Specific heat capacity is present in Figure 3.8. This parameter represents the energy that must be supplied to the material in order for a body of one kilogram to increase one Joule.



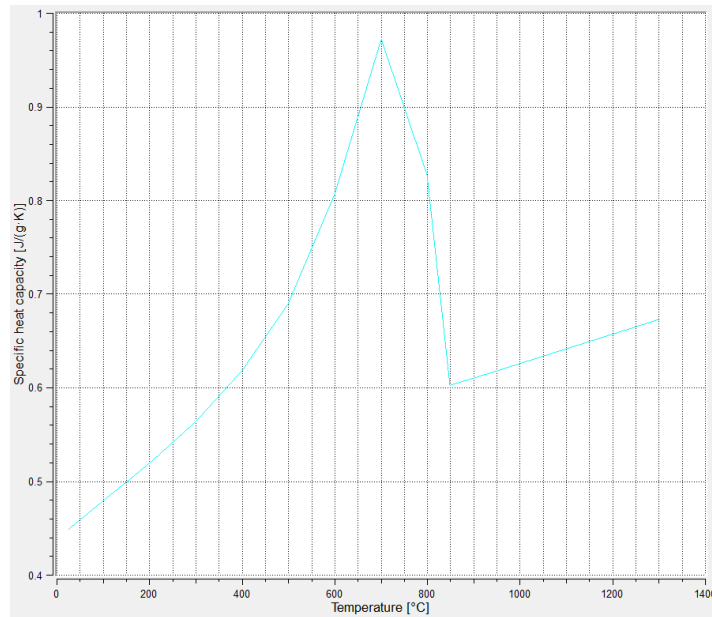


Figure 3.8 – Specific heat capacity

### 3.1.4.2. Mechanical properties

For welding simulation the software needs 4 mechanical properties: Young’s modulus, density, thermal expansion coefficient and Poisson’s ratio.

Poisson’s ratio is a constant value (0.3) and represents how much a material that is stretched in one direction, expands or contracts in the other direction. This value is constant because having this parameter dependent on temperature is insignificant for the results relative to the welding process.

Young’s modulus ( $E$ ) is temperature dependent as shown in Figure 3.9. It describes the relationship between the stress and the elastic strain. It is possible to observe that near the melting temperature the values of the Young modulus are extremely low.

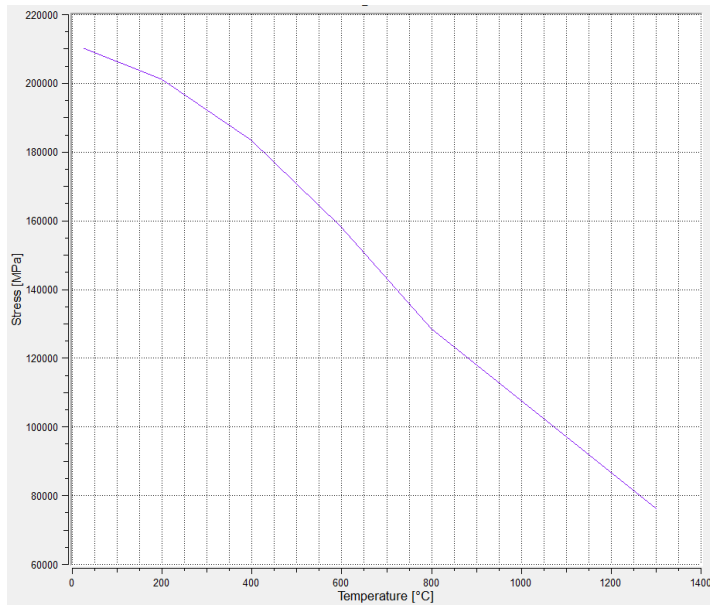


Figure 3.9 – Young's modulus

It is mandatory to have the density (Figure 3.10) dependent on the temperature, since the welding process is characterized by releasing high amounts of heat, and this is solid material that changes its volume with temperature.

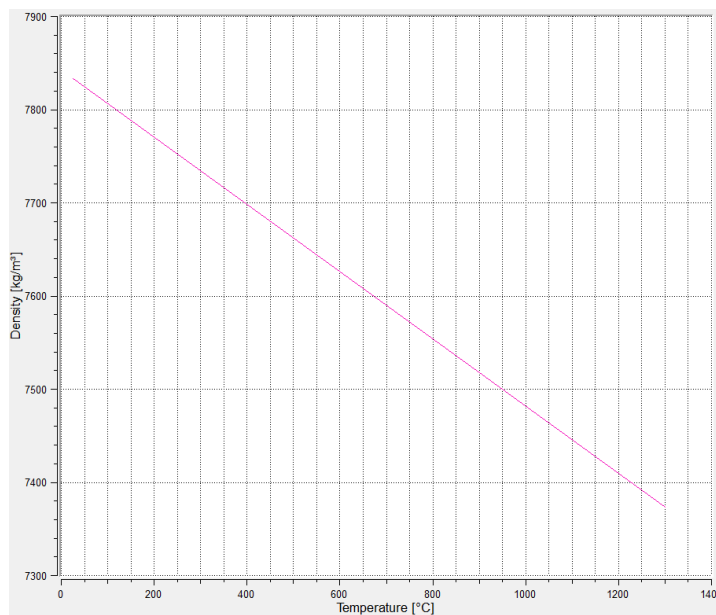


Figure 3.10 - Density

Finally the thermal expansion coefficient (Figure 3.11) is also temperature dependent. This mechanical property describes how the material changes its volume with a change in temperature.

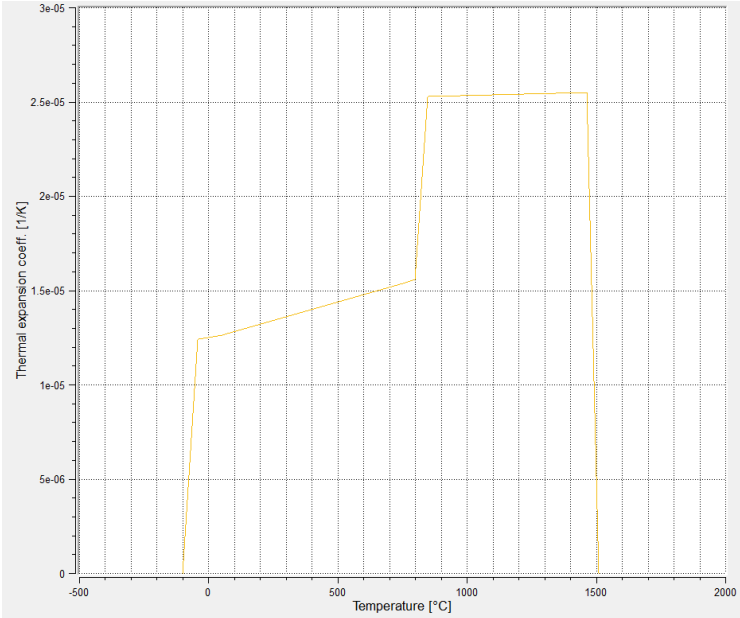


Figure 3.11 – Thermal expansion coefficient

**3.1.4.3. Flow curves**

Flow curves (Figure 3.12) are extremely important to understand the relationship between the true stress and the true plastic strain at different temperatures. The figure shows the different behaviours at different temperatures (25, 100, 20, 300, 400, 500, 600, 700, 800, 900, 1000, 1100, 1200 and 1300 °C). As the temperature increases, the smaller this curve will be.

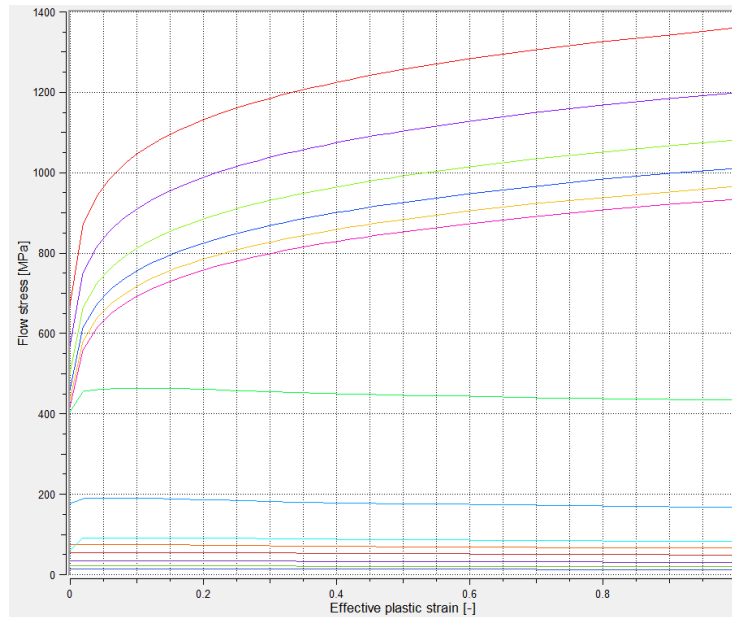


Figure 3.12 – Flow curves

### 3.1.5. Mesh

To run the simulation, it is necessary to perform a spatial discretization (meshing) of the continuous workpiece in finite elements. There are several meshing strategies available to discretize the model according to the complexity of the part's geometry. The convergence of the mesh was done to eliminate the results' dependency on the element size. Only then is it possible to obtain accurate results, and avoid excessive mesh refinement that has no influence on the results but will require more computational time. Several models with different types of mesh refinement have been compared. Initially, a simple mesh was used and the number of elements was increased until convergence was reached. The parameter was the maximum temperature in the centre of the weld bead. The convergence was reached when the defined parameter stabilized, not depending anymore on the mesh density.

The final 3D mesh was divided into the three typical zones to analyse the stresses and deformations of the welding process: base material (BM), heat affected zone (HAZ) and fusion zone (FZ). This procedure was made to speed up processing time, since there are areas that are not very relevant to analyse. The mesh in the weld seam area is always more refined because it is the area where most transformations take place and therefore, the most

important to be studied. The auto refinement tool was used in this area to ensure that all physical changes, such as elements with high temperature or high Von Misses equivalent stress, are correctly detected and adjusted. Hexahedral elements were chosen to create the mesh. The butt joint model is composed by 11544 elements and 8160 nodes (Figure 3.13). The T-joint model uses 17956 elements and 12960 nodes (Figure 3.14). Three elements across thickness were used in all models. The smallest element is 0.25 x 0.25 x 0.33 mm, while the largest element is 1.0 x 1.0 x 0.33 mm.

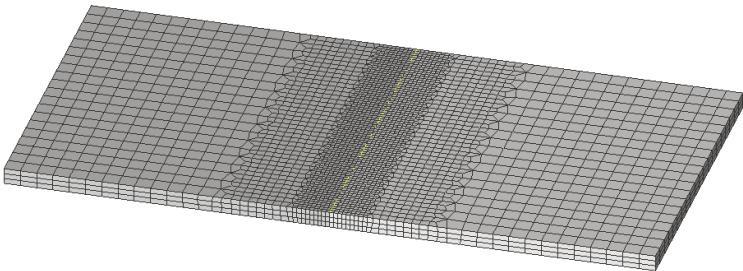


Figure 3.13 – Butt joint mesh

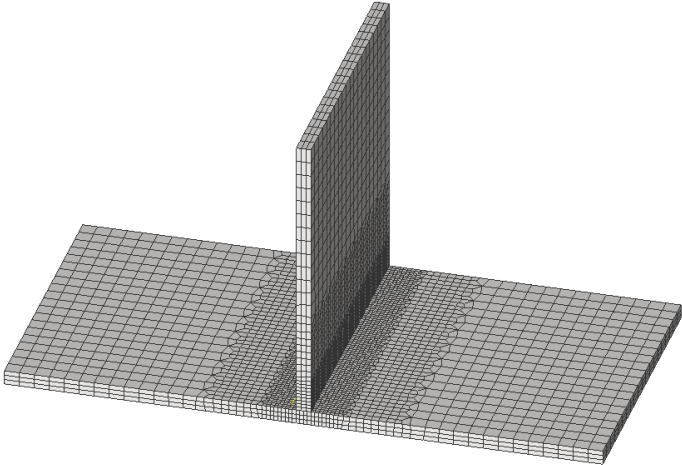


Figure 3.14 – T-joint mesh

### 3.1.6. Process parameters

In addition to the parameters previously defined, there are others that have an influence on the results of the analysis. The selected room temperature is 20 °C. However, when the welding is over, the cooling step is active and only ends when the workpiece achieves 300

°C. If the cooling phase only ended when the entire part reached room temperature, the processing time would be substantially longer. Furthermore, limiting the cooling phase to 300 °C does not have much influence on the results since the parts are made of steel.

All models took into consideration the action of the gravitational force with a value of 9.80665 m/s<sup>2</sup> in (0, 0, -1) direction. The analysis mode chosen was the Precision that improves the results quality especially in the heat-affected zone. Thermal and mechanical analyses are performed together. No phase transformation was taken into account. There are no stress fields present in the components before the simulation.

To speed up the calculation of the results, the parallelization feature was used. This consists of dividing the simulation into several parts that are calculated at same time using several CPU cores. Two parallelization options supported by the software were used: shared memory parallelization (SMP) combined with domain decomposition method (DDM). The number of domains used in all simulation was 4 and the number of cores per domains was 9. The core number used is calculated by multiplication of the number of domains and the number of cores per domain, so a total of 36 cores were used. This means that the model was subdivided into 4 sub models (domains) and the calculation time decreased in ¼.

The total processing time selected for all models was 35 s to ensure that plates have a cooldown phase after the robot finished the welding. The chosen method to calculate the increment length was the Adaptive, where time steps are chosen based on the convergence behavior of the model. Table 27 shows the values selected that define the frequency of mechanical calculation relative to thermal calculation and the results output frequency for welding and cooling cycles. This procedure was adopted in order to accelerate processing time and to achieve accurate results.

Table 27 – Increment and steps control

Parameter	Welding step	Cooling step
Mechanical solution every n thermal increment	3	5
Result output every n increment	6	5

## 3.2. Post-processing stage

---

In this topic all the results of the models are presented and analysed in detail. The following numerical results refer to the end of the cooling step. Before the results presentation, the method used to obtain them is explained for both models: butt joint and T-joint.

### 3.2.1. Stress measurement

#### 3.2.1.1. Butt joint models

To quantify the residual stresses in transverse (x) and longitudinal direction (y), two lines have been defined. The longitudinal line has 20 mm and coincides with the weld bead. The transverse line is perpendicular to the weld bead and is positioned in the middle of the plate with a total length of 40mm. Figure 3.15 shows a top view of the butt joint model where it is possible to see the positions of the lines. There are 40 tracking points for each mm.

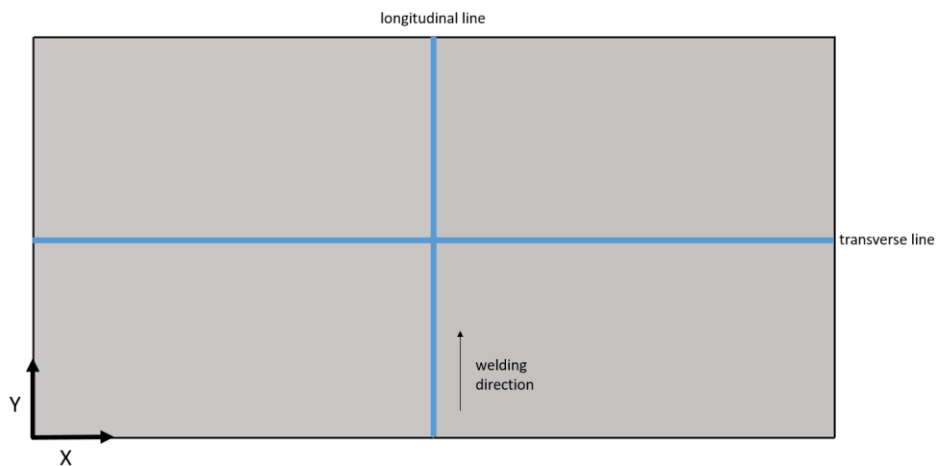


Figure 3.15 – Positioning of transverse and longitudinal lines of butt joint models

The lines are positioned on two surfaces (Figure 3.16) so that it is possible to compare the stresses along the plate thickness. The top surface (orange) corresponds to the surface of the laser beam side, where there are 2 lines as mentioned above: the transverse top line and the longitudinal top line. The bottom surface (green) is opposite to the laser beam, where

transverse bottom and longitudinal bottom lines are present. In total, the butt joint model has 4 lines to monitor the stress distribution in longitudinal and transverse direction.

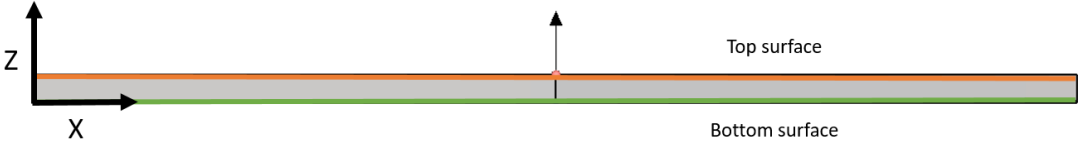


Figure 3.16 – Positioning of top and bottom surfaces of butt joint models

**3.2.1.2. T-Joint model**

In T-joint model, since the plates are not on the same plane, the only way to quantify the transverse stresses is to make the analysis separately. Consequently, different transverse monitoring lines are created for vertical and horizontal plates. The longitudinal line is the same since it is common for both plates due to being positioned on the weld bead.

In the vertical plate of T joint model, two lines were defined to monitor the transverse (z-direction) and longitudinal (y-direction) residual stresses present after the welding and cooling cycle (Figure 3.17). All lines in this plate have a 20 mm length. There are 40 tracking points for each mm.

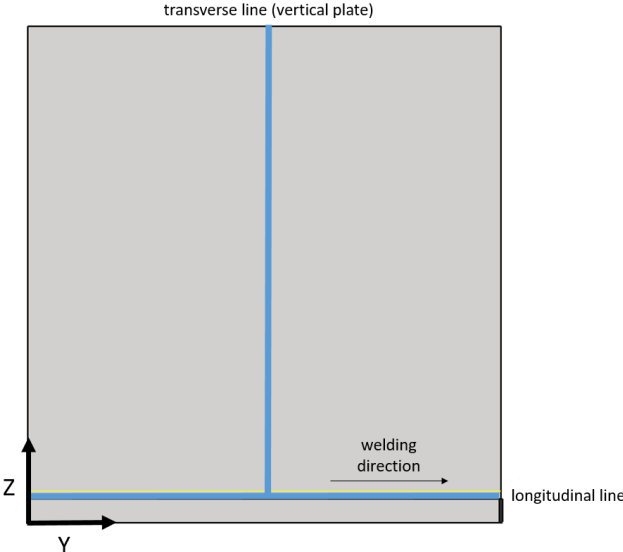


Figure 3.17 - Positioning of transverse and longitudinal lines of vertical plate (model 3 - T joint)



In order to compare the residual stress along the thickness of the vertical plate, the previous lines are positioned on two surfaces presented in Figure 3.18. The right surface (green) corresponds to the surface of the laser beam side. In this surface there are 2 lines as mentioned: the transverse right line and the longitudinal line (line that is common to the vertical plate and the horizontal plate). The left surface (purple) is opposite to the laser beam, where only the transverse left line is present.

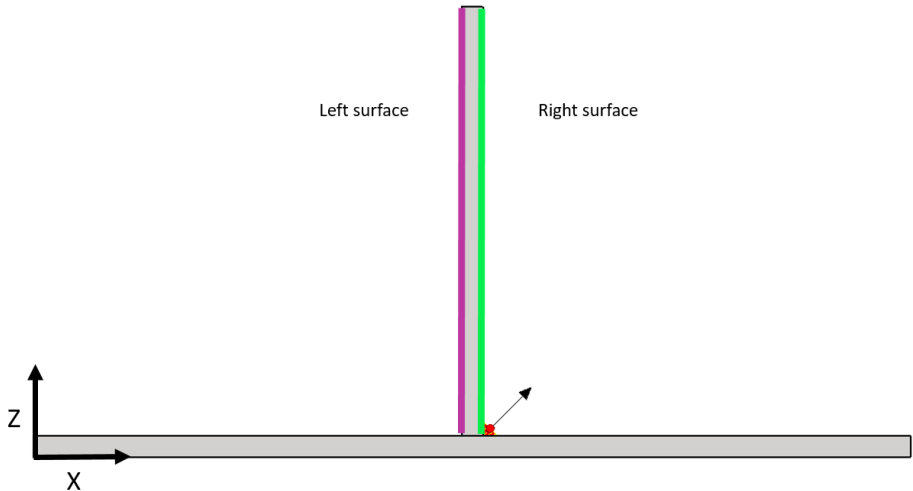


Figure 3.18 – Positioning of left and right surfaces (model 3 - T joint)

In the horizontal plate of the T-joint model, the transverse and longitudinal lines to quantify the transverse (x-direction) and longitudinal (y-direction) residual stress are very similar to those used for the butt joint model. This means that there are 4 monitoring lines (Figure 3.19) on the horizontal plate: 2 transverse and 2 longitudinal. Two are positioned (Figure 3.20) on the top surface (orange) and the other two are on the bottom surface (green). The only difference has to do with the transverse lines that have a length of 41 mm due to the thickness of the vertical plate.

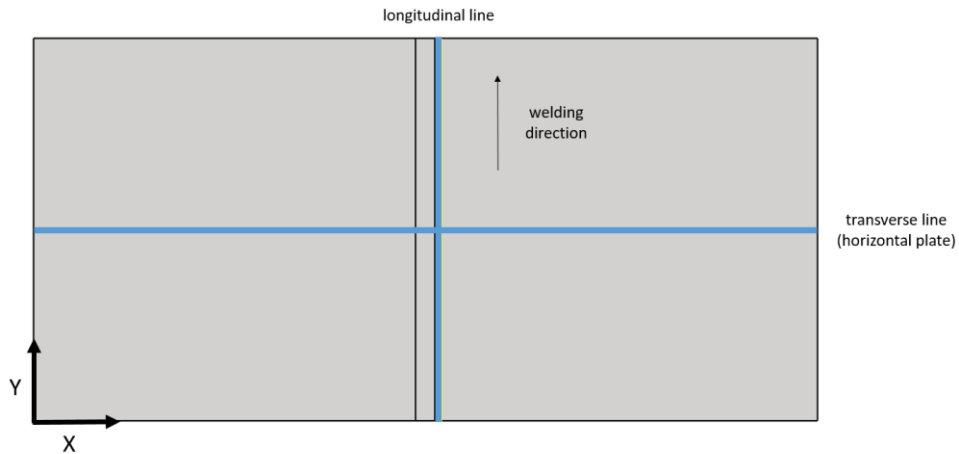


Figure 3.19 - Positioning of transverse and longitudinal lines of horizontal plate (model 3 – T joint)

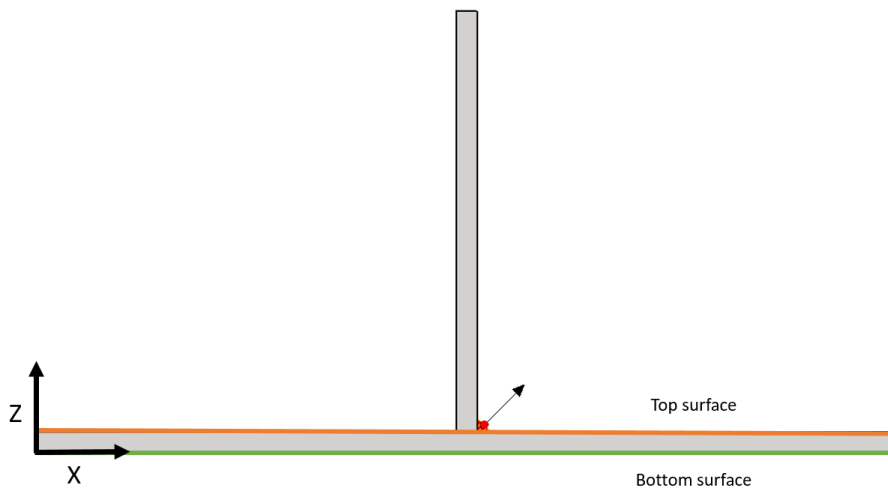


Figure 3.20 - Positioning of top and bottom surfaces (model 3 – T joint)

## 3.2.2. Displacement measurement

### 3.2.2.1. Butt Joint model

To quantify the Y and Z displacement in butt joint models, three transverse lines (a, b and c) are defined (Figure 3.21). The first line (a) and the last line (c) are positioned at the beginning and the end of the plate, respectively, according to the welding direction. The middle line (b) is equidistant from both other lines. The transverse lines have a total length of 40 mm. The two longitudinal lines (lines d and e) are at the edges of the plate and are defined to

calculate the displacement in x-direction (Figure 3.22). These lines have a total length of 20 mm.

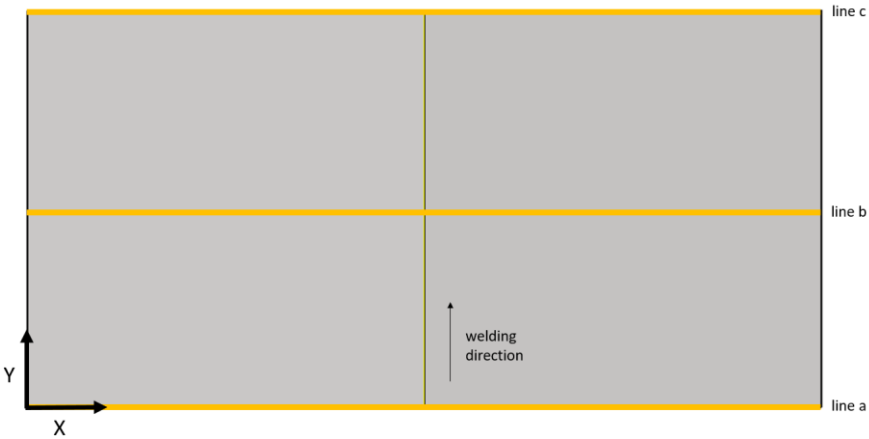


Figure 3.21 - Positioning of transverse lines to calculate Y and Z displacement on butt joint models

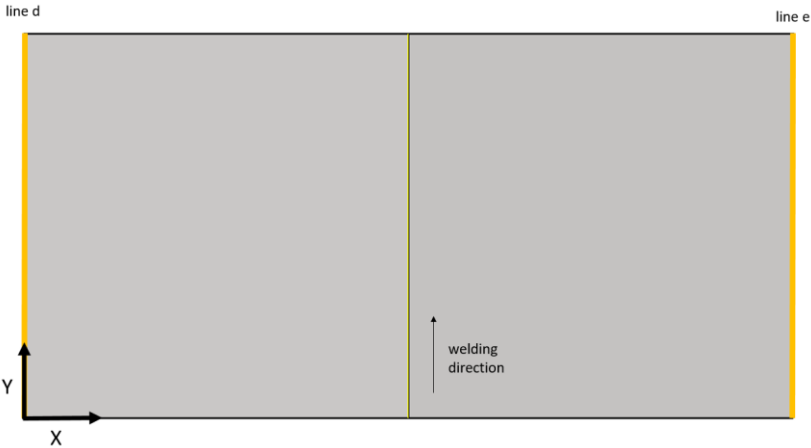


Figure 3.22 - Positioning longitudinal lines to calculate X displacement on butt joint models

These lines are positioned on the top surface of the plate. The lines on the bottom surface have not been taken into account since the deformation at the top surface of the plate is equal to the deformation at the bottom surface. This happens because the plate is thin.

**3.2.2.2. T-Joint model**

To calculate the displacement of the vertical plate in x-direction, three lines are defined (Figure 3.23). These lines are positioned on the same side of the weld bead (right surface).

No lines have been placed on the other side since the thickness is very small. The positioning of longitudinal lines to calculate Z displacement are in Figure 3.24.

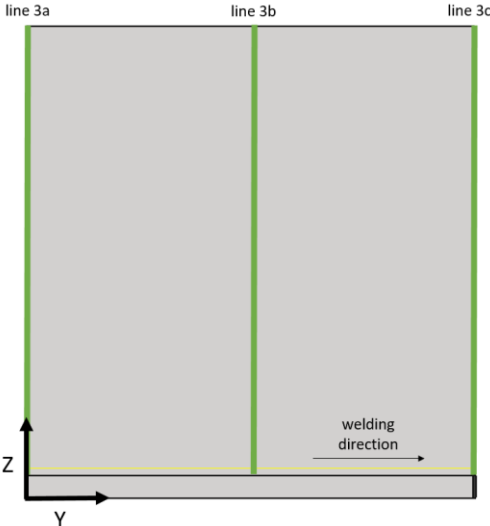


Figure 3.23 – Positioning of transverse lines to calculate X and Y displacement (model 3 – T joint)

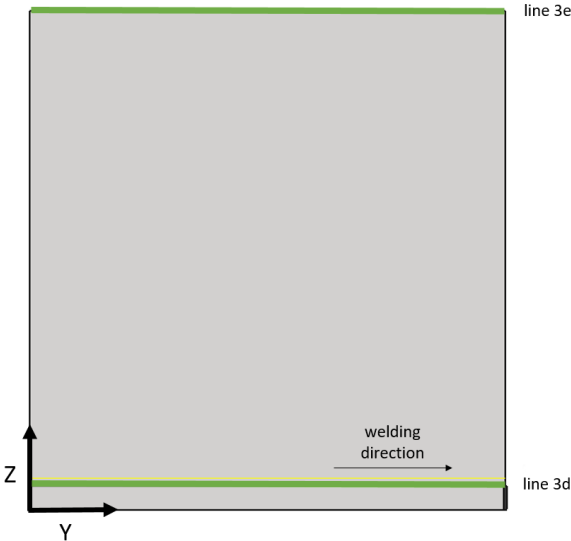


Figure 3.24 - Positioning of longitudinal lines to calculate Z displacement (model 3 – T joint)

The existing deformation on the horizontal plate was quantified using the same three transverse lines (a, b and c) and two longitudinal lines (d and e) that were used in the butt joint models. The position of the lines is exactly the same. The only difference is the length of the transverse lines which is 41 mm.

### 3.2.3. Model 1 results

This model is composed by two plates welded in a butt joint configuration. The plates are clamped during the entire process (welding and cooling phases). The following Table 28 shows all the results that will be presented for this model.

Table 28 - Results resume (model 1 – butt joint)

Item	Line(s)
Longitudinal stress (y-direction)	Transverse (top, bottom)
	Longitudinal (top, bottom)
Transverse stress (x-direction)	Transverse (top, bottom)
	Longitudinal (top, bottom)
Out of plane deformation (z-direction)	Transverse (a, b, c)
Longitudinal deformation (y-direction)	Transverse (a, b, c)
Transverse deformation (x-direction)	Longitudinal (d, e)

#### 3.2.3.1. Longitudinal stress

This is the stress that occurs parallel to the welding path (y-direction). Figure 3.25 shows an isometric view of the longitudinal stress distribution in both plates. It is possible to see that there is a higher stress concentration in the weld bead area. The reason for this is that heat causes the material to expand and when it cools down, it creates residual stresses. To better understand how this stress is distributed along the part, an analysis is made through the transverse and longitudinal lines previously defined.

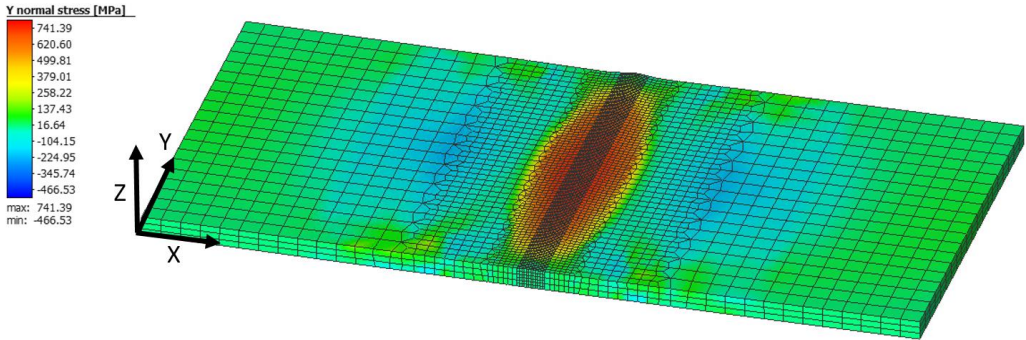


Figure 3.25 - Longitudinal stress mapping in butt joint (model 1 – butt joint)

Through the analysis of the results, it is possible to verify that the behavior of the longitudinal residual stress is identical on the top and bottom surfaces of the plates. In addition, there is a symmetrical distribution of the longitudinal stress on both plates.

Figure 3.26 shows the longitudinal stress along the transverse lines. The edges are those with minimum residual stresses because these are less thermally affected during welding. In the central zone, the plates are under a compression state that reaches approximately -225 MPa. The area near the weld bead, located  $\pm 5$  mm from the weld line, is under a high tensile state. The peak is positioned in the middle of the plates and has a value close to 730 MPa. This area corresponds to the melted region. This happens due to the high temperatures released by the laser beam, when the material changes its phase and consequently, the microstructure suffers significant variations. Moreover, this model has all the clamping conditions active during welding and cooling stages, which has a high influence on the magnitude of the residual stresses.

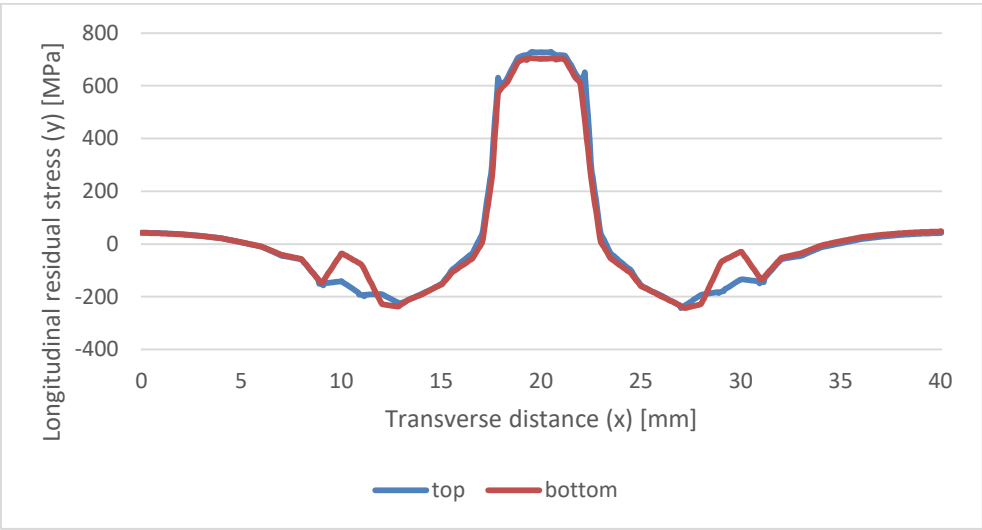


Figure 3.26 – Longitudinal residual stress along transverse lines (model 1 – butt joint)

The presence of longitudinal residual stresses along the weld bead is contemplated in Figure 3.27. There is a slight difference between the top and bottom surfaces in stress magnitude and how it is distributed along the longitudinal line. This happens because the heat reaches the top surface first and with more intensity. In the edges of the plates, the stress is equal to

zero. However, the closer to the weld bead, the higher the stress is, reaching a maximum residual stress of 710 MPa.

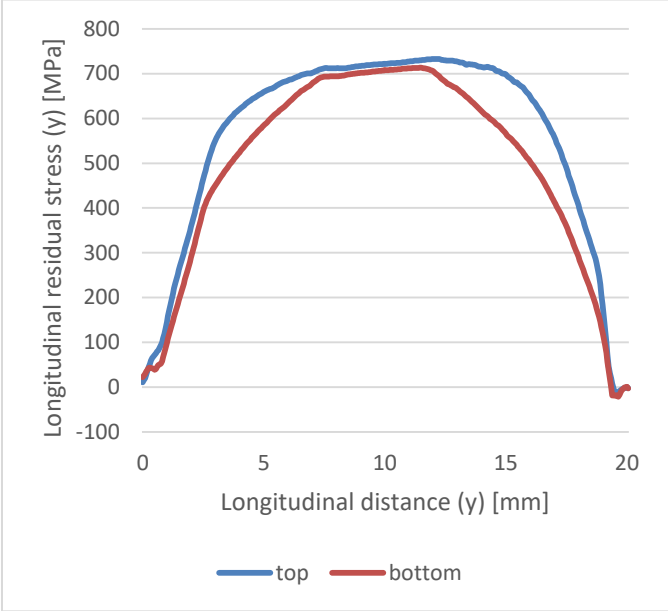


Figure 3.27 - Longitudinal residual stress along longitudinal lines (model 1 – butt joint)

**3.2.3.2. Transverse stress**

This is the stress perpendicular to the welding route (x direction). It is highly influenced by the clamping conditions as shown in the stress overview (Figure 3.28). The highest concentration of stress is between the weld bead and the clamping tools. Outside this area, the plates present an extremely reduced stress due to being free to expand during welding and contract during cooling stage.

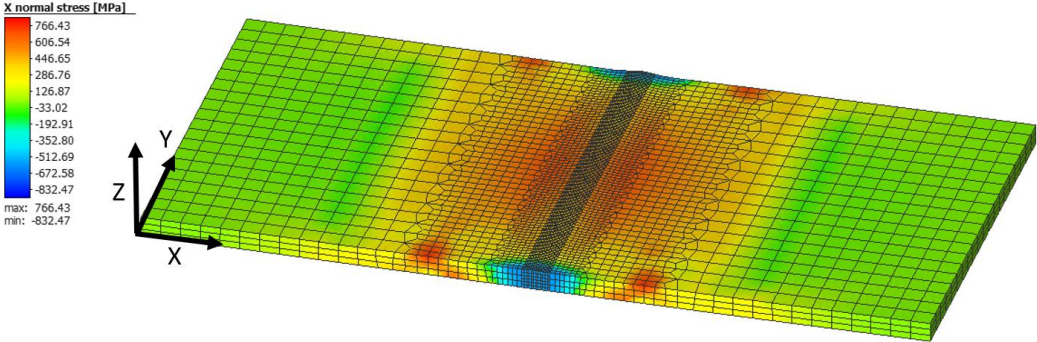


Figure 3.28 – Transverse stress mapping in butt joint (model 1 – butt joint)

The presence of transverse stresses along the thickness is nearly the same, the bottom surface having a slightly lower magnitude. This behavior is easily justified due to the laser beam not reaching this surface. So the heat transfer will be lower and consequently the magnitude of thermal cycles, that cause the stresses, will be inferior. The profile of the transverse residual stresses is symmetrical to the joint.

The maximum stress along the transversal lines occurs in the weld bead area with a magnitude of approximately 650 MPa as shown in the graph present in Figure 3.29. The plates are under a tension state (+) along the transverse direction. There are small areas of the plates, near the end of the clamping tools, where there is a small state of compression (-). At the edges of the plates the transverse stress is zero.

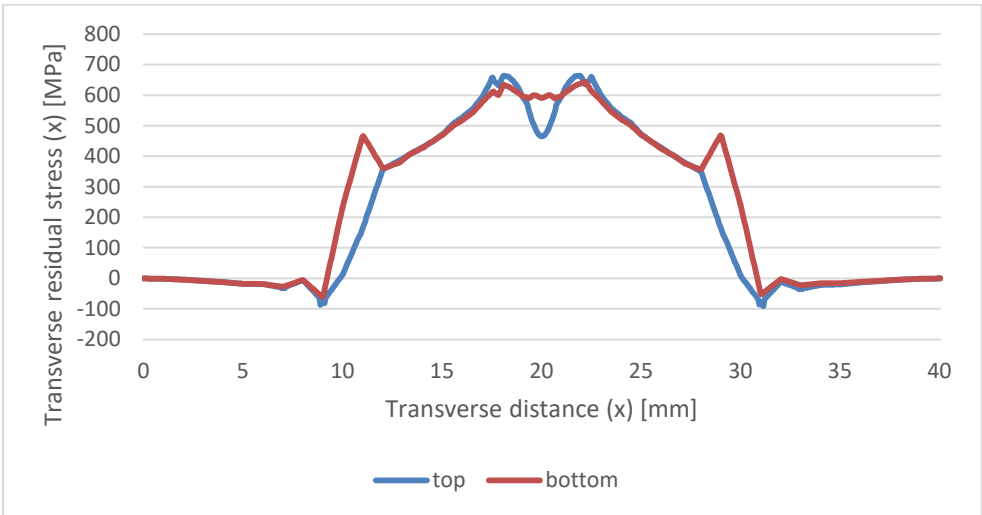


Figure 3.29 – Transverse residual stress along transverse lines (model 1 – butt joint)

Along the longitudinal lines, there is a state of compression at the edges of both metal sheets that starts in the order of -450 MPa and -600 MPa. Outside these zones, the plates are under a state of tension that reaches over 600 MPa on the bottom surface. On the top surface, the maximum transverse stress is near 450 MPa (Figure 3.30).



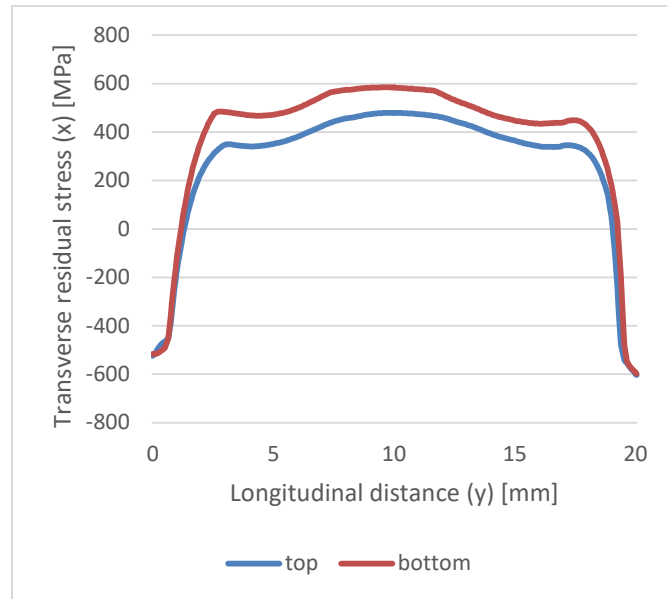


Figure 3.30 – Transverse residual stress along longitudinal lines (model 1 – butt joint)

### 3.2.3.3. Out-of-plane deformation

The out-of-plane deformation regards to the displacement that occurs perpendicular to the top and bottom surfaces. The top surface can be seen in Figure 3.31, where the displacement in z-direction is presented. This model has the plates clamped during the welding and cooling stages. Therefore, in the clamping zones, the displacement is zero (Figure 3.32).

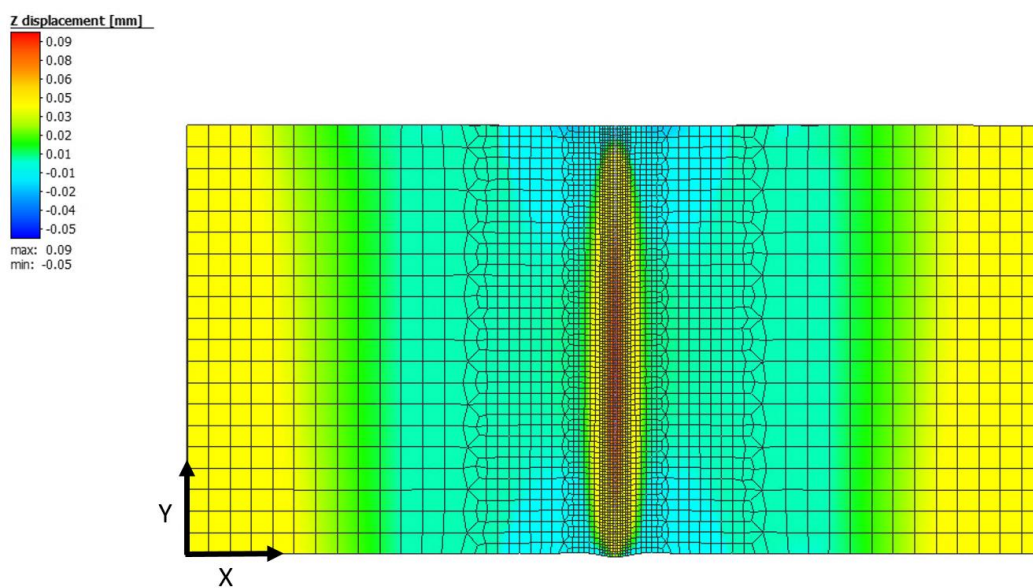


Figure 3.31 – Top view of Z displacement (model 1 – butt joint)

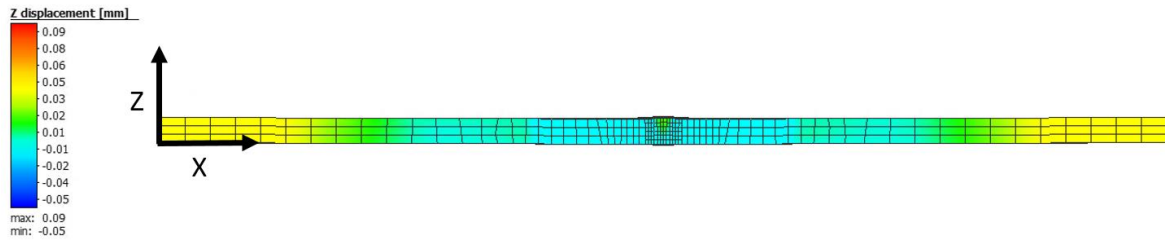


Figure 3.32 – Side view of Z displacement (model 1 – butt joint)

The graph in Figure 3.33 displays the deformation in z-direction of the three lines defined previously. It is possible to see that the deformation presents a symmetrical behavior in relation to the joint (symmetry plane). In the areas where the plates are locked, the deformation is zero, which is predictable. There is positive deformation at the edges of both plates, around 0.05 mm. This deformation only happens outside the clamping zone, where the plates are free to move. The deformation at the beginning and end zone of the laser beam passage presents a similar behavior in the weld zone: they both have a negative displacement around -0.02 mm in both cases.

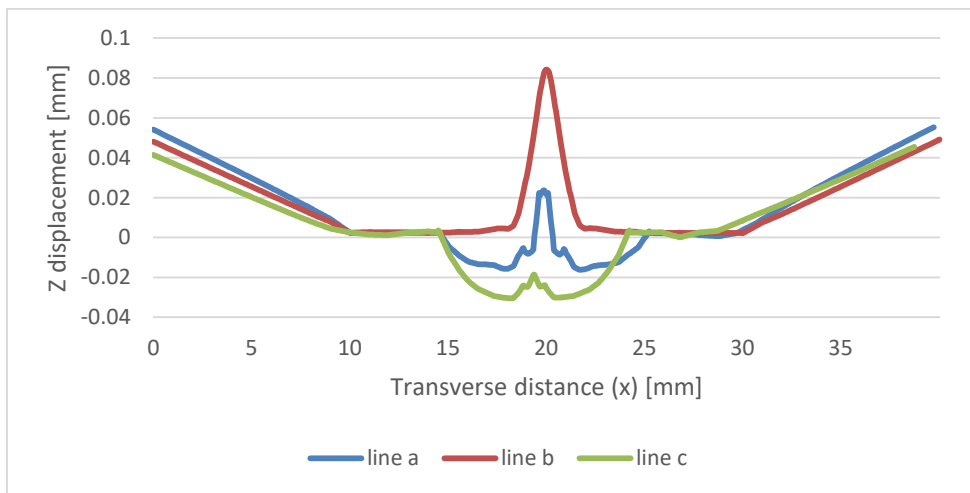


Figure 3.33 – Z displacement along transverse lines (model 1 – butt joint)

### 3.2.3.4. Longitudinal deformation

This deformation occurs parallel to the laser path. Since the plates are fixed and have a small width (20 mm) there is a slight deformation in y-direction. Figure 3.34 presents a top view of the sample, showing the results for displacement in y-axis direction. Excluding the center

of the weld bead, the edges of the plate in y-direction (lines a and c) have a symmetrical longitudinal shrinkage with a magnitude of 0.04 mm (Figure 3.35).

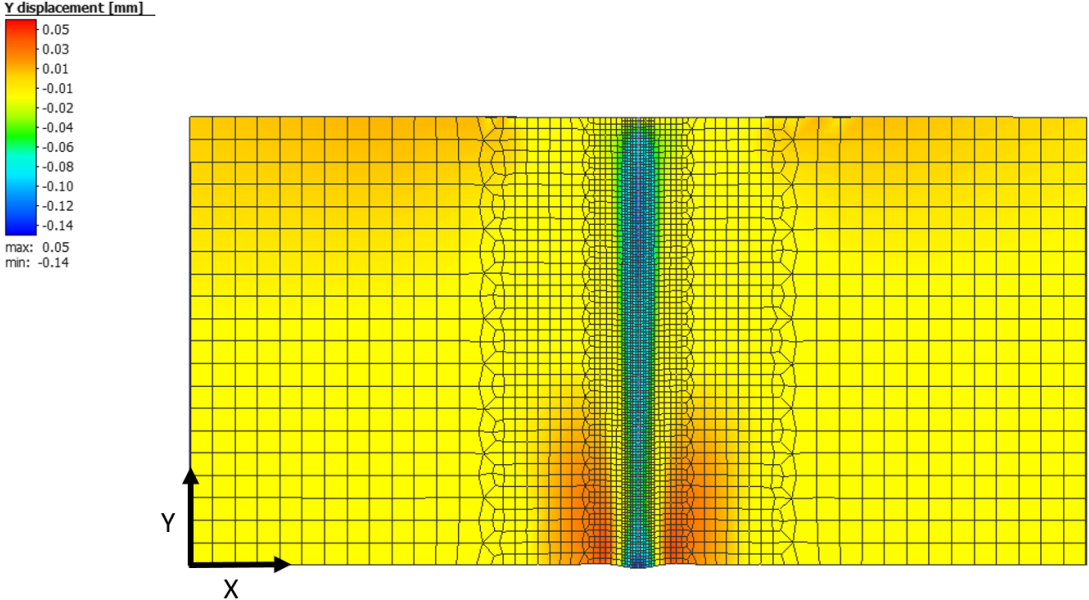


Figure 3.34 – Top view of Y displacement (model 1 – butt joint)

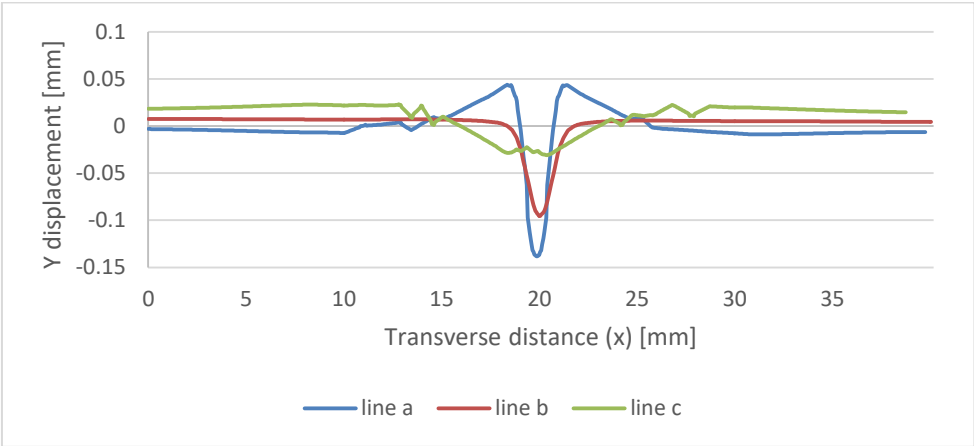


Figure 3.35 - Y displacement along transverse lines (model 1 – butt joint)

**3.2.3.5. Transverse deformation**

This deformation occurs in the transverse way of the plate. Figure 3.36 shows the deformation in the x-direction that occurs on the plate after the welding process. It is possible to verify that the largest deformation occurs in the zone between the weld bead and the clamps. The deformation that exists in the x direction is symmetrical. Outside this zone the

deformation is insignificant. This deformation has a direct influence on the length of the plate; however the change is minimal.

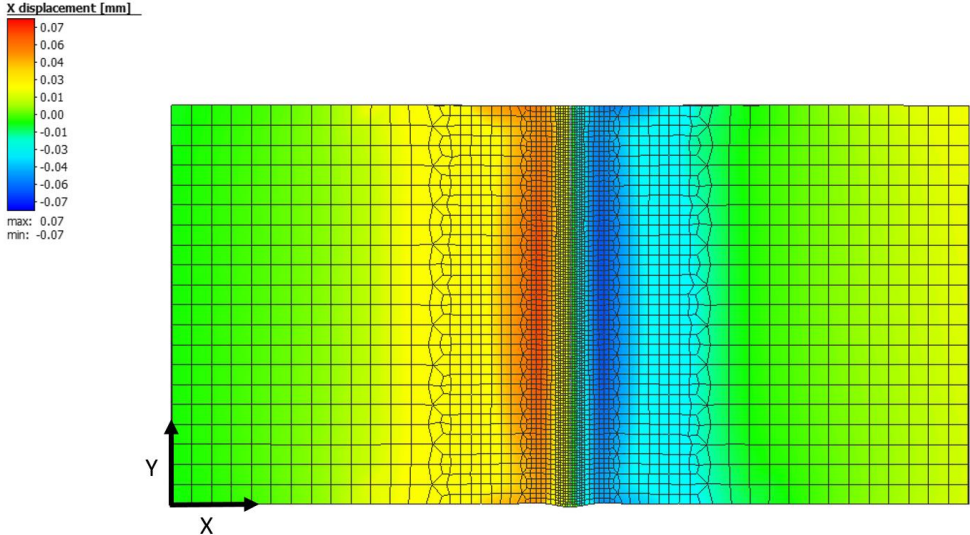


Figure 3.36 – Top view of X displacement (model 1 – butt joint)

Figure 3.37 shows the displacement of the plate’s edges in the x-direction. It can be seen that the total length increases less than 0.02 mm.

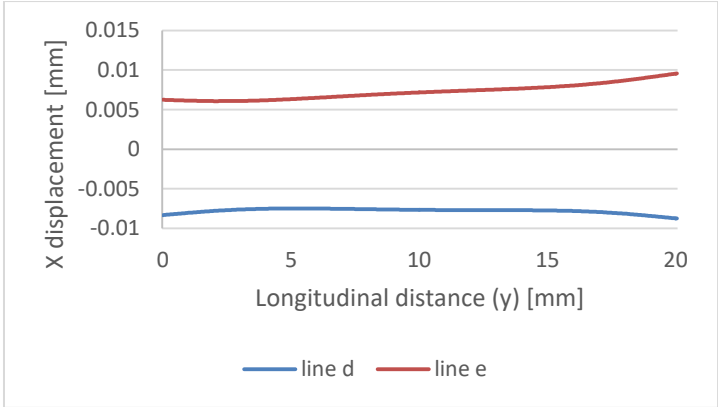


Figure 3.37 - X displacement along longitudinal lines (model 1 – butt joint)

### 3.2.4. Model 2 results

The second model is very similar to model 1. The main difference is in the duration of the clamping. The clamps of one of the plates are released after the tack weld. This means that during the welding process, this plate is free. Table 29 shows a summary of the results that will be demonstrated.

Table 29 – Results summary (model 2 – butt joint)

Item	Line(s)
Longitudinal stress (y-direction)	Transverse lines (top, bottom)
	Longitudinal lines (top, bottom)
Transverse stress (x-direction)	Transverse lines (top, bottom)
	Longitudinal lines (top, bottom)
Out of plane deformation (z-direction)	Transverse line (a, b, c)
Longitudinal deformation (y-direction)	Transverse lines (a, b, c)
Transverse deformation (x-direction)	Longitudinal lines (d, e)

#### 3.2.4.1. Longitudinal stress

This is the stress that occurs parallel to the welding path (y-direction). The following results, presented in Figure 3.38, are related with the end of the cooling phase. It is possible to notice that the greatest magnitude of the stresses in the longitudinal direction are concentrated near the weld bead.

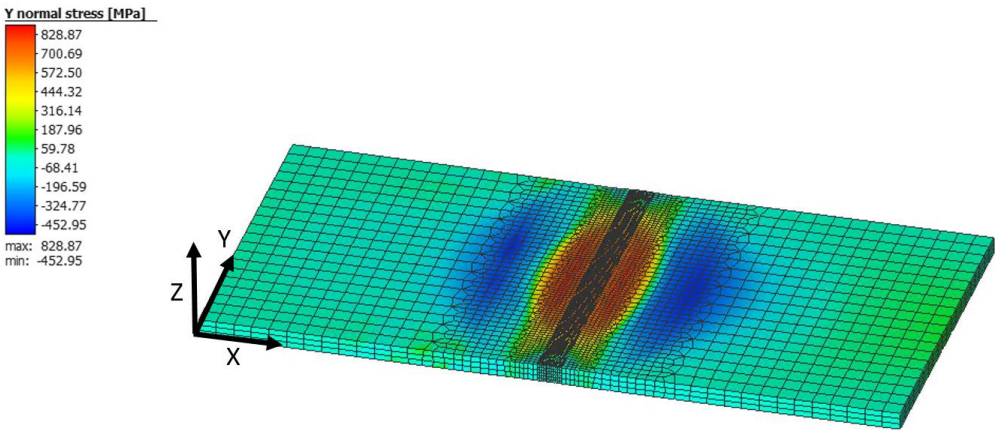


Figure 3.38 – Mapping of longitudinal stress in butt joint (model 2 – butt joint)

The longitudinal stress along transverse lines (Figure 3.39) has similar magnitude on the top and bottom surfaces of the plates. In addition, there is symmetry from the weld joint. In the area surrounding the weld bead, there are transverse stresses in a state of tension. Outside this zone, the plate is under compression. The maximum value of the residual stresses in the transverse direction is approximately 800 MPa. The minimum value is close to -450 MPa.

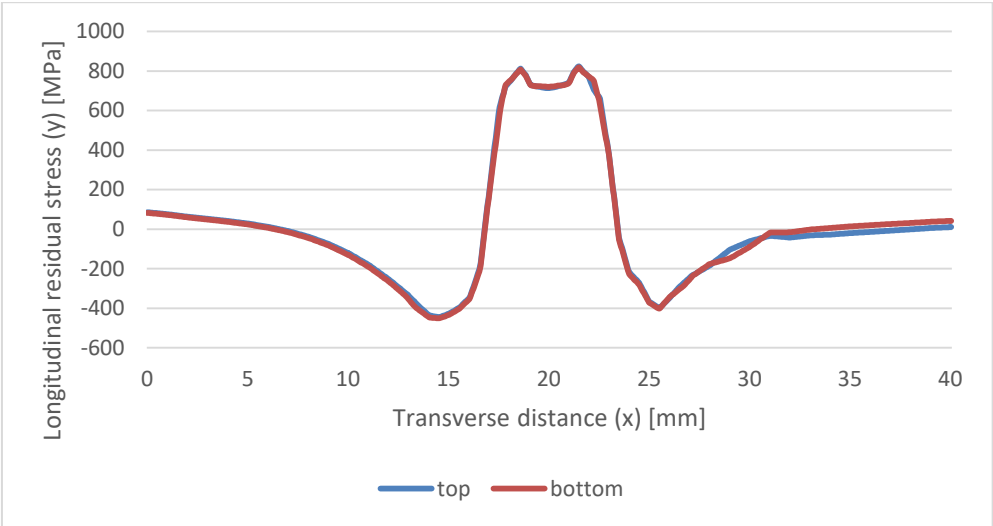


Figure 3.39 – Longitudinal residual stress along transverse lines (model 2 – butt joint)

Along the longitudinal lines the values of the longitudinal stress are very identical in the two surfaces (top and bottom). There is a slight difference at the beginning and at the end of the plate, being higher at the top. The residual stress profile (Figure 3.40) is symmetric with the center of the plate reaching a maximum at the point where the residual stress reaches 710 MPa.

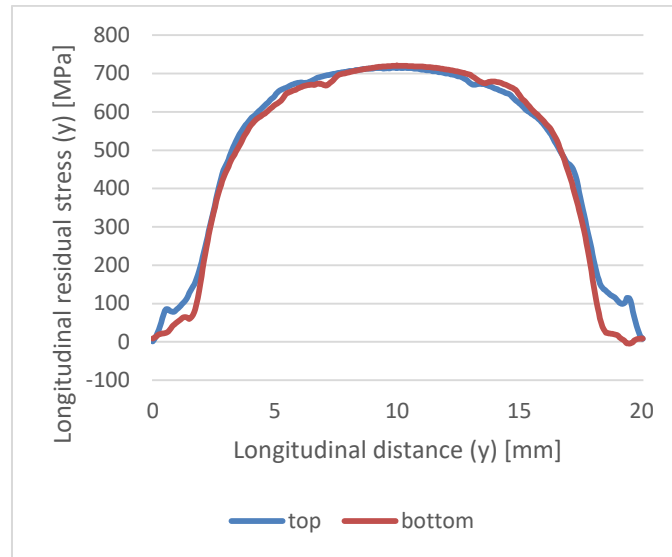


Figure 3.40 – Longitudinal residual stress along longitudinal lines (model 2 – butt joint)

### 3.2.4.2. Transverse stress

This is the stress that occurs in x-direction (Figure 3.41). The following numerical results show that the residual stresses have a constant distribution along the metal sheets. Since one of the plates (Plate B) is free during the welding process, it is possible to see some differences. Plate B is positioned between 0 and 20 mm, and plate A is between 20 mm and 40 mm.

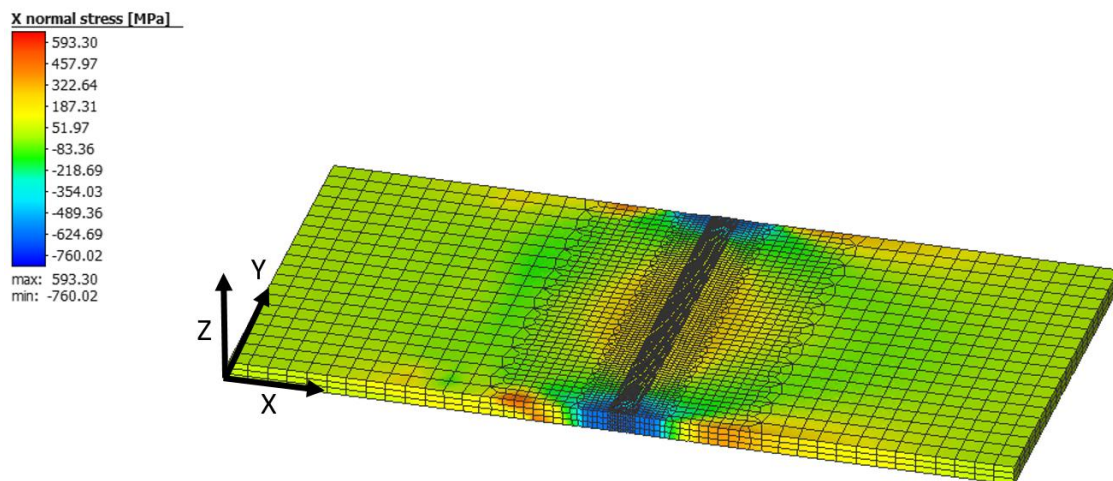


Figure 3.41 – Mapping of transverse stress in butt joint (model 2 – butt joint)

The transverse stresses along transverse lines have a difference between bottom and top surfaces, and there is no symmetry between the plates. Plate A is fixed during the whole process and it is possible to see in Figure 3.42 that it presents a more unstable stress. Plate B, which is free to move, initially presents a slight state of compression reaching its maximum value near  $-50$  MPa. From this point on, the magnitude of the residual stress in the transverse direction begins to increase until reaching a maximum close to  $250$  MPa. Plate B presents a bigger state of compression and a more severe difference between the two surfaces. The minimum value reaches  $-210$  MPa.

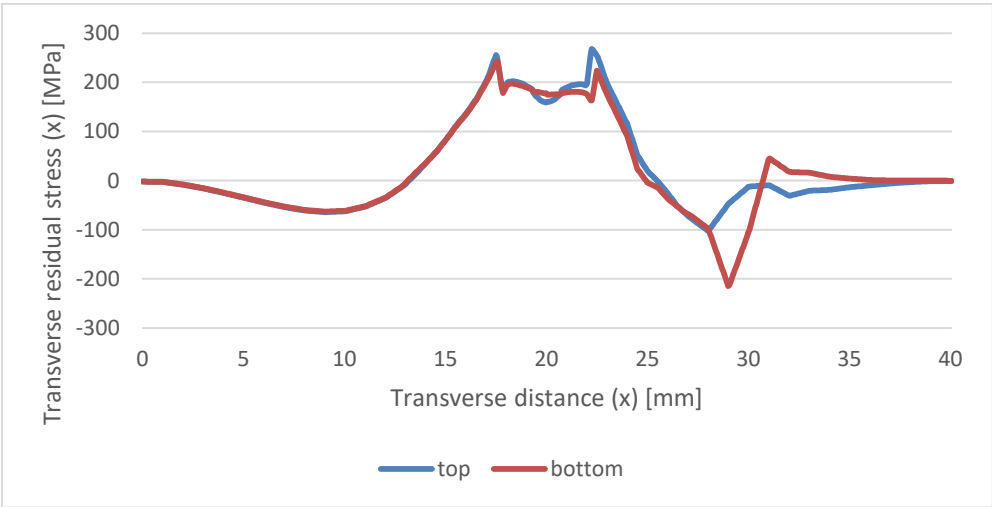


Figure 3.42 – Transverse residual stress along transverse lines (model 2 – butt joint)

There is a symmetrical behavior of the profile of the transverse stresses along the longitudinal lines, centered on the weld bead. The difference between the top and bottom surfaces is minimum. Initially, the plates are under compression with a maximum value around  $-650$  MPa. The maximum value is in the center of the weld bead where it reaches close to  $200$  MPa as Figure 3.43 illustrates. A large area of the plates is under a tension state.



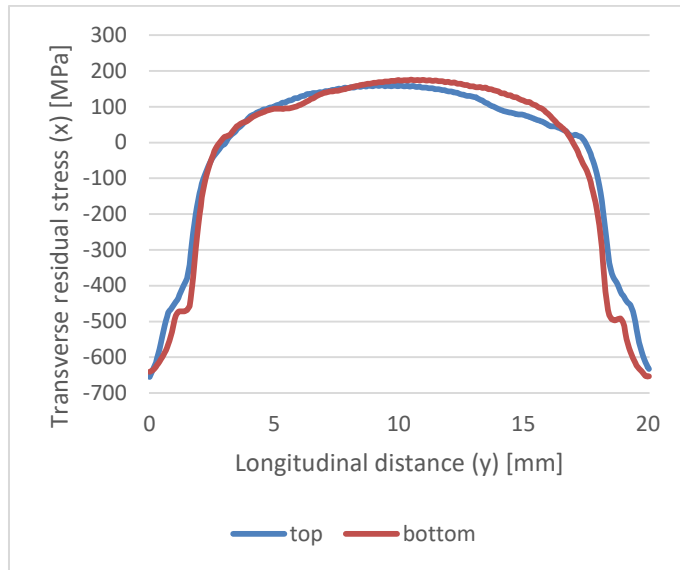


Figure 3.43 – Transverse residual stress along longitudinal lines (model 2 – butt joint)

### 3.2.4.3. Out-of-plane deformation

The displacement in the normal direction is minimum in this model as shown in Figures 3.44 and 3.45. Plate B is free to move during the welding process. However, there is lower deformation of this plate in the z-direction. The greatest deformation occurs in the joint area due to the formation of the weld bead.

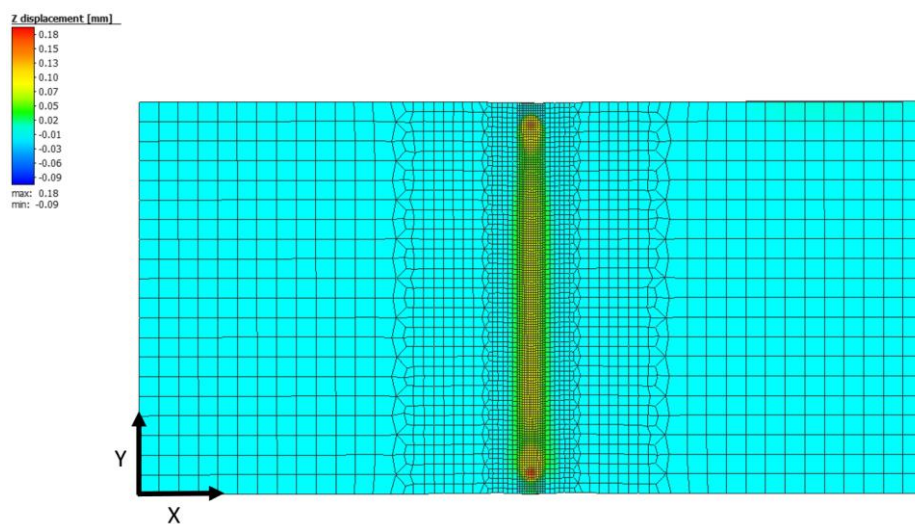


Figure 3.44 – Top view of Z displacement (model 2 – butt joint)

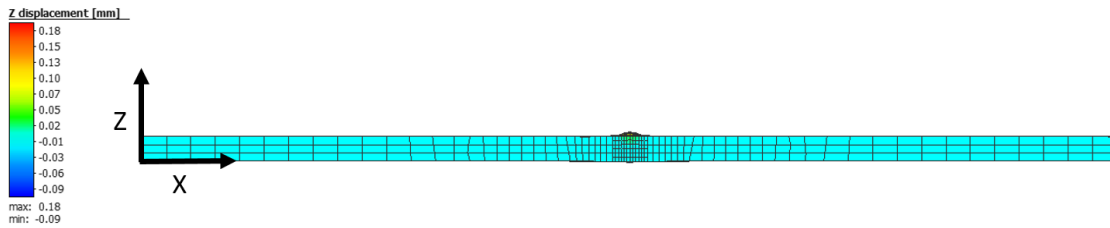


Figure 3.45 – Side view of Z displacement (model 2 – butt joint)

The deformation of three lines is presented in Figure 3.46. Plate B is positioned between 0 and 20 mm and it is the one that is free to move. This plate has a negative displacement right after passing the weld bead area. At the beginning of plate B the displacement is zero. Plate A is between 20 mm and 40 mm and is locked during the entire process. In the area, where the clamps are applied (27.5 mm to 32.5 mm), the displacement in z direction is zero. From this point there is a displacement with a magnitude of -0.01 mm.

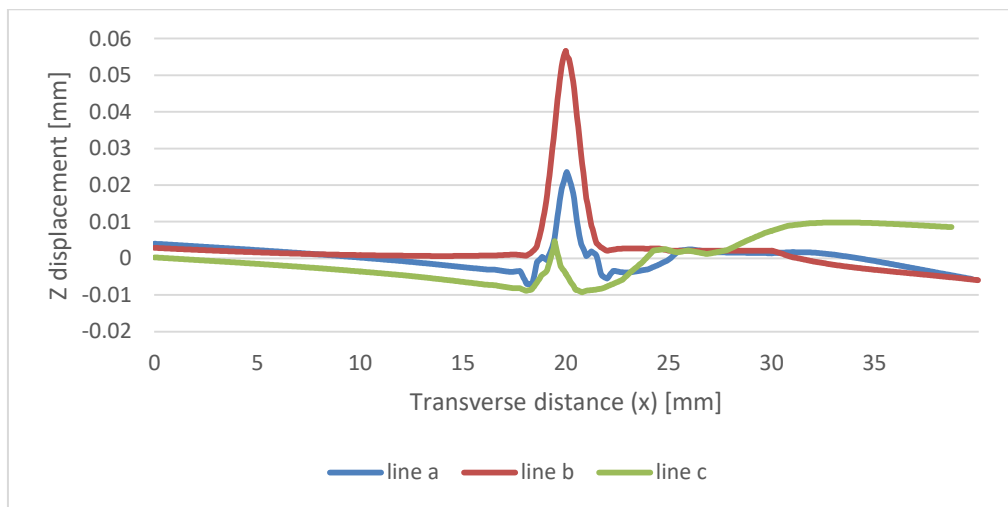


Figure 3.46 - Z displacement along transverse lines (model 2 – butt joint)

#### 3.2.4.4. Longitudinal deformation

This deformation occurs parallel to the welding direction (y direction). Through the analysis of Figure 3.47, it is possible to verify that there is a rotational deformation due to the B plate being free to move. This means that transverse shrinkage is not the same along the weld bead. In this case, there is a bigger shrinkage at the end of the weld bead than at the beginning, which means that the welding speed is high.

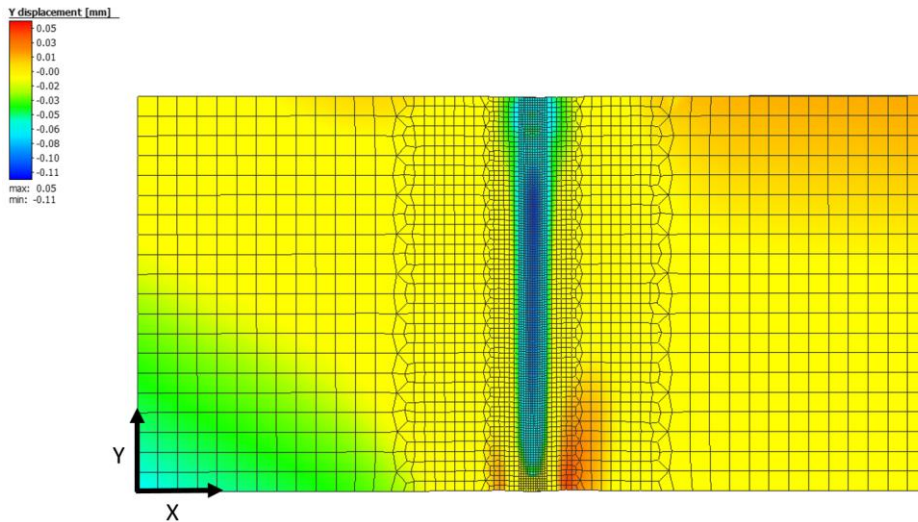


Figure 3.47 – Top view of Y displacement (model 2 – butt joint)

The deformation in the y direction is significantly higher on plate B, which is free during the process. Through the graph in Figure 3.48 it is possible to conclude that plate B has a maximum negative displacement close to -0.06 mm. The behavior along the width is not uniform. At the beginning the displacement is negative and at the end it is slightly positive. This is directly related to the welding direction. Plate A, which is clamped, has a minimum displacement. However, in the area most thermally affected by the heat released by the laser beam, there is a symmetrical longitudinal shrinkage.

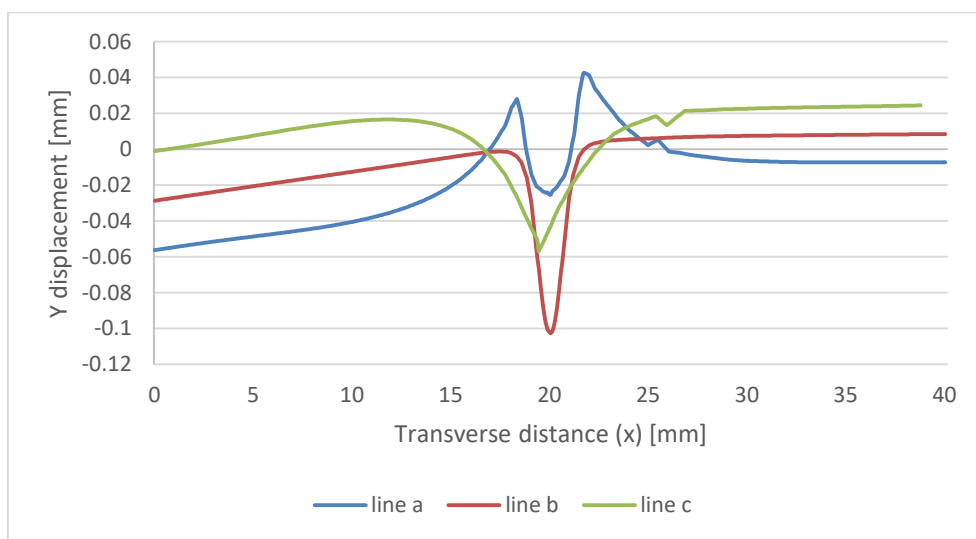


Figure 3.48 – Y displacement along transverse lines (model 2 – butt joint)

**3.2.4.5. Transverse deformation**

The deformation that occurs in the x direction (Figure 3.49) is directly related to the total length of the assembly after the welding process. Since one of the plates is free and the other fixed, there is no symmetry between the two lines positioned at the longitudinal edges of the two plates.

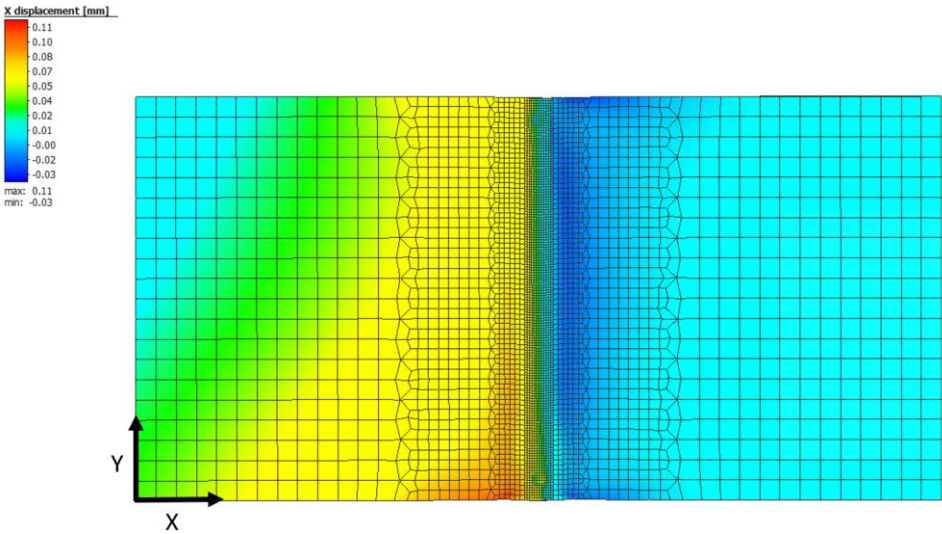


Figure 3.49 – Top view of X displacement (model 2 – butt joint)

Figure 3.50 shows the displacements in x-direction. Line e, which is positioned at the end of plate A, which is fixed, shows that there is a constant displacement in the x direction near 0.017 mm. It is possible to verify that there has been a rotational deformation of plate B that is free during the whole welding process.

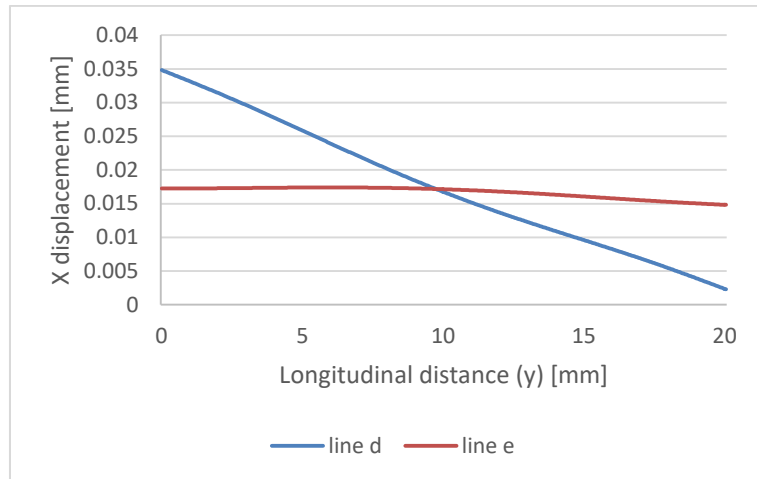


Figure 3.50 - X displacement along longitudinal lines (model 2 – butt joint)

### 3.2.5. Comparison between Butt joint models

To better understand the differences between the two butt joint models, the results from both models are compared. The plates of the first model are clamped during the welding and cooling phases. In the second model, plate B is free to move after the tack weld. All other factors that can influence the residual stress, such as material, geometry and welding procedure are exactly the same.

#### 3.2.5.1. Longitudinal stress

Longitudinal stress acts parallel to the welding direction (y direction). According to Figure 3.51, it is possible to conclude that these stresses are very similar in both models. So, the clamping conditions have little influence on the presence of the longitudinal stresses along the longitudinal and transversal lines of the two models. It can be observed that there are compressive (-) and tensile (+) states on both plates. The area near the weld bead is under a state of tension (+) while the area further away, which is thermally less affected, has a low state of compression (-). The maximum residual stress is near the weld bead due to the high amount of heat released in this zone. The difference between top and bottom surfaces is insignificant.

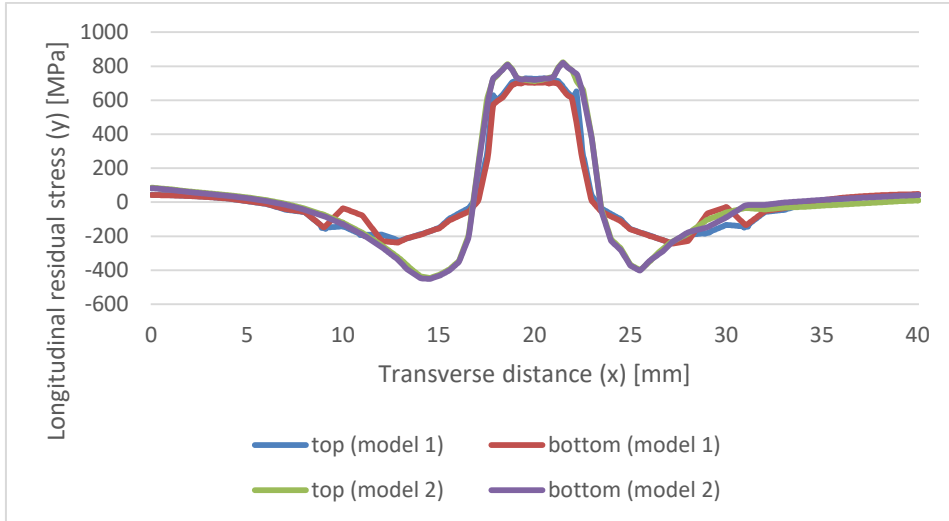


Figure 3.51 – Comparison of longitudinal residual stress along transverse line of butt joint models

The longitudinal stresses along the longitudinal lines present a superior magnitude compared to the stresses along the transverse lines. These are in tension state (+) and the maximum is at the centre of the weld bead (Figure 3.52). This happens because the temperature gradient in this area is significantly higher, causing higher concentration of residual stresses. The stress magnitude decreases with the increase of the distance from the weld bead.

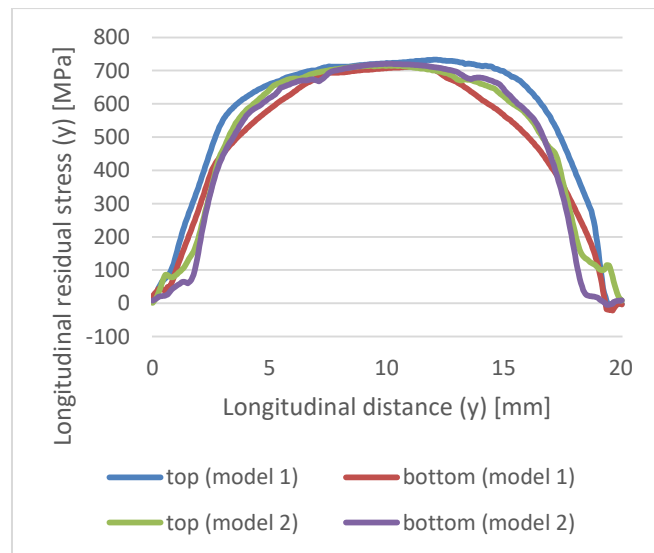


Figure 3.52 - Comparison of longitudinal residual stress along longitudinal line of butt joint models

**3.2.5.2. Transverse stress**

There is a great discrepancy in the stress profile in x direction between the two models. That means that transverse stress magnitude is strongly dependent on the clamping conditions. Model 1, which is fixed during the whole process, has higher transverse residual stresses. The plates in model 2 are not clamped and are free to expand in transverse direction, so the transverse stress is lower.

Figure 3.53 shows the comparison of transverse residual stresses along transverse lines of both models. In the first 10 mm of each plate, residual stresses are low, since this area is not as affected by the heat released by the laser beam. However, approaching the weld bead, the existing stresses are higher. There is a difference close to 400 MPa between model 1 (fully constrained) and model 2 (which has 1 plate free). There is a tensile state (+) on both plates. However, in model 2, in the area between the joint and the extremity of the plate, there is a state of compression (-).

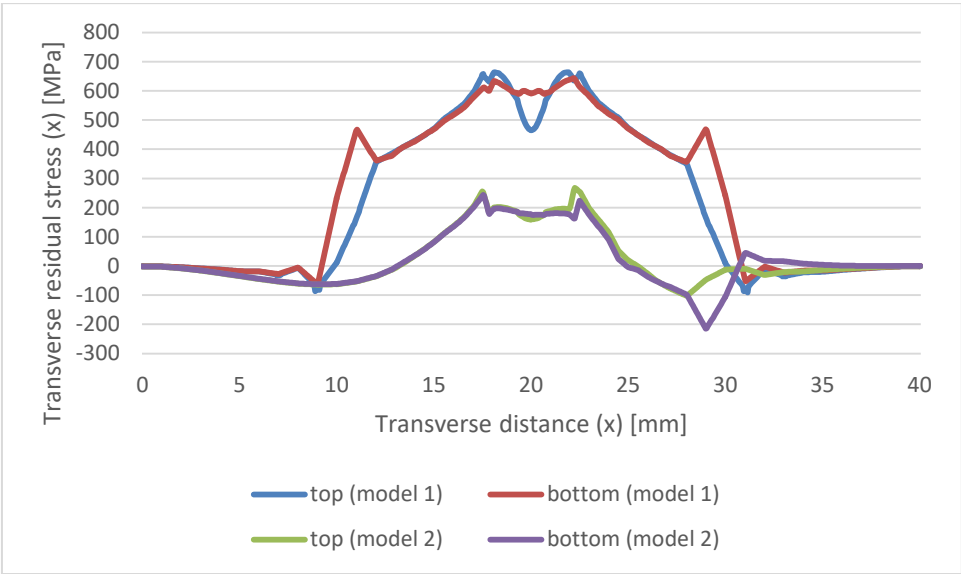


Figure 3.53 - Comparison of transverse residual stress along transverse lines of butt joint models

The transverse residual stress along longitudinal lines is presented in Figure 3.54. The profile of residual stresses is identified in both models. At the edges of the plate, there is a compression state (-) near -600 MPa for both models. It is possible to verify that there are higher transverse residual stresses in model 2. In addition, there is a larger discrepancy

between the top and the bottom surfaces of the model 2. The maximum in the bottom surface is near 600 MPa and in the top surface is close to 500 MPa. Model 1 has lower residual stresses along longitudinal lines. The peak value in this model is 200 MPa.

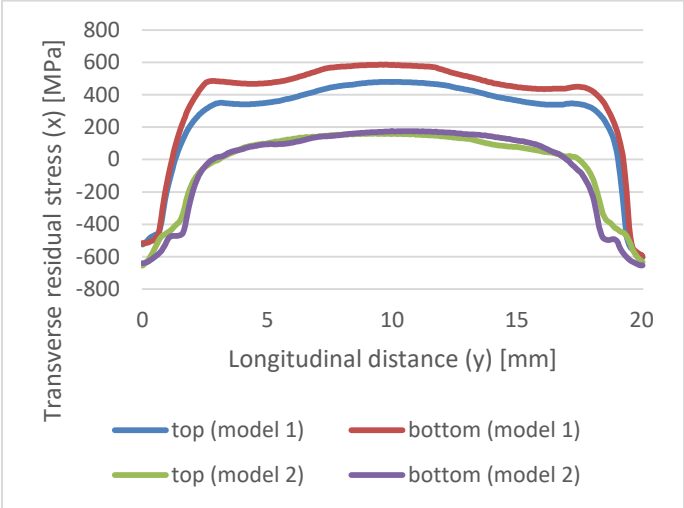


Figure 3.54 - Comparison of transverse residual stress along longitudinal lines of butt joint models

**3.2.5.3. Z displacement**

There is greater deformation at the edges of the plates in model 1, which has the plates fixed throughout the process. In the weld bead area the behaviour is similar for both models as shown in Figure 3.55.

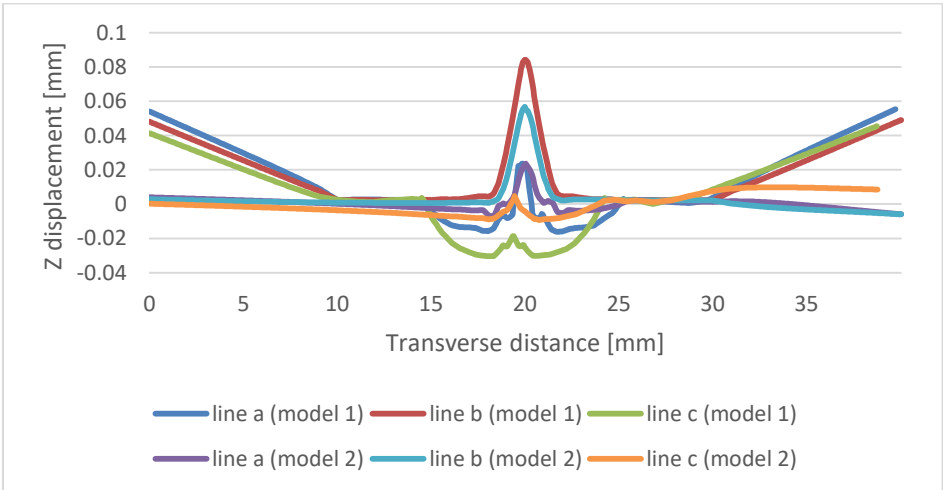


Figure 3.55 - Comparison of Z displacement of butt joint models



**3.2.5.4. Y displacement**

In model 2 there is a greater deformation in y-direction (Figure 3.56). This happens due to the existing rotational deformation, a consequence of the high welding speed.

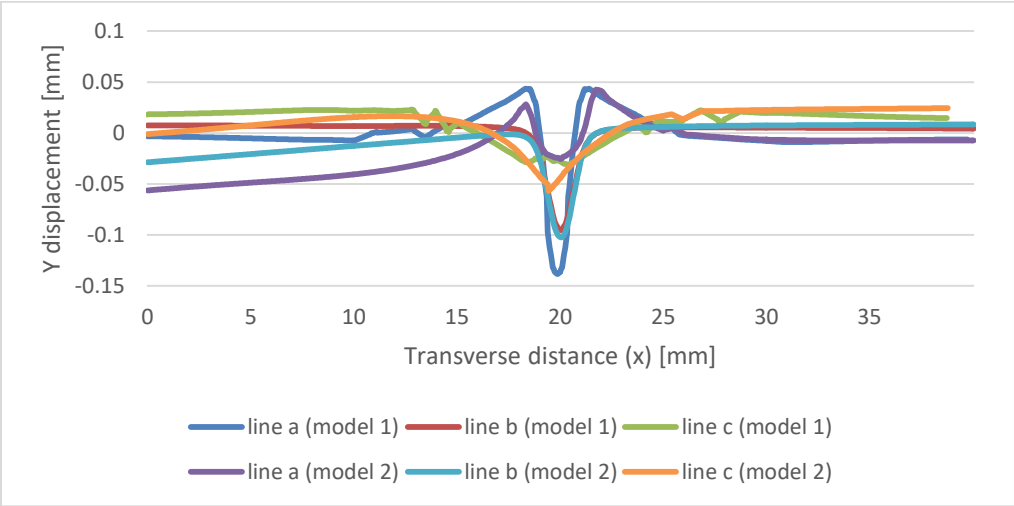


Figure 3.56 - Comparison of Y displacement of butt joint models

**3.2.5.5. X displacement**

There is a smaller displacement in x-direction in model 1, as can be seen in Figure 3.57.

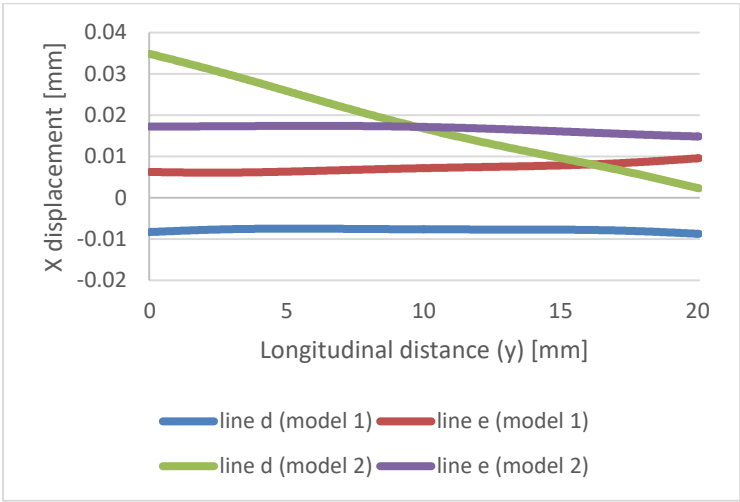


Figure 3.57 - Comparison of X displacement of butt joint models

### 3.2.6. Model 3 results

The last model consists of welding two plates in a T-joint configuration. Initially, all the plates are clamped and after the tack welds, the vertical plate is released to become free to move. Table 30 shows a summary of the results of the stresses and deformations of the vertical plate and horizontal plate of the T joint model.

Table 30 – Results summary (model 3 – T joint)

Item	Plate	Line(s)
Transverse Stress	Vertical (z-direction)	Transverse (left, right)
		Longitudinal (weld bead)
	Horizontal (x-direction)	Transverse (top, bottom)
		Longitudinal (weld bead)
Longitudinal Stress	Vertical (y-direction)	Transverse (left, right)
	Horizontal (y-direction)	Longitudinal (weld bead)
		Transverse (top, bottom)
X displacement	Vertical	Transverse (3a, 3b, 3c)
	Horizontal	Longitudinal (d, e)
Y displacement	Vertical	Transverse (3a, 3b, 3c)
	Horizontal	Transverse (a, b, c)
Z displacement	Vertical	Longitudinal (3d, 3e)
	Horizontal	Transverse (a, b, c)

#### 3.2.6.1. Transverse stress

The residual transverse stress occurs perpendicular to the weld bead. In the vertical plate it is in the z-direction and in the horizontal plate, it is in the x-direction.

The z-stress is the transverse residual stress of the vertical plate. At the lower extremity of the vertical plate, there is a higher concentration of transverse stress as can be seen in Figure 3.58. However, in the center of the plate, where the monitoring transverse lines (left and right surface) are positioned, these stresses are slightly lower.

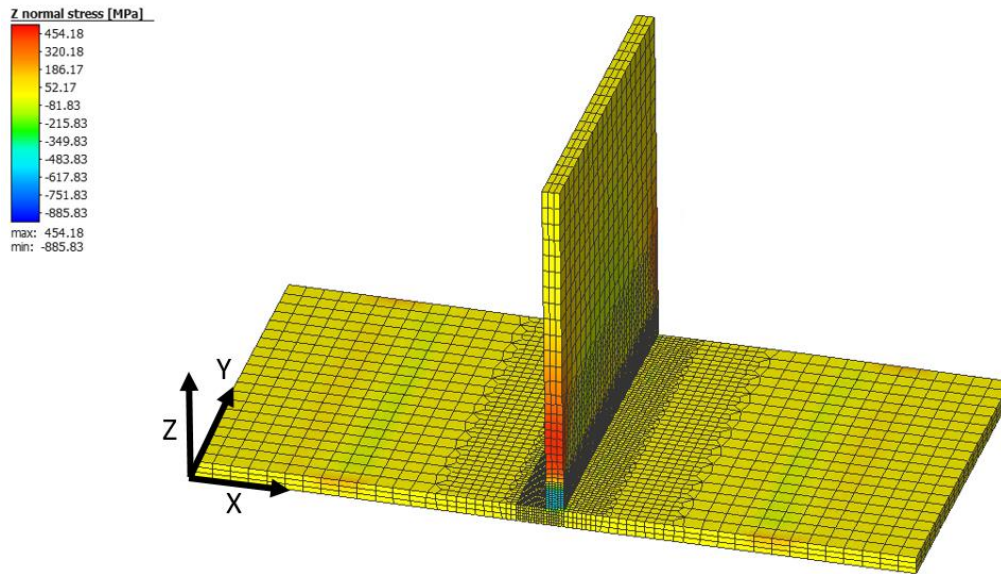


Figure 3.58 – Mapping of the stress in z-direction (model 3 – T joint)

Figure 3.59 shows the magnitude of the transverse residual stresses along the two transverse monitoring lines. The origin corresponds to the weld bead and the 20 mm to the top of the vertical plate. First, it is possible to conclude that there is a very small influence of the residual stress along the thickness of the vertical plate. Secondly, there is a higher residual stress near the weld bead. Initially, between 0 mm and 1 mm, there is a state of compression that reaches -70 MPa. The state of tension occurs between 1 and 3 mm. From this point, there is again a state of compression, which reaches its peak near -100 MPa and decreases until it reaches 0 MPa, which coincides with the top of the vertical plate.

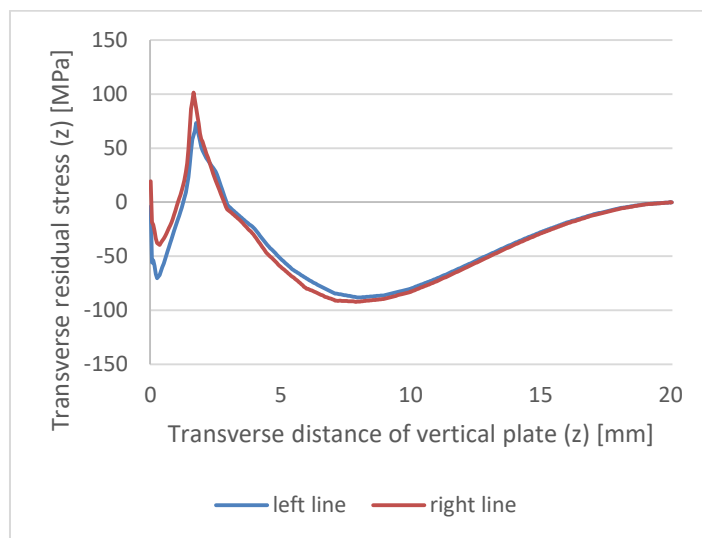


Figure 3.59 - Transverse residual stress along transverse lines of vertical plate (model 3 – T joint)

Figure 3.60 shows the presence of transverse residual stresses of the horizontal plate, which occur in the x-direction. By the analysis, it is possible to verify that there are 2 zones of the horizontal plate with a higher concentration of stress in tension state: in the edges and in the centre of the weld bead.

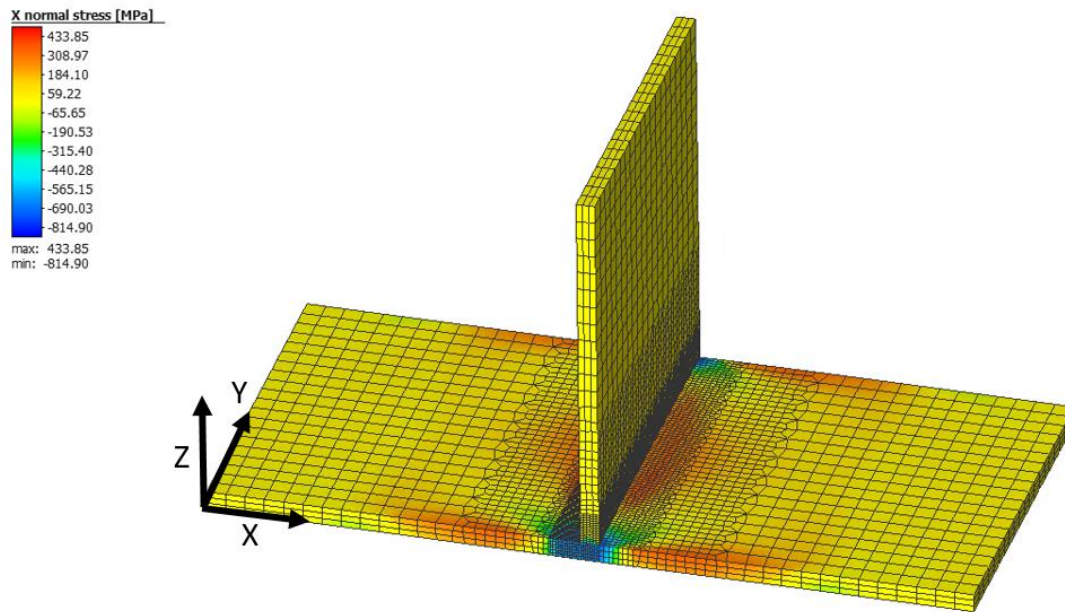


Figure 3.60 - Mapping of the stress in x-direction (model 3 – T joint)

Figure 3.61 shows the transverse stresses that occur on the top and bottom surfaces of the horizontal plate, monitored through the transverse lines. It is possible to verify that the stresses that exist along these lines are in tension state, reaching a maximum in the central zone of the weld bead, near 350 MPa. There is an insignificant difference between the magnitudes of the stresses along the horizontal plate thickness. The residual stresses are zero at the edges of the horizontal plate and increase symmetrically as it approaches the joint. In the centre of the weld bead, there is a significant decrease of the residual tension close to 170 MPa.

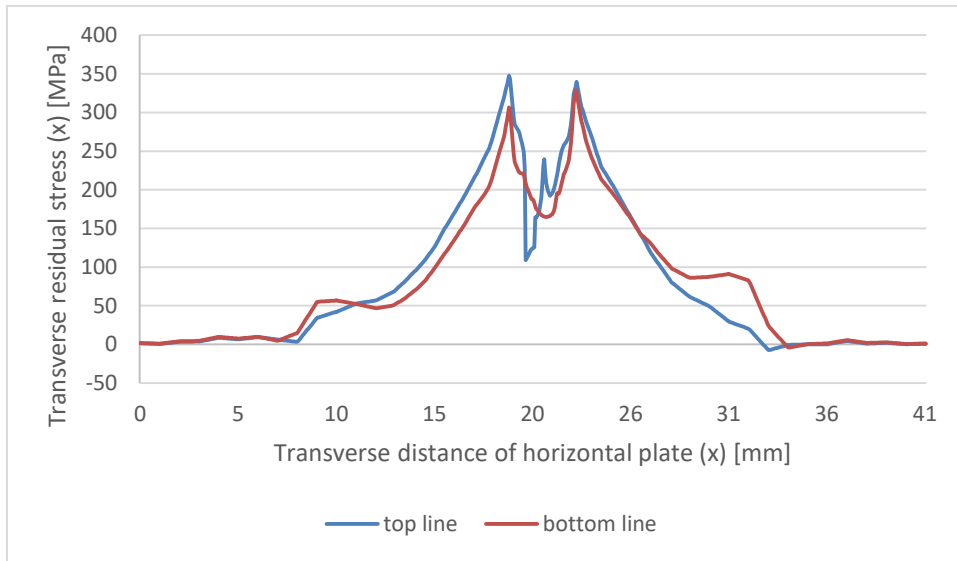


Figure 3.61 - Transverse residual stress along transverse lines of horizontal plate (model 3 – T joint)

The transverse residual stress along the longitudinal line (Figure 3.62) occurs in x-direction on the horizontal plate and in z-direction on the vertical plate. There is a significant difference between the values of the vertical plate and the horizontal plate. Both curves are symmetrical relatively to the centre of the weld bead.

The horizontal plate has a greater range of residual stresses in the transverse direction. It starts with a state of compression that reaches -700 MPa. From  $y = 3$  mm, it passes to a tension state with a maximum close to 200 MPa in the centre ( $y = 10$  mm).

The vertical plate has practically no residual stress in the transverse direction. This happens since it is free to move during the welding process. However, there is a slight state of compression at both edges near - 290 MPa.

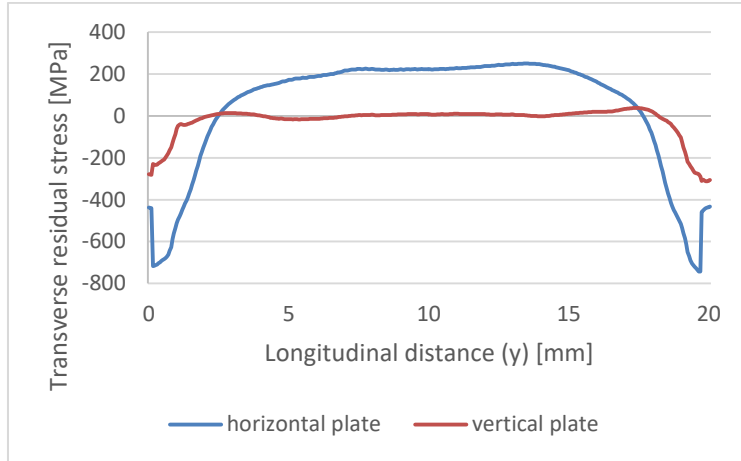


Figure 3.62 - Transverse residual stress along longitudinal line (model 3 – T joint)

### 3.2.6.2. Longitudinal stress

The stress in vertical and horizontal plates that occurs in the direction parallel to the welding path (y-direction) is present in Figure 3.63. It is possible to visualize that the area with the highest presence of residual tensions is near the welding bead.

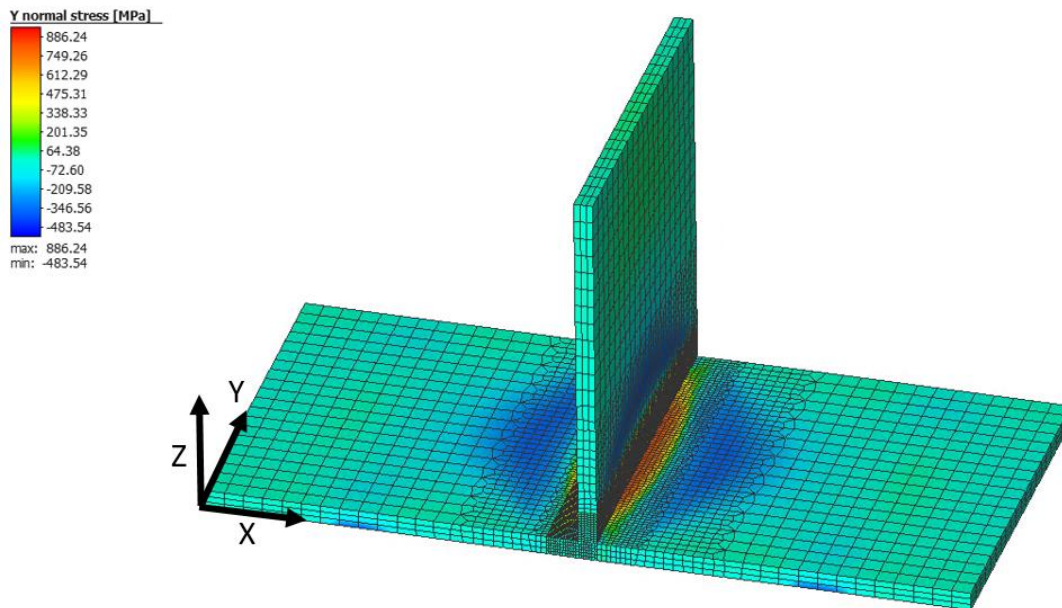


Figure 3.63 - Mapping of the stress in y-direction (model 3 – T joint)

The longitudinal residual stress (Figure 3.64) along the horizontal plate transverse lines has a very identical behavior at the top and bottom surfaces. In addition, there is a symmetry in

residual stresses, centered on the joint ( $y = 21 \text{ mm}$ ). At both edges, the residual stress is zero. As we approach the weld bead, a state of compression begins to exist with a peak near  $-400 \text{ MPa}$ . In the central zone, there is a state of tension with a maximum around  $800 \text{ MPa}$ .

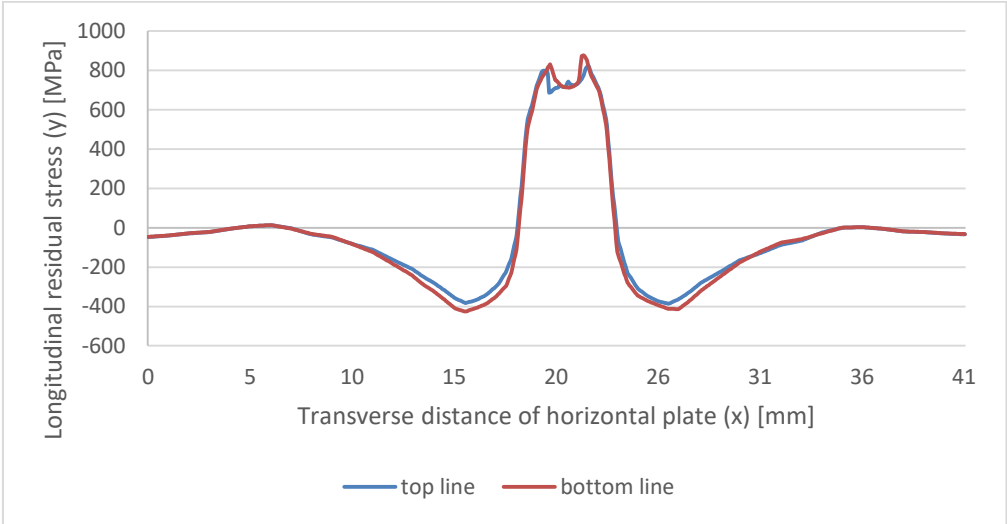


Figure 3.64 - Longitudinal residual stress along transverse lines of horizontal plate (model 3 – T joint)

The longitudinal residual stress in the vertical plate is shown in Figure 3.65. At the edge of the vertical plate, near the weld bead, there is a tension state close to  $800 \text{ MPa}$ . This state decreases up to  $y = 3 \text{ mm}$ , when it changes to a compression state. The minimum value is  $-400 \text{ MPa}$ , which increases until zero is reached.

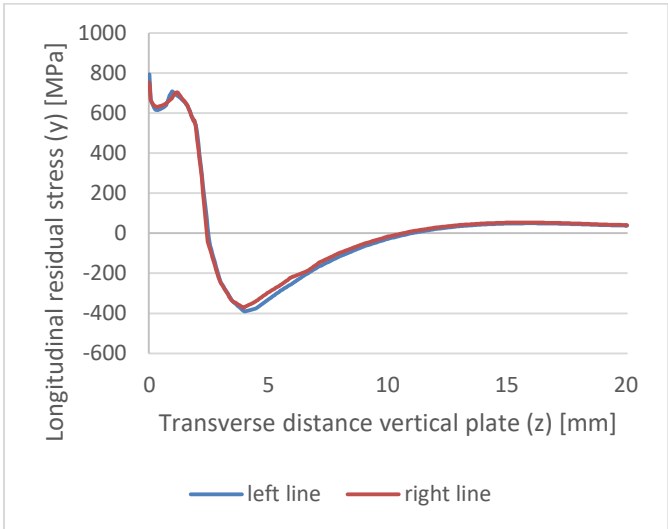


Figure 3.65 - Longitudinal residual stress along transverse lines of vertical plate (model 3 – T joint)

The longitudinal residual stress (y-direction) that occurs in the longitudinal line, which is common to vertical and horizontal plates, is presented in Figure 3.66. There is symmetry relatively to the center of the weld bead. Excluding the edges, the longitudinal residual stresses existing after the welding process are in tension state with a maximum close to 740 MPa.

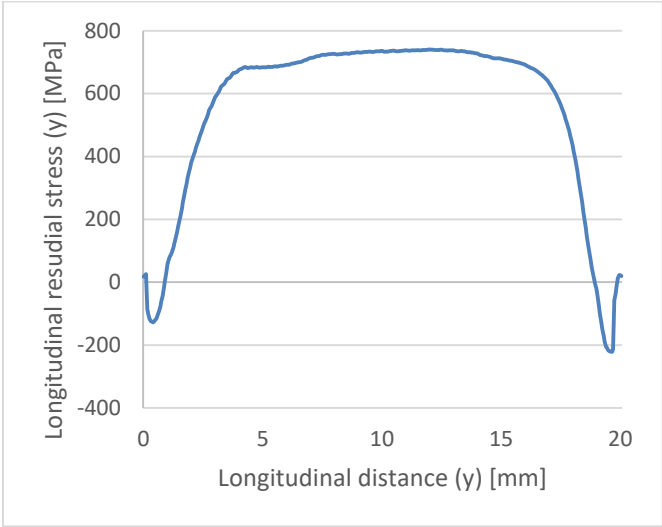


Figure 3.66 - Longitudinal residual stress along longitudinal line (model 3 – T joint)

### 3.2.6.3. X displacement

The deformation in the x-direction is significantly higher on the vertical plate since it is free during the welding process. Figure 3.67 shows that the horizontal plate has minimum displacement. This happens because the horizontal plate is clamped during the whole process. The angular rotation that exists on the vertical plate in relation to the horizontal plate is visible in Figure 3.68.



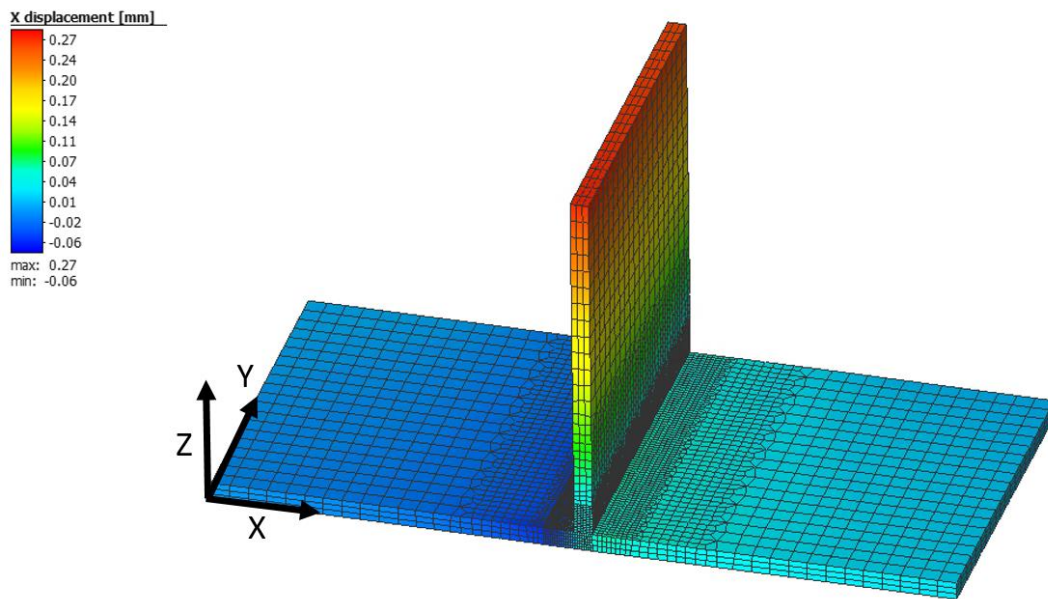


Figure 3.67 - Overview of X displacement (model 3 – T joint)

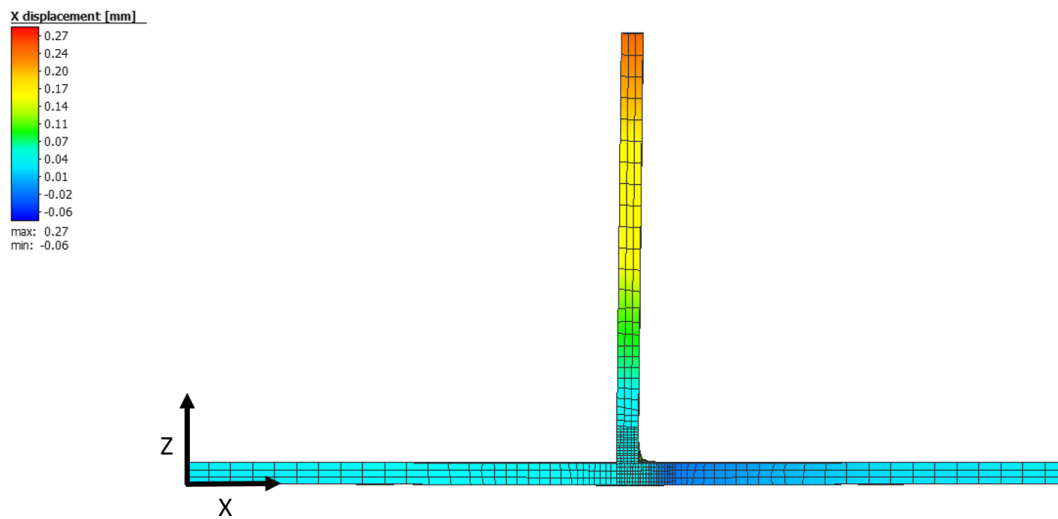


Figure 3.68 – Side view of X displacement (model 3)

In Figure 3.69, it is possible to verify that the vertical plate deformed in a linear way and has an equal behaviour along the width (y-direction). The average maximum displacement of the three lines has a magnitude of 0.26 mm and it is at the top of the plate. The vertical plate has a total length of 20mm. This means that the plate has an angular deformation of approximately 1.6 degrees after the cooling cycle. The bend occurs in the side where the weld bead is. The deformation at the beginning of the plate, related to the generation of the

weld bead, is negligible since it corresponds to a very small portion of the plate and has no influence on the angular deformation.

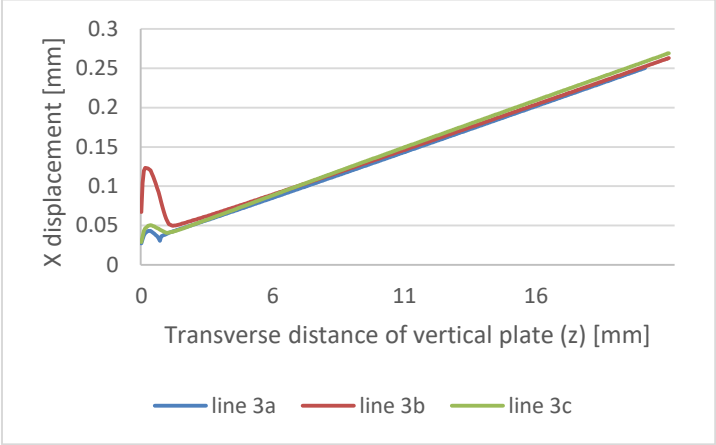


Figure 3.69 – X displacement along transverse lines of the vertical plate (model 3 – T joint)

It is possible to observe in Figure 3.70 that there is a positive rotational deformation (scissor effect) in the horizontal plate. This means that the distance between the edges of the horizontal plate tends to decrease. This effect is more significant as we move away from the starting point of the welding. There is a symmetrical behaviour in relation to the joint.

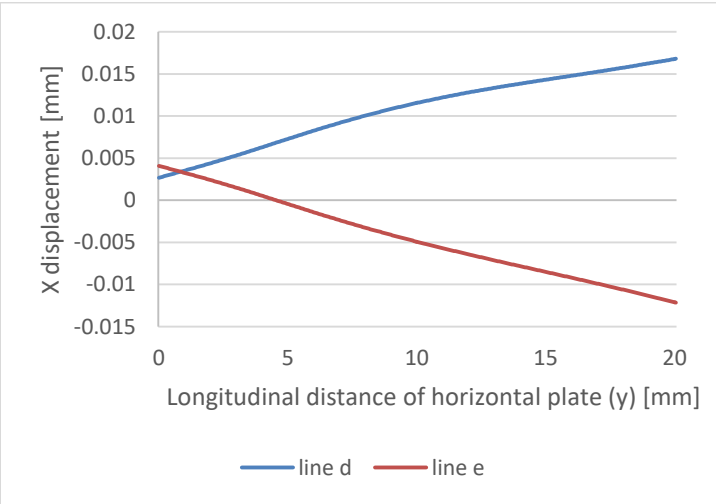


Figure 3.70 – X displacement along longitudinal lines of horizontal plate (model 3 – T joint)

### 3.2.6.4. Y displacement

The displacement in the direction of the weld bead (y-direction) is practically zero on both plates, except in the area of the weld bead, as shown in Figure 3.71.

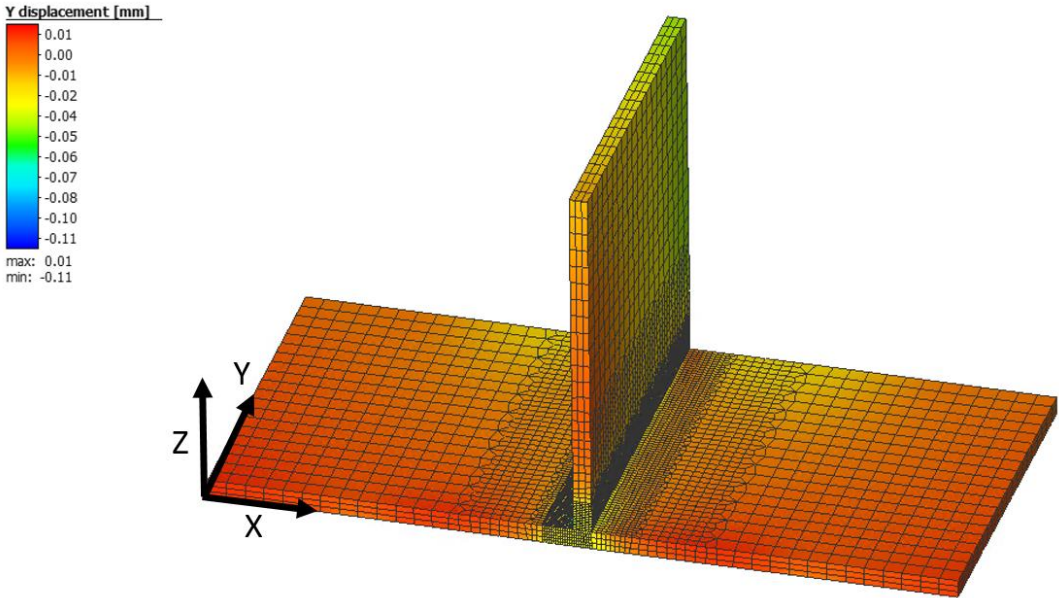


Figure 3.71 - Overview of Y displacement (model 3 – T joint)

The horizontal plate has a small transverse shrinkage effect along the edges. In Figure 3.72, it is possible to see that there is a higher shrinkage magnitude near the centre of the weld bead with  $\pm 0.02$  mm. At the joint area, where the metal reaches high temperatures, there is a large displacement in the y-direction that reaches -0.1 mm. However, this displacement represents a small portion of the plate and therefore, it is insignificant.

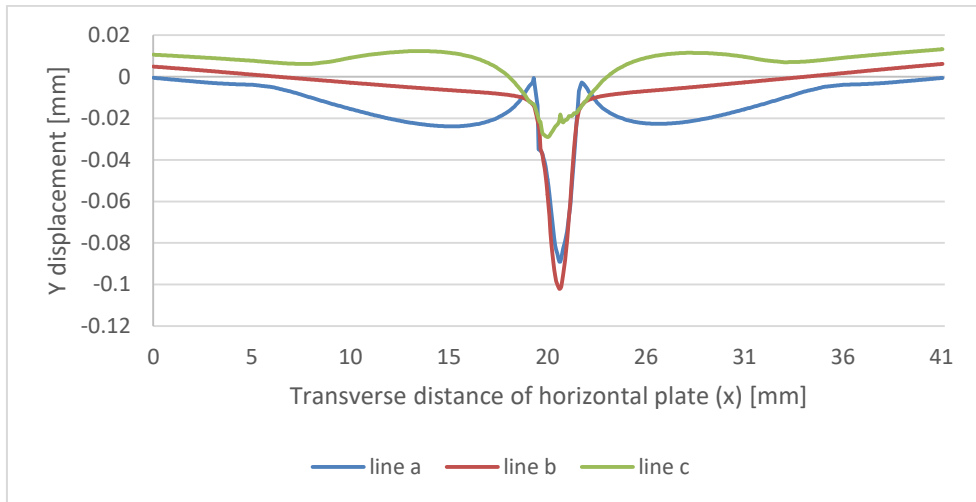


Figure 3.72 – Y displacement along transverse lines of the horizontal plate (model 3 – T joint)

Analysing the vertical plate, it is possible to verify that there is also a small transverse shrinkage as shown in Figure 3.73. However, this behaviour is not uniform along the plate. At the beginning (line 3a) it is possible to see that there is a displacement near -0.04 mm. At the middle of the plate (line 3b) these displacements are already lower: -0.02 mm. Finally at the end of the plate (line 3c), this displacement is practically 0. As with the horizontal plate, there is a severe displacement in the weld bead area that reaches -0.1mm.

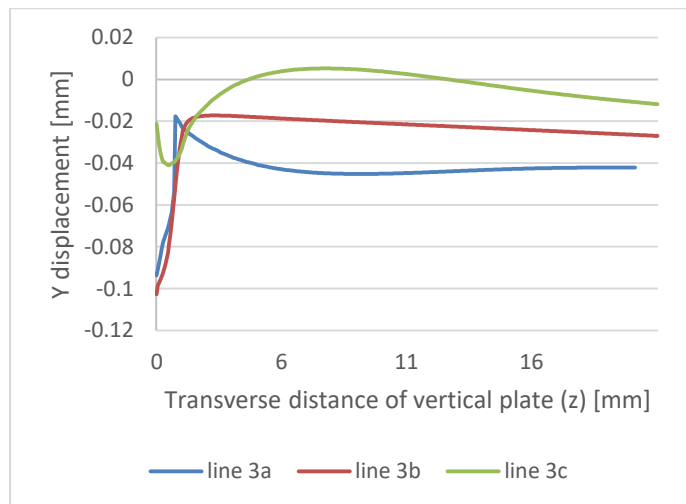


Figure 3.73 – Y displacement along transverse lines of the vertical plate (model 3 – T joint)

### 3.2.6.5. Z displacement

The Z displacement at the end of the cooling stage is present in Figure 3.74. Outside the weld bead zone, this displacement is practically zero. The displacement of the vertical plate influences its length.

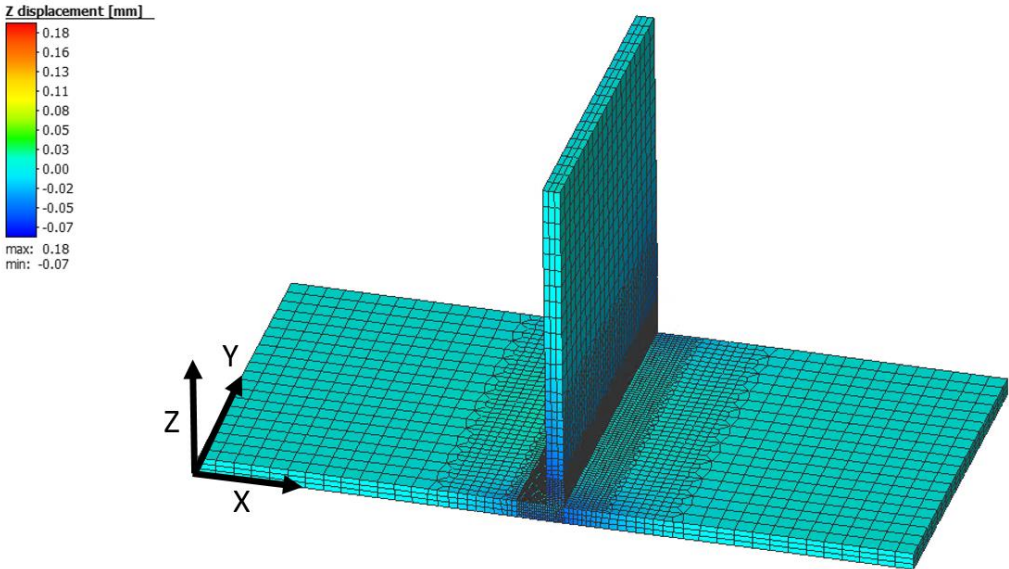


Figure 3.74 – Overview of Z displacement (model 3 – T joint)

The out-of-plane displacement of the horizontal plate is shown in Figure 3.75, through the three transversal lines previously defined. There is a symmetry behaviour in relation to the joint ( $x = 21$  mm). It is important to notice that the horizontal plate is clamped and therefore, in these zones the displacement in z-direction is zero. In the area between the clamps and the weld bead, there are 2 types of behaviour. In the central zone, represented by line b, there is a positive displacement peak with a maximum of 0.08 mm. At the edges (lines a and b), there is a negative displacement with a maximum near -0.04 mm.

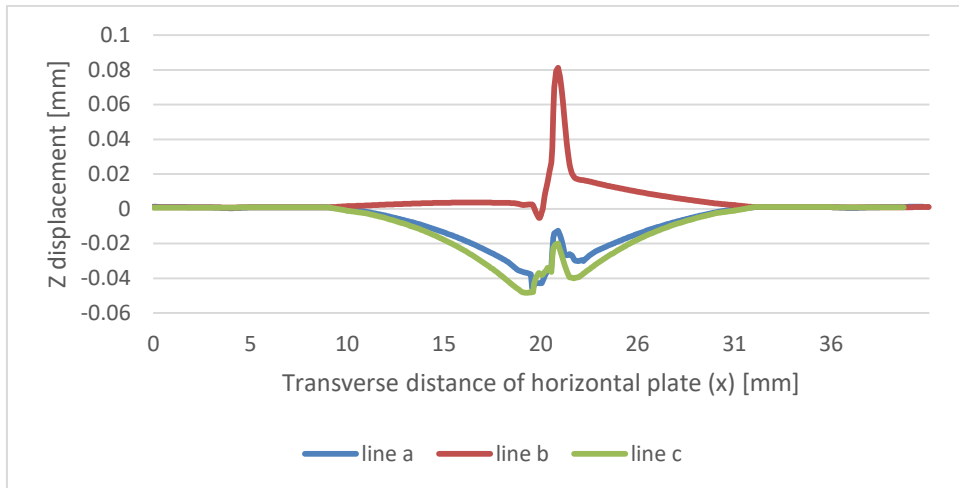


Figure 3.75 – Z displacement along transverse lines of horizontal plate (model 3 – T joint)

In Figure 3.76, it is possible to verify that there is practically no increase in the length of the vertical plate after the welding process. The 3e line, which is positioned on the top surface of the plate, has a very small displacement. The largest value is at the beginning of the plate ( $y = 0$ ), where the welding bead begins to be generated, and has a magnitude of -0.01 mm. The line that is positioned at the base of the vertical plate (line 3d), presents a different behaviour compared with the line 3e. At the edges, there is a displacement peak that reaches 0.08 mm. This displacement decreases significantly to 0 and then increases again, stabilizing at 0.02 mm. There is a symmetric behaviour in relation to the centre of the plate ( $y = 10$ ).

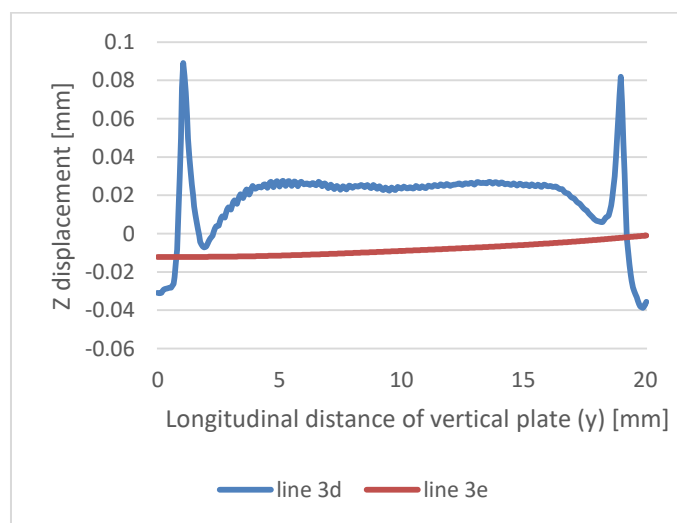


Figure 3.76 - Z displacement along longitudinal lines of the vertical plate (model 3 – T joint)



## 4. CHAPTER 4 – GENERAL CONCLUSIONS

This chapter discusses the obtained results and their conclusions. The difficulties experienced in carrying out this work are explained after the conclusions. In order to ensure the continuity of the work developed, some proposals for future works are presented.

### 4.1. Conclusions

---

Predicting the behaviour of the parts after the welding process is extremely important and mandatory in product development. Numerical simulation is a powerful tool, used in this work.

This work allowed the study of the stresses and strains resulting from the Nd:YAG laser welding process. Two types of assemblies (butt and T-joint) of two AHSS metal sheets with 1mm of thickness were studied. Three numerical models with different parameters were developed using the Simufact software. A fixed power of 4 kW and a welding speed of 3m/min was used.

This work represents the kick-off of welding simulation in the Mechanical Engineering Department of the University of Aveiro. Consequently, the development of this work was challenging because there was no in-depth knowledge on this theme or previous/reference works.

With this work, some conclusions were achieved:

- a) In the butt joint models, the **longitudinal residual stress**, which acts parallel to the welding direction, is not affected by the clamping conditions.
  - i. The longitudinal stress along the transverse lines has a symmetrical profile in relation to the weld bead. At the edges of the plate the residual stress is zero, going through a state of compression (-). In the weld bead area the stresses are in tension state (+).



- ii. The longitudinal stresses along longitudinal lines are all in tension state (+). At the edges the residual stresses are zero, reaching a maximum in the central zone of the weld bead. There is a symmetry behaviour in relation to this point.
- b) In the butt joint models, clamping conditions have a huge influence on the magnitude of the **transverse residual stress**, which acts perpendicular to the weld bead. However, the profile of the residual stresses remains equivalent. When there is restriction of movement on both plates in the transverse direction, the residual stresses are higher.
- i. The transverse stresses along the transverse lines have a symmetrical behaviour in relation to the weld bead. At the edges, the magnitude is zero, passing to a tension state (+) just after passing the clamp zones. The maximum stress is in the weld bead area. There is a difference between the models of 400 MPa (maximum stress).
  - ii. The transverse residual stress along longitudinal lines shows a difference between models of 300 MPa (maximum stress). Although there is a difference in magnitude, the stress profile is identical, with symmetry in relation to the central point of the weld bead. The edges of the plates are in a state of compression (-), moving immediately to a state of tension (+).
- c) In the butt joint models, the **z-displacement** has a very small magnitude. In both models, there is a higher deformation near the area around the weld bead due to the high temperature. The model that has one of the plates free to move presents little deformation, while the one that has both plates fixed, presents a small deformation after passing the clamping zones. The deformation is not uniform along the width.
- d) In the butt joint models, the **y-displacement** is quite different between models. In the model that has both plates fixed there is no deformation in the edges. However, in the model that has the plate free to move during the welding process, there is a rotational deformation. There is a longitudinal shrinkage (y-direction) near the weld bead on both models.

- e) In the butt joint models, the **x-displacement** is insignificant in the model that has the fixed plates. However, due to the existing rotational deformation, there is a deformation in model 2.
- f) In the T-joint model, the **transverse residual stress**:
- i. In the vertical plate (transverse lines) has a higher concentration near the weld bead, being zero at the opposite extremity. It starts with a small state of compression, moving to a tension state and goes back to the compression state.
  - ii. In the horizontal plate (transverse lines) the stress profile is symmetrical to the weld bead, being null at the edges and increasing next to the centre. It is always in the tension state.
  - iii. Along longitudinal lines, there is a significant difference between the stresses of the horizontal and the vertical plates.
- g) In the T-joint model, the **longitudinal residual stress**:
- i. The horizontal plate (transverse lines) presents a symmetrical behaviour in relation to the weld bead. At the edges the stress is zero, going through a state of compression. In the area near the weld bead the stresses are maximum and in the state of tension.
  - ii. In the vertical plate (transverse lines) there are more stresses near the weld bead. Initially the stresses are in tension state, passing to compression state and reaching the zero at the extremity.
  - iii. Along the longitudinal line, there is a small compression state at the edges and outside these areas the stresses are in tension state.
- h) In the T-joint model, there is a rotational deformation of the vertical plate of approximately 2 degrees to the side where the welding is done (in **x-direction**). There is a slight scissor effect at the edges of the horizontal plate.
- i) In the T-joint model, there is a small transverse shrinkage effect (**y-direction**) along the transverse edges. The same effect happens in the vertical plate.

- j) In the T-joint model, the displacement in **z-direction** is practically zero.
- k) In both models, the difference in the magnitude of the residual stresses is insignificant along the **plate thickness**. There is no difference in deformation along the plate thickness;
- l) To perform the numerical simulation of the welding process it is mandatory to have the following **temperature dependent properties**: thermal conductivity, specific heat capacity, Young's modulus, density, thermal expansion coefficient and flow curves. In addition, the temperature range must be between the room and melting temperatures of the material;
- m) The heat source that best adapts to the laser welding process is the conical heat source, since it is the one that best represents the energy distribution of the beam. This must have a depth equal to the thickness of the plate to be welded;
- n) The quantification of internal residual stresses and strains must be done after a cooling period to ensure the stabilization of the temperature gradient in the whole part. There was no significant difference between completing the analysis when the part reached 300 or 20 °C (room temperature);
- o) The discretization of the model has a great influence on the results. It is crucial to perform a mesh convergence study. The maximum temperature in the centre of the weld bead was the chosen parameter and proved to be efficient. The refinement should be superior in areas where there is a higher temperature gradient (near weld bead);
- p) The use of the tools shared memory parallelization (SMP) combined with the domain decomposition method (DDM) shows to be beneficial. The processing time decreases substantially and the available results are exactly the same;

- q) The Adaptive mode that calculates the length increment automatically is the best option. For simulations aiming only the calculation of stresses and strains (mechanical simulation), it is not necessary to write an output in each increment. As the output frequency increases, the simulation becomes faster and has little influence on the results;
- r) The monitoring lines, composed of several intermediate tracking points, must be defined through the node coordinates. It is enough to select the starting and ending points and the number of points between these two. It is fundamental to guarantee a high number of tracking points to detect all changes.
- s) Two clamp modes were tested (stiffness & force vs stiffness). There was no difference in the results;
- t) Simufact proved to be a relatively easy software to perform laser welding simulation.

In general, the work developed and its numerical results are in accordance with the theory and literature.

## 4.2. Future work

---

As I developed this work, reading several articles, master's thesis from other institutions and other documents, I realized that the work I developed was the tip of the iceberg. I hope that the work developed is the starting point of the numerical simulation of the welding process in my department (DEM-UA).

Here are some recommendations for future work that can be developed:

- Development of **experimental tests** to validate the robustness of the numerical model;

- Development of **new numerical models using other FEM software** (*Sysweld, Abaqus, Ansys*) to compare;
- Experimentally **determine the material properties** for welding simulation (temperature dependent data);
- Perform a numerical analysis with **metallurgical approach** to predict the phase transformations and calculate the microstructure;
- Study in more detail the **areas affected by the heat input** (HAZ and FZ) and the size of the melt pool;
- Determine the **influence of laser welding parameters** and optimize it to ensure the quality of the welded structure;
- Execute new simulations for other **welding types** and other **joints geometries**.



## REFERENCES

- [1] T. R. Lima, “Determinação do campo de tensões residuais e distorções resultantes de processos de soldadura recorrendo ao Sysweld,” pp. 1–228, 2014.
- [2] N. S. M. Nasir, M. K. A. A. Razab, S. Mamat, and M. I. Ahmad, “Review on Welding Residual Stress,” *ARPN J. Eng. Appl. Sci.*, vol. 11, no. 9, pp. 6166–6175, 2016.
- [3] C. Seang, “Evaluation numérique des contraintes résiduelles appliquée à l’acier DP600s soudé par laser de haute puissance Nd:YAG,” 2013.
- [4] T. Schenk, *Modelling Welding Distortion - Influence of Clamping and sequencing*. .
- [5] A. B. Pereira, “Tecnologia dos Processos de Ligação - Tensões e deformações na soldadura (Capítulo 13).” pp. 1–11.
- [6] G. Agarwal, *Study of solidification cracking during laser welding in advanced high strength steels*. .
- [7] J. Zheng, A. Ince, and L. Tang, “Modeling and simulation of weld residual stresses and ultrasonic impact treatment of welded joints,” *Procedia Eng.*, vol. 213, no. 2017, pp. 36–47, 2018, doi: 10.1016/j.proeng.2018.02.005.
- [8] H. M. Esteves Ramos, “Modelação numérica de processos de soldadura usando ESI Sysweld,” 2015.
- [9] C. Dawes, *Laser Welding: A Practical Guide*. 1992.
- [10] F. A. O. Fernandes, D. F. Oliveira, and A. B. Pereira, “Optimal parameters for laser welding of advanced high-strength steels used in the automotive industry,” *Procedia Manuf.*, vol. 13, no. January, pp. 219–226, 2017, doi: 10.1016/j.promfg.2017.09.052.
- [11] P. H. Geri van Krieken, “Practical guideline Laser welding - including certification scheme,” *Laser Appl. Cent.*, p. 368.
- [12] W. Steen and J. Mazumder, *Laser material processing - fourth edition*. 2008.
- [13] A. B. Pereira, R. O. Santos, B. S. Carvalho, M. C. Butuc, G. Vincze, and L. P. Moreira, “The evaluation of laser weldability of the third-generation advanced high strength steel,” *Metals (Basel)*, vol. 9, no. 10, 2019, doi: 10.3390/met9101051.
- [14] J. P. Oliveira and Z. Zeng, “Laser welding,” *Metals (Basel)*, vol. 9, no. 1, pp. 9–10, 2019, doi: 10.3390/met9010069.
- [15] F. A. O. Fernandes, A. B. Pereira, B. Guimarães, and T. Almeida, “Laser welding of transmitting high-performance engineering thermoplastics,” *Polymers (Basel)*, vol.

- 12, no. 2, 2020, doi: 10.3390/polym12020402.
- [16] J. Wu, H. Zhang, Y. Feng, and B. B. Luo, “3D multiphysical modelling of fluid dynamics and mass transfer in laser welding of dissimilar materials,” *Metals (Basel)*, vol. 8, no. 6, 2018, doi: 10.3390/met8060443.
- [17] M. Dal and R. Fabbro, “An overview of the state of art in laser welding simulation,” *Opt. Laser Technol.*, vol. 78, pp. 2–14, 2016, doi: 10.1016/j.optlastec.2015.09.015.
- [18] W. Piekarska, M. Kubiak, and Z. Saternuns, “Computer Simulation of Temperature Field in Laser Beam Welded Lap Joint,” vol. 7.
- [19] W. Arif, “Numerical modeling and failure prediction of laser welded joints in a support of car seat,” 2017.
- [20] M. Sokolov and A. Salminen, “Methods for improving laser beam welding efficiency,” *Phys. Procedia*, vol. 56, no. C, pp. 450–457, 2014, doi: 10.1016/j.phpro.2014.08.148.
- [21] W. Piekarska, M. Kubiak, and Z. Saternus, “Application of Abaqus to analysis of the temperature field in elements heated by moving heat sources,” vol. 10, no. 4, pp. 177–182, 2010.
- [22] T. Kik and J. Górka, “Numerical simulations of laser and hybrid S700MC T-joint welding,” *Materials (Basel)*, vol. 12, no. 3, 2019, doi: 10.3390/ma12030516.
- [23] H. T. Kashani, P. Kah, and J. Martikainen, “Laser Overlap Welding of Zinc-coated Steel on Aluminum Alloy,” *Phys. Procedia*, vol. 78, no. August, pp. 265–271, 2015, doi: 10.1016/j.phpro.2015.11.037.
- [24] A. B. Pereira, F. A. O. Fernandes, D. G. Afonso, and R. J. A. de Sousa, “Maintenance of cast brass taps by pulsed Nd:YAG LASER welding,” *Procedia Manuf.*, vol. 41, pp. 1001–1008, 2019, doi: 10.1016/j.promfg.2019.10.026.
- [25] B.L.Kinsey, “Tailor welded blanks for the automotive industry,” p. 2011, 2011.
- [26] D. F. Oliveira, “Parâmetros da soldadura LASER pulsado de Nd:YAG em aços avançados de alta resistência,” *Univ. Aveiro*, p. 132, 2015.
- [27] W. Piekarska, M. Kubiak, Z. Saternus, and K. Rek, “Computer modelling of thermomechanical phenomena in pipes welded using a laser beam,” *Arch. Metall. Mater.*, vol. 58, no. 4, pp. 1237–1242, 2013, doi: 10.2478/amm-2013-0156.
- [28] N. D. Bahar, S. Marimuthu, and W. J. Yahya, “Pulsed Nd: YAG laser drilling of aerospace materials (Ti-6Al-4V),” *IOP Conf. Ser. Mater. Sci. Eng.*, vol. 152, no. 1,



- 2016, doi: 10.1088/1757-899X/152/1/012056.
- [29] W. Castro and J. R. Almirall, “Elemental analysis of biological matrices by laser ablation high resolution inductively coupled plasma mass spectrometry (LA-HR-ICP-MS) and high resolution inductively coupled plasma mass spectrometry (HR-ICP-MS),” vol. 3358431, no. May, p. 207, 2008.
- [30] I. Ashraf, “Laser Systems and Their Applications,” 2013.
- [31] M. Berczeli and G. Buza, “Relationship between the keyhole laser welding and the plasma,” *IOP Conf. Ser. Mater. Sci. Eng.*, vol. 448, no. 1, 2018, doi: 10.1088/1757-899X/448/1/012051.
- [32] D. A. De Moraes and A. Czekanski, “Thermal modeling of 304L stainless steel for Selective Laser Melting: Laser power input evaluation,” *ASME Int. Mech. Eng. Congr. Expo. Proc.*, vol. 2, no. November, 2017, doi: 10.1115/IMECE2017-72224.
- [33] C. Seang, A. K. David, and E. Ragneau, “Nd:YAG laser welding of sheet metal assembly: Transformation induced volume strain affect on elastoplastic model,” *Phys. Procedia*, vol. 41, pp. 448–459, 2013, doi: 10.1016/j.phpro.2013.03.101.
- [34] X. Ruan, Q. Zhou, L. Shu, J. Hu, and L. Cao, “Accurate prediction of the weld bead characteristic in laser keyhole welding based on the stochastic kriging model,” *Metals (Basel)*, vol. 8, no. 7, 2018, doi: 10.3390/met8070486.
- [35] J. Gonçalves, “Análise da soldabilidade entre titânio e alumínio por laser pulsado.” 2019.
- [36] K. I. Yaakob, M. Ishak, and S. R. A. Idris, “The effect of pulse welding parameters on weld geometry of boron steel using low power fibre laser,” *J. Mech. Eng. Sci.*, vol. 11, no. 3, pp. 2895–2905, 2017, doi: 10.15282/jmes.11.3.2017.10.0261.
- [37] M. Sokolov and A. Salminen, “The effect of joint edge surface preparation on the efficiency of fiber laser welding of low-alloyed steels,” *Mechanika*, vol. 21, no. 3, pp. 220–225, 2015, doi: 10.5755/j01.mech.21.3.8798.
- [38] T. P. Hung, H. E. Shi, and J. H. Kuang, “Temperature modeling of AISI 1045 steel during surface hardening processes,” *Materials (Basel)*, vol. 11, no. 10, 2018, doi: 10.3390/ma11101815.
- [39] J. Kaars, P. Mayr, and K. Koppe, “Determining material data for welding simulation of presshardened steel,” *Metals (Basel)*, vol. 8, no. 10, 2018, doi: 10.3390/met8100740.

- [40] S. Lemkeddem, F. Khelfaoui, and O. Babahani, “Calculation of energy lost by radiation and convection during laser welding of TA6V titanium alloy,” *J. Theor. Appl. Phys.*, vol. 12, no. 2, pp. 113–120, 2018, doi: 10.1007/s40094-018-0288-x.
- [41] T. Kik, “Computational techniques in numerical simulations of arc and laser welding processes,” *Materials (Basel)*, vol. 13, no. 3, pp. 1–18, 2020, doi: 10.3390/ma13030608.
- [42] J. D. Caprace, G. Fu, J. F. Carrara, H. Remes, and S. B. Shin, “A benchmark study of uncertainty in welding simulation,” *Mar. Struct.*, vol. 56, pp. 69–84, 2017, doi: 10.1016/j.marstruc.2017.07.005.
- [43] T. A. Cirne Ramos, “Numerical simulation of multi-stage hydroforming process of tubular parts,” 2005.
- [44] M. Klingler, “Laser Beam Welding Simulation with Two Different Approaches,” no. January 2007, 2018.
- [45] E. S. V Marques, F. J. G. Silva, and A. B. Pereira, “Comparison of Finite Element Methods in Fusion Welding Processes — A Review,” pp. 1–19, 2020, doi: 10.3390/met10010075.
- [46] L. E. Lindgren, “Finite element modeling and simulation of welding part 1: Increased complexity,” *J. Therm. Stress.*, vol. 24, no. 2, pp. 141–192, 2001, doi: 10.1080/01495730150500442.
- [47] S. Liu, A. Kouadri-Henni, and A. Gavrus, “DP600 dual phase steel thermo-elasto-plastic constitutive model considering strain rate and temperature influence on FEM residual stress analysis of laser welding,” *J. Manuf. Process.*, vol. 35, no. October, pp. 407–419, 2018, doi: 10.1016/j.jmapro.2018.07.006.
- [48] S. Dragi and I. Vasović, “Finite Element Analysis of Residual Stress in Butt Welding Two Similar Plates,” *Computer (Long. Beach. Calif.)*, no. 1, pp. 57–60, 2009.
- [49] D. Kollár and B. Kövesdi, “Numerical Simulation of Welding Process,” *Young Weld. Prof. Int. Conf. YPIC2015*, no. October 2015, p. 6, 2015.
- [50] A. C. Nunes, “An Extended Rosenthal Weld Model: A moving heat source weld model can be extended to include effects of phase changes and circulations in the weld pool,” *Am. Weld. Soc.*, no. 62, pp. 165–170, 1983.
- [51] R. J. A. de Sousa, F. Teixeira-Dias, J. Pinho-da-Cruz, R. A. Fontes Valente, *Método dos Elementos Finitos - Técnicas de Simulação Numérica em Engenharia*. 2018.

- [52] M. Frunza, F. Gheorghe, and R. Luca, “The Use of Numerical Applications in the Study of Dental contacts,” no. June, 2010.
- [53] M. Zubairuddin, S. K. Albert, S. Mahadevan, M. Vasudevan, V. Chaudhari, and V. K. Suri, “Experimental and finite element analysis of residual stress and distortion in GTA welding of modified 9Cr-1Mo steel,” *J. Mech. Sci. Technol.*, vol. 28, no. 12, pp. 5095–5105, 2014, doi: 10.1007/s12206-014-1132-0.
- [54] F. Billur, J. Dykeman, and T. Altan, “Three generations of advanced high strength steels for automotive applications,” *Stamp. J.*, no. December 2013, 2014.
- [55] M. Ozsoy, E. Esener, S. Ercan, and M. Firat, “Springback Predictions of a Dual-phase Steel Considering Elasticity Evolution in Stamping Process,” *Arab. J. Sci. Eng.*, vol. 39, no. 4, pp. 3199–3207, 2014, doi: 10.1007/s13369-013-0910-9.
- [56] S. Winzer, Jami; Heibel, “Lightweight car body construction with new high strength steels,” no. June 2017, 2018.
- [57] P. R. Spena, M. De Maddis, F. Lombardi, and F. D’Aiuto, *Resistance spot welding of advanced high strength steels*, vol. 423–426, no. March. 2013.
- [58] Z. Bézi, B. Baptiszta, and S. Szávai, “Experimental and numerical analysis of resistance spot welded joints on DP600 sheets,” no. JANUARY 2014, pp. 7–12, 2015.
- [59] T. Hilditch, S. Toman, and D. Fabijanic, “Post-forming heat treatment of dual phase steel components for automotive applications using a fluid bed furnace,” *Mater. Forum*, vol. 31, no. March, pp. 24–30, 2007.
- [60] S. Krajewsk and J. Nowacki, “Artificial Intelligence in the AHSS Steel Mechanical Properties and Microstruture Analysis,” *Prz. Elektrotechniczny*, vol. 92, no. 6, pp. 102–105, 2016, doi: 10.15199/48.2016.06.19.